THE BETA DECAY OF ^{105}Ru

THE BETA DECAY OF ^{105}Ru

by

STANLEY OWEN SCHRIBER

A Thesis

Submitted to the Faculty of Graduate Studies

in Partial Fulfilment of the Requirements

for the Degree

Doctor of Philosophy

McMaster University

October, 1966

DOCTOR OF PHILOSOPHY (1967) McMASTER UNIVERSITY

(Physics) Hamilton, Ontario.

TITLE: The Beta Decay of ^{105}Ru

AUTHOR: Stanley Owen Schriber, B. Sc. (University of Manitoba)

M. Sc. (University of Manitoba)

SUPERVISOR: Professor M. W. Johns

NUMBER OF PAGES: vii, 132

SCOPE AND CONTENTS:

Twenty-two energy levels of ^{105}Rh populated in the beta decay of ^{105}Ru have been determined. The internal conversion coefficients of the eighteen strongest transitions were measured using a magnetic spectrometer and were used to obtain their multipole assignments. The energies and intensities of seventy gamma rays were measured using germanium detectors and scintillation counters. Gamma-gamma and beta-gamma coincidence measurements carried out with magnetic spectrometers, NaI(Tl) and Ge(Li) detectors were used with these energy measurements to establish a decay scheme. An interpretation of the decay scheme in the light of current nuclear models was attempted.

ACKNOWLEDGEMENTS

I wish to thank my research director, Dr. M. W. Johns for his invaluable guidance and assistance and the other members of my supervisory committee, Dr. T.J. Kennett and Dr. D. W. L. Sprung for their interest and support.

I would like particularly to acknowledge the help which I received from Dr. T.J. Kennett and his entire research group for generously making available their equipment for my use and for their advice in writing computer programs.

The members of the beta and gamma spectroscopy group to which I belong have not only helped me with experiments but have been interested in every phase of this work. It is a pleasure to recall the fun we have had as a team.

Thanks are due to Dr. A. Artna who first suggested the problem and who, with Dr. D.G. Burke made some of the preliminary measurements and to Dr. Ziem Sujkowski who has been interested in the final phases of the investigation.

The financial assistance from the National Research Council in the form of studentships and operating grants is gratefully acknowledged.

Special appreciation goes to my wife who has not only given constant encouragement but who has been inveigled into plotting graphs and typing the rough manuscript.

Finally, I would like to thank Mrs. Helen Kennelly for typing the thesis and wrestling with the tables.

TABLE OF CONTENTS

LIST OF FIGURES

LIST OF TABLES

CHAPTER I

INTRODUCTION

In the study of nuclear levels one is interested in the properties of a collection of protons and neutrons which form a stable, quasi-stable or unstable configuration. Since the heaviest nucleus known to date has less than three hundred particles, attempts to depict the nucleus as a medium with an infinite number of constituent nucleons is indeed an approximation (Weisskopf et al (1958), Brueckner et al (1958)). These nuclear matter calculations yield, however, many interesting clues as to actual nuclear properties (Preston (1962)). At the other extreme, the treatment of a group of a hundred particles by one-body or two-body techniques is out of the question unless some "a priori" approximations about nuclear forces binding the nucleons together are made. Since the many-body problem is prohibitively complex, physicists have attempted to make progress by inventing models of nuclei which possess some of the properties of real nuclei. Some of the more useful models will be discussed in the next chapter. As will be seen the models work only in certain regions of the periodic table. To date, no one model is able to predict all the properties of all nuclei.

With the tools and techniques available to the nuclear spectroscopist, he can, by studying induced radioactivity or by observing naturally occurring transitions between nuclear states, deduce such properties of the energy levels as the energy, spin and parity of the state. For a complete understanding of the work that is to follow, an explanation of some of the terms used will be found in the next section.

This thesis deals with the energy levels in $^{105}_{45}Rh_{60}$, as populated in the beta decay of $^{105}_{44}Ru_{61}$. The measurements of beta and gamma ray energies and intensities together with a determination of internal conversion coefficients give a good deal of information about these levels.

1.1 Spin and Parity

The excitation energies are obtained by observing the transitions which occur when the nucleus de-excites itself from one nuclear state to another. It should be noted that the de-excitation may proceed by several competing paths, each with its own characteristic decay probability.

The expression "spin" refers to the intrinsic angular momentum of a particle, a quantum mechanical concept. Protons and neutrons are both fermions obeying Fermi-Dirac statistics and the exclusion principle and hence each particle has an intrinsic angular momentum $\frac{1}{2}\hbar$ ($\hbar = h/2\pi$ and h, Planck's constant, 6.625×10^{-27} erg-sec). The term "spin" is also used to represent the vector sum of the orbital angular momentum and the intrinsic angular momentum of a particle. The spin of a nucleus is the vector sum of the spins of all the individual constituent nucleons.

It can be seen that, in terms of $\hbar$, a nucleus made up of an even number of protons and neutrons will have an integral value of spin while a nucleus with an uneven number of particles will have a half integral spin. It is an experimental fact that nucleons tend to pair off their spins giving a resultant spin of zero. Also, all even-numbered proton, even-numbered neutron nuclei have a zero spin ground state with-

out exception.

Symmetry suppositions lead to conservation principles. For example, the rotational symmetry property of space leads to the conservation of angular momentum principle and the conservation of energy principle follows from the homogeneity properties of space and time. The space inversion invariance leads to the parity conservation principle. Parity is a quantum mechanical concept with no classical analog. Stated mathematically, a wave function $\psi(x,y,z)$ describing a system with co-ordinates (x,y,z) is of even parity if upon inversion of the co-ordinates through the origin the wave function is unaltered, i.e. $\psi(x,y,z) = \psi(-x,-y,-z)$. A wave function is of odd parity if upon inversion one obtains $\psi(x,y,z) = -\psi(-x,-y,-z)$. Parity is a good quantum number for strong and electromagnetic interactions; however, in recent years it has been found that parity is not conserved in weak interactions. This will be discussed in the next section.

1.2 Beta Decay

There are four different types of interactions in the physical world. These are, listed in order of decreasing strength, the strong interaction (neutron-proton scattering), the electromagnetic interaction (gamma emission), the weak interaction (beta decay) and the gravitational interaction (attraction between celestial bodies). Representative numbers describing comparative orders of magnitude for these interactions are 10, 10^{-2}, 10^{-23} and 10^{-45}, respectively. (Preston (1962)).

The weak interaction is responsible for beta decay which is a nuclear transformation accompanied by the emission of an electron or positron, or by the capture of an orbital electron. The three modes of

decay are listed below:

(i) The reaction $n \rightarrow p + e^- + \bar{\nu}$ describes the decay of neutron-rich nuclei and the free neutron, a neutron decaying into a proton, electron and antineutrino.

(ii) The reaction $p \rightarrow n + e^+ + \nu$ describes the decay of proton-rich nuclei, a proton decaying into a neutron, positron and neutrino. (A free proton cannot decay in this manner since its mass is less than the products and therefore the process is energetically impossible. However, a proton in the nucleus can decay in this manner due to the influence of other nucleons in the nucleus.)

(iii) The reaction $p + e^- \rightarrow n + \nu$ describes the capture of an orbital electron by a proton with a resulting transformation into a neutron and neutrino.

Beta rays were one of the first types of radioactivity discovered. Since the force mechanism which accomplishes beta decay was not known at first, theoretical and experimental ventures went hand in hand, each in turn leading the other. Since the theoretical understanding of the weak interaction required both the development of relativistic quantum electrodynamics and the development of many experimental techniques, it is perhaps not surprising that a precise theory took over fifty years to mature. Chadwick and Ellis (1922) were the first to distinguish between the beta ray continuum and the monoergic conversion electrons. The monoergic electrons are emitted after the primary beta ray and neutrino pair have been produced and compete with gamma ray transitions in the manner discussed in the section on internal conversion. The existence of a continuum was baffling to physicists since

it appeared that the conservation of energy law was being violated. The upper energy limit of the continuum was shown energetically to represent the energy available for the beta decay (Gurney (1925)). The conservation of angular momentum principle was also being violated as indicated in the following example. A half-integral fermion decaying into two half-integral fermions whose resultant spin would be of integral value cannot be consistent with the conservation of angular momentum because, somehow, a half-integral value of spin is missing, ie.

$$n \rightarrow p + e^-$$

$$\frac{1}{2} \rightarrow \frac{1}{2} + \frac{1}{2}$$

Pauli (1933) suggested the existence of a third decay product which would allow for the continuous distribution of beta rays. This postulated particle, the neutrino, would then have to have the following properties; possess zero charge, one-half spin, and nearly zero mass, obey Fermi statistics, and interact only through the weak interaction. The neutrino postulate saved the conservation of energy and the conservation of angular momentum principles.

Fermi (1934) showed how the neutrino could fit into a beta decay theory using currents in the nucleus in analogy to electromagnetic gamma ray emission. Perturbation theory yields the following transition probability per second for the emission of an electron of energy E to E + dE in beta decay

$$W(E) = \frac{2\pi}{\hbar} \left| \langle \psi_f^* \varphi_f^* | H_{if} | \psi_i \varphi_i \rangle \right|^2 \rho(E)$$

where ψ_i and ψ_f are the initial and final representations of the nu-

clear states (neutron, proton), φ_i and φ_f are the initial and final representations for the leptonic states (electron, neutrino), H_{if} is the interaction Hamiltonian which must not only contain the type of weak interaction but must destroy the initial states and create the final ones, and $\rho(E)$ is the density of final states per unit energy interval available for the decay.

For the wave functions one first assumes that there is no interaction between the nucleus and the participating particles. Therefore one can use plane waves as a good approximation ($\psi = A \exp(-i\underline{k}\cdot\underline{r})$, $\underline{r}$-position vector and $\underline{k} = \frac{2\pi}{\lambda}$ where λ is the wave length of the radiation). Rewriting $\exp(i\underline{k}\cdot\underline{r})$ in a series expansion gives $1 + i\underline{k}\cdot\underline{r} + (\frac{\underline{k}\cdot\underline{r}}{2})^2 + \cdots$. Since λ is large compared to nuclear dimensions, the first term of the expansion is dominant and can be used as an approximation for the electron and neutrino wave functions. This leads to what is known as allowed order of decay. If the resultant $|\langle f|H|i\rangle|^2$ upon integration is zero, higher order terms in the plane wave expansion can become important. In this manner forbidden orders of decay arise. The more terms in the approximation that are required, the higher the degree of forbiddenness. This expansion is analogous to the multipole expansion of a radiation field. Upon integrating the transition probability 'W' over appropriate variables, the probability of obtaining an electron of momentum between p and p + dp becomes, with a few correction factors added,

$$N(p)dp = C|M_{if}|^2 F(Z,E)\ p^2(E_o - E)^2 S_n dp$$

where C is a constant, M_{if} is the nuclear matrix element containing the neutron and proton states and the interaction Hamiltonian, $F(Z,E)$ is

the Fermi function which corrects for the Coulomb interaction between nucleons and electrons (assumed plane waves) and the effects of the atomic electrons, p is the momentum of the electrons, E_o is the maximum energy of the emitted electrons, E is the energy of the electrons and S_n is the shape factor which corrects the expression when higher degrees of forbiddenness are required (n indicates the degree of forbiddenness). It should be noted that S_n is constant for all allowed and for most first forbidden decays.

It can be seen that plotting $(N(p) / p^2F(Z,E))^{\frac{1}{2}}$ versus energy results in a straight line plot known as a Fermi plot with intercept E_o on the energy axis. Departures from a straight line indicate a forbidden shape factor or the admixture of several beta groups.

Integrating N(p)dp over all possible momenta yields the total probability of decay

$$\lambda = \frac{\ell n 2}{T_{\frac{1}{2}}} = C\left|M_{if}\right|^2 f_n(Z,E)$$

where $T_{\frac{1}{2}}$ is the half-life for the decay and f_n contains the dependence on the integral with S_n (ie. $f_n = \int p^2(E_o-E)^2 F(Z,E)S_n dp$. Rewriting this expression gives $f_nT = \frac{C}{\left|M_{if}\right|^2}$ which is dependent only on the type of transition occurring and gives information about nuclear properties. The expression f_nT is known as the comparative half-life. The following table shows characteristic values of $\log_{10} f_nT$ for different types of transitions. In reality, one can only work out f_oT since S_n is not uniquely defined for most forbidden decays. We therefore use $\log_{10} f_oT$ except for special cases such as first forbidden unique decays.

Type	$\log_{10}$ fT
Super allowed	3.2-3.8 transitions between mirror nuclei
Allowed	4.2-6.6
First Forbidden	6.5-8.5
First Forbidden Unique	8.0-8.8
Second Forbidden	10 - 13

The $\log_{10}$ fT value is not a very reliable indication of the type of transition but it is often the only clue one can find.

From the properties postulated for the neutrino it can be seen that it would be a difficult particle to detect. Indirect evidence for its existence was first obtained by recoil experiments in which the direction of the beta particle and the direction of the nucleus suggested the need for a third particle which would conserve linear momentum (Sherwin (1948), Allen (1948)), but difficulties with source thicknesses made these results somewhat inconclusive. It took almost twenty-five years to obtain direct evidence for the existence of the neutrino. The difficult experiments of Reines and Cowan (1953, 1959) finally provided direct evidence for the neutrino using the inverse reaction $\bar{\nu} + p \rightarrow n + e^+$. Davis (1955) in his experiments on ^{37}Cl showed that the neutrino and antineutrino were not the same, a result confirmed by experiments on double beta decay (Ingraham and Reynolds (1950), Primakoff (1952)).

In 1956, Lee and Yang (1956) pointed out that the question of parity violation in the weak interaction had never been investigated and that experiments on aligned nuclei would give clear cut information on this point. Wu et al (1957) showed that the electrons emitted from oriented ^{60}Co nuclei were emitted predominantly in a direction opposite

to the nuclear spin, confirming parity violation for weak interactions. Experimental evidence acquired over the next few years gave a great deal of new insight into the nature of beta decay. In particular, one might mention the work of Goldhaber et al (1958) which showed that the neutrino has negative helicity, i.e. that the intrinsic spin and the linear momentum vectors of the neutrino are always antiparallel.

Konopinski and Uhlenbeck (1941) first listed the five types of interactions that were Lorentz invariant. These were vector (displacement), axial vector (angular momentum), scalar (scalar product of vector with vector or axial vector with axial vector), pseudoscalar (scalar product of vector with axial vector) and tensor interactions. These forms are represented by V, A, S, P and T, respectively. In principle, the beta interaction can be a combination of all of these. Because beta decay does not conserve parity, each interaction can consist of two terms, one which preserves parity and the other which does not. Since the helicity of the neutrino is known to be negative and the helicities of electrons and positrons are -v/c and v/c, respectively (Frauenfelder et al (1957), Page (1957)), the ten possible coupling constants are reduced to two; the vector and axial-vector interactions. In principle, it had been known that two types of interactions existed from experimental results on angular momentum changes for various allowed spectra. The vector interaction gives the Fermi selection rules and the axial-vector interaction gives the Gamow-Teller selection rules. In the Fermi allowed interaction the electron and the neutrino do not remove spin from the nucleus since their spins are antiparallel. The Gamow-Teller allowed interaction removes one unit of angular momentum because the spins

of the electron and neutrino are parallel. Examples of some transitions with spins are shown below.

(i) $O^{14} \longrightarrow N^{14} + e^{+} + \nu$

$I = 0 \longrightarrow I = 0 + \frac{1}{2}\uparrow + \frac{1}{2}\downarrow$ Pure Fermi interaction

(ii) $He^{6} \longrightarrow Li^{6} + e^{-} + \bar{\nu}$

$I = 0 \longrightarrow I = 1 + \frac{1}{2}\downarrow + \frac{1}{2}\downarrow$ Pure Gamow-Teller interaction

(iii) $H^{3} \longrightarrow He^{3} + e^{-} + \bar{\nu}$

$I = \frac{1}{2}\uparrow \longrightarrow \frac{1}{2}\uparrow + \frac{1}{2}\uparrow + \frac{1}{2}\downarrow$

$\longrightarrow \frac{1}{2}\downarrow + \frac{1}{2}\uparrow + \frac{1}{2}\uparrow$

Mixture of Fermi and Gamow-Teller contributing with approximately the same strengths

(iv)

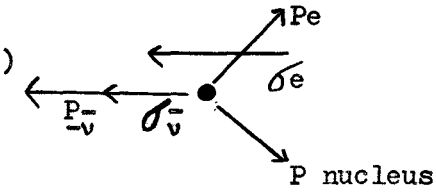

Allowed Gamow-Teller decay

P - momentum

σ - spin

(v)

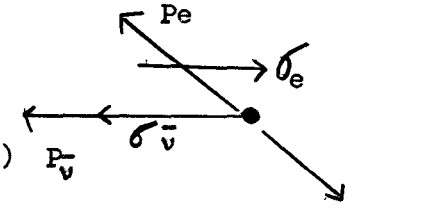

Allowed Fermi decay

Transition	Spin	Parity	Comment
Allowed	$\Delta I = 0$	$\Delta\pi$ = no	Fermi
"	$\Delta I = \pm 1, 0$	$\Delta\pi$ = no	G-T except $0 \longrightarrow 0$
First Forbidden	$\Delta I = \pm 1, 0$	$\Delta\pi$ = yes	Fermi except $0 \longrightarrow 0$
" "	$\Delta I = \pm 2, \pm 1, 0$	$\Delta\pi$ = yes	G-T except $0 \longrightarrow 0$, $\frac{1}{2} \longrightarrow \frac{1}{2}$, $0 \longrightarrow 1$
Second Forbidden	$\Delta I = \pm 3, \pm 2$	$\Delta\pi$ = no	

Higher orders of forbidden decays are observed only in exceptional cases. Since none of these higher order decays were observed in this study, no further discussion seems warranted here.

1.3 Gamma Ray Emission

After beta decay or some other appropriate type of nuclear interaction the nucleus can be left in an excited state. This state is de-excited to the ground state by a direct transition or by a series of cascade events involving intermediate states. The transitions between the excited nuclear states are accomplished predominantly by the emission of electromagnetic radiation.

This electromagnetic radiation is classified by its multipole order "L" according to the angular momentum "L" which the radiation field removes from the nucleus. This angular momentum is related to the spin change between the nuclear states participating in the transition. There are two classes of radiation differing in parity for each angular momentum change. Their names stem from classical theory where an oscillating electric (E) or magnetic (M) 2^L pole will produce a radiation field designated as EL or ML, respectively. The selection rules which must be satisfied for a transition between two nuclear states are

$$\left| I_i - I_f \right| \leq L \leq I_i + I_f$$

$$M = M_i - M_f$$

$$\Delta\pi = (-1)^L \text{ for electric transitions}$$

$$\Delta\pi = (-1)^{L+1} \text{ for magnetic transitions}$$

In this description $\Delta\pi = +1$ or the term "no" means no parity change and $\Delta\pi = -1$ or the term "yes" means a parity change while I_i and I_f are the spins of the initial and final states respectively.

The predominant multipole order emitted will be that consistent with the smallest transfer of angular momentum possible between the states. The situation is summarized in the following table.

Type of Transition	E1	E2	E3	E4	M1	M2	M3	M4
$\Delta\pi$	yes	no	yes	no	no	yes	no	yes
$\Delta J \leqslant$	1	2	3	4	1	2	3	4

It can be seen that the spin and parity quantum numbers of a state can often be uniquely determined if one can establish the multipole order and character of the gamma ray transitions to and from this state.

Gamma ray emission is due to the fact that nucleons are charged and possess magnetic moments and therefore set up charge or magnetic currents which are confined to the nuclear region. For a pure electromagnetic field, expressing the electric, $\underline{E}$, and magnetic, $\underline{H}$, fields in terms of the vector potential, $\underline{A}$, Maxwell's equations will be satisfied if

$$\left(\nabla^2 - \frac{1}{c^2}\,\frac{\partial^2}{\partial t^2}\right)\underline{A} = 0 \quad , \quad \nabla \cdot \underline{A} = 0$$

$$\text{with} \quad \underline{E} = -\frac{1}{c}\,\frac{\partial \underline{A}}{\partial t} \quad \text{and} \quad \underline{H} = \nabla \times \underline{A}$$

Upon quantization of the radiation field and the introduction of the angular momentum operator $\underline{L}$, one obtains two solutions for $\underline{A}$ which have opposite parities. These give rise to the electric and magnetic radiation fields. The interaction Hamiltonian between a charged system of A particles and the electromagnetic field is

$$H_{int.} = -\sum_{i=1}^{A}\left[\frac{e_i}{m_i c}\,\underline{p}_i \cdot \underline{A}(\underline{r}_i) + \mu_i\,\underline{s}_i \cdot \underline{H}(\underline{r}_i)\right]$$

where e_i, μ_i, $\underline{s}_i$, m_i and $\underline{p}_i$ are the charge, intrinsic magnetic moment,

intrinsic spin, mass and momentum of the i^{th} particle, respectively, and $\underline{A}(\underline{r}_i)$ and $\underline{H}(\underline{r}_i)$ are the vector potential and magnetic field, respectively, due to the i^{th} particle at position $\underline{r}_i$. The transition probability for the emission of a gamma ray involving the initial state "i" and the final state "f" is given by

$$T_{i\rightarrow f} = \frac{2\pi}{\hbar} \left| \langle f \right| H_{int} \left| i \rangle \right|^2 \rho(E)$$

where $\rho(E)$ is the density of final states available per unit energy interval. The transition probability for the emission of a photon of energy $\hbar\omega$ with angular momentum L, M and of either electric or magnetic type is given by (Preston (1962)).

$$T(\sigma L) = \frac{8\pi(L+1)}{L\left[(2L+1)!!\right]^2} \frac{k^{2L+1}}{\hbar} B(\sigma L) \quad \text{where } k = \omega/c \text{ and}$$

the reduced matrix element $B(\sigma L, J_i \rightarrow J_f) = (2J_i + 1)^{-1} \sum_{M_i, M_f} \left| \langle f \left| O_{LM} \right| i \rangle \right|^2$

O_{LM} stands for $E_{L,M}$ or $M_{L,M}$ the electric and magnetic operators respectively, σ is a subscript standing for either electric or magnetic type of radiation.

Upon making a rough estimate for the matrix elements, it can be shown that the ratio of the electric and magnetic transition probabilities for the same multipole order is approximately $\left(\frac{McR}{\hbar}\right)^2$ (25-1000) where R is the nuclear radius. The ratio between transition rates of successive multipole orders (L and L + 1) of the same type is approximately $\left(\frac{kR}{2L+3}\right)^2$. Since $kR \ll 1$, it can be seen that only the lowest order multipole possible by the selection rules will take part in the transition. However, in some instances there may be multipole mixing between the two types of radiation, such as M1 and E2 admixtures in regions where

E2 transition rates have been enhanced due to some nuclear properties discussed in the next chapter.

It is very difficult to obtain an accurate formulation for the initial and final nuclear states. Hence one reverts to models which give a simplified representation. Weisskopf (1951) and Moszkowski (1953) used wave functions for a single particle in the shell model picture and obtained for the transition rates

$$T_W(EL) = \frac{2(L+1)}{L[(2L+1)!!]^2}\left(\frac{3}{L+3}\right)^2 \frac{e^2}{\hbar c}\left(\frac{\omega R}{c}\right)^{2L} \omega \text{ sec}^{-1}$$

$$T_W(ML) = \frac{20(L+1)}{L[(2L+1)!!]^2}\left(\frac{3}{L+3}\right)^2 \frac{e^2}{\hbar c}\left(\frac{\omega R}{c}\right)^{2L} \omega \text{ sec}^{-1}$$

$$T_M(ML) = \frac{1}{10}\left(\frac{L+3}{L+2}\right)^2 \left(\mu_p L - \frac{L}{L+1}\right)^2 T_W(ML)$$

where the W and M subscript on the T apply to the results of Weisskopf and Moszkowski, respectively (Preston (1962), Siegbahn (1965)). These "single particle estimates" are often used for convenience in discussing experimentally measured transition rates and it is common practice to refer to lifetimes in terms of "Weisskopf units". It should be noted that a gamma ray transition cannot take place between two nuclear states both having spin zero. The internal conversion process is the mechanism by which a transition between such states occurs.

1.4 Internal Conversion

Gamma emission is not the only mechanism by which an excited nuclear state can be de-excited. Another type of process, of interest here, is the internal conversion process. In this process the nuclear de-excitation energy is transferred directly to an orbital electron which is thereupon ejected from the atom with an energy $E_\gamma - B_j$ (B_j is

the binding of the j^{th} shell). Therefore the beta spectrum of most nuclides consists of a continuous beta momentum distribution upon which is superposed a line spectrum. The conversion electrons emitted are labelled as K, L_1, L_2, L_3, etc. electrons according to the subshell from which they originate. Since the electrons closest to the nucleus have the greatest probability of interacting with it, the K lines are stronger than the L lines, the L lines are stronger than the M lines and so on.

The transition probability per second for the internal conversion process is given by

$$T_e = \frac{2\pi}{\hbar} \left| \langle f | H_{int} | i \rangle \right|^2 \rho(E)$$

where the initial state (i) and the final state (f) are products of nucleon and electronic wave functions. If the nucleus is treated as a point nucleus this expression will have the same nuclear matrix elements as for the gamma emission process. The internal conversion coefficient, α_i, for the ejection of an electron from the i^{th} shell is defined as the ratio T_e/T_γ for that shell. Since the nuclear matrix elements appearing in the numerator and denominator of this expression cancel out leaving only electronic wave functions and multipole operators to be evaluated, the conversion coefficients, α_i, can be calculated with some degree of accuracy. The total internal conversion coefficient $\alpha = \Sigma\alpha_i$, is related to the total decay probability of a transition by $T_T = (1+\alpha)\, T_\gamma$ or $T_T = (1+\frac{1}{\alpha})\, T_e$. It should be noted that α decreases with increasing energy and that it increases with increasing L for either EL or ML transitions. The internal conversion coefficients of a transition give a very good means of determining the type of transition between levels. Such ratios as $\alpha_K, \alpha_K/\Sigma\alpha_L$ $\alpha_{L1}/\alpha_{L2}/\alpha_{L3}$ are also useful in yielding information as to the parities and spins of nuclear levels. Extensive tables of internal conversion coefficients have been computed by Rose et al (1951) treating the nucleus as a point. Corrections to these calculated values were made

by Rose (1958) in a more detailed calculation which took into account the size of the nucleus. A still better compilation of internal conversion coefficients has been made by Sliv and Band (1956,1958) who have corrected for the finite size of the nucleus and for the time that the electron spends in the nuclear volume.

1.5 Isomeric Transitions

In some cases the selection rules governing transitions mentioned in section 1.3 can result in a small probability for a transition or it can be said that the transition has a long half-life for decay (order of seconds-years). This type of transition when first observed was called an isomeric transition. Since the time of the measurement of the first transition rates, it has been found that there is no distinct dividing line between prompt transitions and so-called delayed transitions. Because these transitions must be highly forbidden there usually is a large spin change and a small energy difference between participating levels. These transitions will therefore have large internal conversion coefficients. It was noticed a number of years ago that isomers are not distributed evenly through the mass table but are concentrated in certain mass regions, the so called "islands of isomerism". The shell model accounts reasonably well for the observed facts concerning isomerism.

1.6 Interaction of Gamma Rays with Matter

In traversing matter, electrons lose energy by a large number of successive collisions which lead either to ionization or to the production of Bremsstrahlung radiation. A photon, on the other hand, is removed from the beam by a single event. The reduction in photon

intensity is therefore given by the exponential absorption law, $N = N_o \exp(-\mu x)$ where μ is the absorption coefficient in cm^{-1}.

The three main types of interactions by which gamma radiation reacts with matter are the photoelectric effect, the Compton effect, and the pair production effect. With the photoelectric effect a third body (the nucleus) is necessary for conservation of energy and momentum. This is why the most tightly bound K electrons are responsible for the largest part of the photoelectric cross-section. In the photoelectric effect the photon energy is transferred to an atomic electron which is ejected with an energy $E_\gamma - B_j$ where B_j is the binding energy of the shell in which the electron was located. The vacancy left by the emitted electron is filled by outer electrons falling into the hole with the emission of either fluorescent radiation or Auger electrons.

The Compton process describes the interaction in which a photon of energy $h\nu$ is incoherently scattered from a free electron at an angle θ with a resultant energy of $h\nu'$ and consequent recoil of the free electron. Conservation of energy and momentum lead to the relations

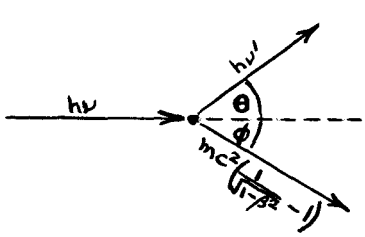

$$h\nu' = h\nu/(1+\alpha(1-\cos\theta))$$

$$T = h\nu 2(1-\cos\theta)/(1+\alpha(1-\cos\theta))$$

where $\alpha = \frac{h\nu}{m_o c^2}$ and T is the kinetic energy of the electron. Klein and Nishina (1929) made a quantum mechanical calculation of the cross-section for Compton scattering which has been shown to agree closely with experimental results (Siegbahn (1965)).

The pair production effect describes a process in which a photon is transformed into an electron-positron pair whose kinetic energy is approximately one MeV less than the energy of the gamma ray. This process must occur in the vicinity of a nucleus in order that the conservation of energy and momentum laws will be fulfilled. This process will be accompanied by gamma radiation when the positron annihilates.

The photoelectric, Compton and pair production cross sections vary as Z^5, Z and Z^2 respectively, and each gives a contribution to the total atomic absorption coefficient as follows $\mu = \mu_{P.E.} + \mu_{C.} + \mu_{P.P.}$ At low energies (less than 100 keV) the photoelectric effect is the dominant process, while at medium energies (approximately 300 keV) the Compton effect is most important and at high energies (above 2 MeV) the pair production effect dominates.

It is the occurrence of multiple interactions that makes a thick body a good absorber of the total energy of an incoming photon. Multiple interactions successively degrade the energy of the scattered radiation and eventually lead to a photoelectric absorption process. Thus, with a large absorber volume, all the incident photon energy is likely to be absorbed, even if the first interaction is Compton scattering. Hence for a large NaI(Tℓ) detector most of the photons interacting with the detector deposit their full energy in the detector and contribute to the full energy photo peak. On the other hand, in the thin, high Z materials used for convertors in external conversion measurements, each photon is likely to interact only once with the converter and the height of the "photo peak" is much less than that of the Compton distribution and corresponds, in energy to $E_\gamma - B_j$ rather than E_γ.

CHAPTER II

NUCLEAR MODELS

INTRODUCTION

Over the last fifty years, it has become clear that the attractive forces between nucleons are non-central, charge independent, short ranged and of the exchange type and that at small enough nucleon-nucleon separations they become repulsive (hard core). The nucleus is composed of from 1 to 250 nucleons, and it ought therefore to be possible to account for all of its properties in terms of the nucleon-nucleon interactions. However, the number of nucleons in the nucleus is far too large for exact mathematical treatment and somewhat too small for a proper statistical treatment. In the case of the atom, the nucleus acts as a strong center of attraction which makes it possible to treat the weaker electron-electron interactions by perturbation methods. The absence of a strong force center in a "blob" of nuclear matter makes the problem much more complicated and leads one to evade the issue by the use of nuclear models which are simpler to manipulate and understand. Only those models which have been useful in the present study of ^{105}Rh will be discussed.

2.1 The Shell Model

A particular nuclide is specified by the number of protons, Z, and the number of neutrons, A-Z, in the nucleus. It has been known for several decades that certain specific values of Z or A-Z have extra stability. These numbers, 2, 8, 20, 28, 50, 82 and 126 were originally called "magic numbers"; we know today that they represent the number

of protons or neutrons required to fill a shell. The situation is completely analogous to that which creates the periodic classification of the elements but the effects of shell closure are much less dramatic in the nucleus than they are in the atom.

The shell model was first proposed in a quantitatively usable form by Mayer (1949, 1950) and independently by Haxel, Jensen and Suess (1949, 1950). In this model, it is assumed that each nucleon moves in a static central potential created by the averaging of the interactions between all the other nucleons in the nucleus. The assumed potential may be a square well, a harmonic oscillator or some more exotic potential of a similar type. The eigenstates for each of these potentials are characterized by a set of quantum numbers (n, ℓ, j) and the Pauli principle limits the number of particles that can go into each of these states. Since these states differ sharply in energy, one would expect differences in nuclear binding as a function of A when one completes the filling of one of these configurations. The square well and harmonic oscillator potential both predicted "magic numbers" at the neutron and proton numbers 2, 8 and 20 but no reasonable potential yielded the other numbers. In order to obtain these, it was necessary to introduce a strong spin-orbit coupling of the form $V(\underline{r})\underline{\ell}\cdot\underline{s}$ in which $V(\underline{r})$ expresses the radial dependence of the force. This $\underline{\ell}\cdot\underline{s}$ coupling splits the $2\ell + 1$ degenerate levels of given ℓ into the two groups with $j = \ell + \frac{1}{2}$ and $j = \ell - \frac{1}{2}$ in which the level with larger j is more tightly bound. In this model $\underline{j} = \underline{\ell} + \underline{s}$ is a constant of the motion. This shell model makes good predictions of ground state spins and parities for all odd A nuclei and does a reasonably good job for excited states

of odd A nuclei with one or two particles (or holes) in a shell. When there are several particles in an unfilled shell, the nucleus tends to become deformed from a spherical shape to an ellipsoidal shape and the assumption of a spherically symmetric potential is no longer valid.

In the early days of the theory, it was difficult to visualize the existence of nuclear "orbits" in densely packed nuclear matter. Today, it is realized that the permanence of these orbits is associated with the fact that all the available states in momentum space are filled with fermions; thus scattering collisions within the nuclear volume cannot take place and each nucleon is able to act as a free particle in the shell model potential.

In the extreme single particle model, the filled shells are regarded as an inert core and particles in the unfilled shells react only with the potential due to this core. In this situation all particles with the same (n,l,j) have the same energy. If there is one particle in an unfilled shell or one hole in a completely filled shell, the spin and parity of the state are given directly by that of the one nucleon or hole. If there are two particles or holes in a shell, these will couple to form degenerate levels with $\underline{j} = \underline{j}_1 + \underline{j}_2$ where j takes all the values permitted by the laws of combination of angular momentum and the Pauli principle. In fact, this degeneracy is always removed by interactions between the two particles. The model which attempts to include the interactions of nucleons within the unfilled shell is called the "single particle model" and introduces a number of new corrections to the oversimplified "extreme single particle" model. In this model, particles within an unfilled shell pair off to yield a resultant zero

spin with an increase in stability which increases with the spin value. Thus in some nuclei a more stable configuration can be obtained by completing a high spin pair and breaking a low spin pair of a lower lying level. The occurrence of this phenomenon explains the absence of high spin ($\frac{11}{2}$ or $\frac{13}{2}$) ground states in nuclei, even though the shell being filled is characterized by a large j value.

The same type of pairing interaction accounts for the zero ground state spins of all even-even nuclei, and gives some guidance through Nordheim's (1950) rules (as modified by Bernstein and Brennan (1960)) for the ground state spins of odd-odd nuclei. The so-called strong rule predicts that the spin of an odd-odd nucleus is $\left|j_p - j_n\right|$ if one of the combining nucleons has $\underline{\ell}$ and $\underline{s}$ parallel and the other has $\underline{\ell}$ and $\underline{s}$ antiparallel. The weak rule states that $j = \left|j_p - j_n\right|$ or $j_p + j_n$ in the case where both the combining nucleons have $\underline{\ell}$ and $\underline{s}$ parallel or both have $\underline{\ell}$ and $\underline{s}$ antiparallel.

Levels other than the ground state for nuclides with more than one particle outside a shell are formed by single particle excitations, pair excitations, or by the promotion of a particle from a filled shell to form a zero spin pair with the consequent creation of a hole in the filled shell.

The shell model explains the existence of the "islands of isomerism" in the regions where N or Z are between 39 and 49, 65 and 81, or 101 and 125. In these regions the model predicts the existence of high spin states in close proximity to low spin states of opposite parity. Thus, if the ground state of the nucleus is one of these states, a nearby excited state is likely to be the other one. The transitions between

them have large "L" values and long half-lives. For example, in elements with Z from 39 to 49, one is placing protons in either a $g_{9/2}(+)$ or a $p_{1/2}(-)$ configuration with almost the same stability. In this case one expects to find a pair of low-lying levels with spins 9/2+ and 1/2- and to observe transitions between them. In the case of $^{105}_{45}Rh_{60}$, the five $g_{9/2}$ protons couple to a 7/2+ spin and one finds a $1/2- \longrightarrow 7/2+$ E3 transition of energy 130 keV. The transition rate for this transition is at least a factor of ten slower than the single particle estimate; this is not unreasonable since a $p_{1/2} \longrightarrow (g_{9/2})^5_{7/2}$ transition is certainly not single particle in character.

The shell model can often make useful predictions of spin and parity changes for ground state beta transitions, but again, these tend to be qualitative rather than quantitative.

As a result of the interactions of nucleons in unfilled shells, a realistic model must include considerations of configuration mixing and a realistic treatment of the residual interaction to obtain any sort of agreement with experimental data concerning such things as excited level parameters. The residual interaction contains idealized nuclear forces (Wigner, Majorana, Heisenberg and Bartlett exchange terms) with adjustable parameters and a suitable radial dependence. Since the real description makes perturbation calculations difficult one uses this analytic form of the force with the introduction of other quantum numbers (seniority, isospin) for calculations of level parameters. An excellent account of how far shell model calculations can be carried has been given by de Shalit and Talmi (1963). The shell model cannot however give reliable results for wave function dependent quantities

such as transition probabilities and quadrupole and magnetic moments.

2.2 Collective Motions and the Unified Model

It is found experimentally that nuclei associated with partially filled shells tend to have large quadrupole moments, level structures characteristic of a rigid rotator, and electric quadrupole transition rates much faster than any single particle model can explain. The collective and unified models have been created to account for these phenomena. While these models were designed originally to describe nuclei with $150 < A < 190$ and $A > 223$, they have been found useful for light nuclei as well.

The nucleons outside a basically spherical core tend to deform the nuclear shape by polarization effects (Rainwater (1950)) and thus, speaking classically, move in their respective orbits under the influence of a slowly changing non-spherically symmetric potential. This collective deformation brings about two types of strongly coupled motions; the rotational or vibrational motion of the nucleus as a whole which causes variations in the orientation or shape of the nuclear field and the intrinsic motion of the nucleons which follow this slowly changing field adiabatically. For convenience rotational, vibrational and intrinsic motions can be separated and treated in much the same way as one deals with the diatomic molecule.

Bohr and Mottelson (1953) developed the collective theory from Rayleigh's (1877) calculations for surface oscillations of a continuous liquid drop. In this description the radius vector of the nuclear surface is described by the function

$$R(\theta,\varphi) = R_o \left[1 + \sum_{\lambda=0}^{\infty} \sum_{\mu=-\lambda}^{\lambda} \alpha_{\lambda\mu} Y_\lambda^\mu(\theta,\varphi)\right]$$

where R_o is the radius of the equilibrium spherical shape, (θ,φ) are the polar angles, and $Y_\lambda^\mu(\theta,\varphi)$ are spherical harmonics. Collective motion is expressed by allowing the coefficients $\alpha_{\lambda\mu}$ to be functions of time. Assuming that the nucleus is incompressible and can be described as an irrotational fluid, one obtains the following expressions for the potential energy, kinetic energy and oscillator frequencies

$$V = \tfrac{1}{2} \sum_{\lambda\mu} C_\lambda \left| \alpha_{\lambda\mu} \right|^2 \quad ; \quad T = \tfrac{1}{2} \sum_{\lambda\mu} B_\lambda \left| \dot{\alpha}_{\lambda\mu} \right|^2 \text{ and } \omega_\lambda = \left(\frac{C_\lambda}{B_\lambda}\right)^{\frac{1}{2}}$$

The energies of the collective states are given by $\sum_\lambda n_\lambda \hbar\omega_\lambda$ where n_λ is the number of phonons of order λ in the excited sate, λ is the total angular momentum of the phonon with parity $(-1)^\lambda$ while μ is the component of λ along a space fixed axis. Hence the states are $2\lambda + 1$ degenerate. Since ω_λ is a rapidly increasing function of λ, one need only consider small values of λ.

The λ=0 mode of vibration is only possible if one permits oscillations in density of nuclear matter; such oscillations would lead to states of very high excitation ($>$20 MeV) and do not concern us. The λ=1 phonon interaction is ignored because it simply represents a change in the position of the nuclear mass centre. The λ=2 term yields quadrupole oscillations which are the most important ones for low lying nuclear levels. For even-even nuclei the one phonon quadrupole oscillation leads to a low lying 2+ excited state, the two phonon oscillation produces three degenerate excited states (0 + 2 + and 4 +) at an energy of approximately twice that for the one phonon 2+ state. These degenerate states are usually separated by perturbation effects. Also since an octupole, λ=3, phonon has approximately the same energy as two λ=2

phonons, a 3-state can be found in the region of the 0+, 2+, 4+ triplet. There should be no cross-over transition from the two quadrupole phonon state to the ground state because two phonons have to be destroyed simultaneously. Such a transition may be observed, however, when there is some configuration mixing amongst the states. Since higher order vibrational states are mixed with particle states, their collective features are obscured. The picture described above works particularly well for nearly spherical nuclei, e.g. those with only a few particles (holes) in unfilled (filled) shells.

When there are a large number of particles outside a closed shell the nucleus is permanently deformed and the expansion of $R(\theta,\varphi)$ is more conveniently carried out about a permanently deformed shape. The description of the motion now resembles that of a rigid rotator and the existence of a rotational level structure becomes prominent.

In this formulation one uses β (a measure of the total deformation of the nucleus) and γ (a measure of the nuclear asymmetry) as parameters where $a_{20} = \beta \cos\gamma$ and $a_{22} = \frac{1}{\sqrt{2}} \beta \sin\gamma$. The $a_{2\mu}$ are coefficients similar to the $\alpha_{\lambda\mu}$ used previously. If γ is not a multiple of $\pi/3$ the nucleus will be asymmetric. Values of $\gamma=0$, $\frac{2\pi}{3}$ or $\frac{4\pi}{3}$ represent prolate spheroids while values of $\gamma = \frac{\pi}{3}$, π or $\frac{5\pi}{3}$ represent oblate spheroids. For an odd A nucleus the spin $\underline{j}$ (with projection Ω on the Z' axis) of the last unpaired particle couples with the rotational angular momentum $\underline{R}$ of the whole system to give a resultant nuclear spin $\underline{I}$ (with projection K on the Z' axis). These values are illustrated in the adjoining figure where $\underline{M}$ is the component of I in a fixed arbitrary direction and Z' is the symmetry axis. K and -K result

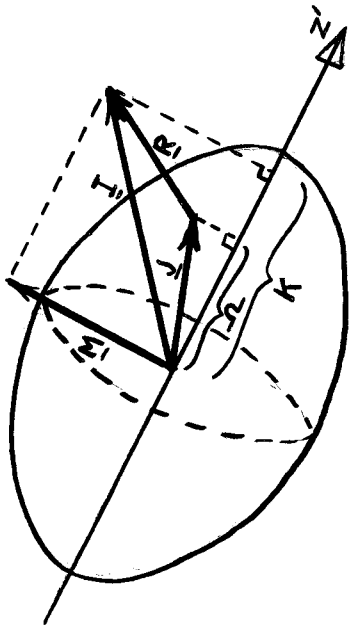

in degenerate states since this change only corresponds to a rotation of the nucleus in a different direction. Because there are no collective variations about the symmetry axis, K is a constant of the motion for a rotational band and $K = \Omega$. K also represents the intrinsic angular momentum. Carrying over the use of quadrupole $\lambda=2$ phonons as lowest excitations of vibrational spectra, one finds for a spheroidal equilibrium nuclear shape that the level spacings are given by $\frac{\hbar^2}{2\mathcal{J}}\left[I(I+1) - K^2\right]$ ($\mathcal{J}$ is the moment of inertia of the nucleus associated with the deformation). The spin sequence for a K = 0 band is 0+, 2+, 4+, 6+, etc. For K = 0, the odd I values are forbidden by symmetry considerations. For non-zero K however, I takes on the values I = K, K + 1, K + 2, etc.

A weak coupling between rotational modes of oscillation and vibrational modes of oscillation results in a correction to this energy level formula proportional to I^2. Here the energy of a state involving an intrinsic energy ϵ_K is given by

$$E_I = \epsilon_K + \frac{\hbar^2}{2\mathcal{J}}\left[I(I+1) - K^2\right] - B\, I^2(I+1)^2$$

It should be noted that just because a nucleus is spherical in its ground state, it does not mean that it has to be spherical in an excited state.

Rotational bands can be built up on collective vibrational states as well as on particle states. β vibrations are oscillations which preserve the symmetry axis of the nucleus but alter its eccentricity. Hence

they have no angular momentum about the symmetry axis and for this vibration K=0, I=0+, 2+, 4+ etc. Gamma vibrations, quadrupole in nature, cause the nucleus to lose its axial symmetry and in this case K = 2, I = 2+, 3+, 4+ etc. Octupole vibrations causing pear-shaped nuclei give rise to negative parity rotational bands since they are not symmetric vibrations. For K=0 the level sequence is I = 1-, 3-, 5-, etc. while for $K \neq 0$ the level sequence is I = K, K+1, etc.

Consideration of the coupling of the rotational motion with the intrinsic particle motion brings in a term proportional to the coupling of their angular momenta similar to the Coriolis force in classical mechanics. This Coriolis term can be neglected except where $K = \frac{1}{2}$ or when different single particle states are close in energy. Using "a" as the decoupling parameter the rotational particle coupling term is given by $\frac{\hbar^2}{2\mathcal{J}}\, a(-)^{I+\frac{1}{2}}\,(I+\frac{1}{2})$. While for $K \neq \frac{1}{2}$, the level sequence follows the normal order of spins, the decoupling term can completely destroy the normal spin sequence for a $K = \frac{1}{2}$ band. Combining this result with the rotational-vibrational interaction, the energy of a level is given by

$$E_{I,K} = \epsilon_K - \frac{\hbar^2}{2\mathcal{J}}\, K^2 + \frac{\hbar^2}{2\mathcal{J}}\left[I(I+1) + \delta_{K,\frac{1}{2}}\, a(-)^{I+\frac{1}{2}}(I+\tfrac{1}{2})\right]$$

$$- B\left[I(I+1) + \delta_{K,\frac{1}{2}}\, a(-)^{I+\frac{1}{2}}\,(I+\tfrac{1}{2})\right]^2$$

Because the Bohr and Mottelson model reveals the existence of distorted nuclei, it became clear that a non-spherically symmetric potential should have been used for shell model calculations in the deformed region. Nilsson (1955) extended the shell model by calculating the energies of the single particle levels in an anisotropic harmonic

oscillator potential. His results together with the collective model yield the so-called "unified model". In the non-spherical potential, the shell model levels lose their degeneracy and change in stability with the nuclear asymmetry. To the oscillator potential with the usual $\underline{\ell}\cdot\underline{s}$ term included Nilsson added a term proportional to $\underline{\ell}^2$ and a deformation parameter β in such a way that the shell model states would still be retained for zero deformation. Since the K degeneracy has not been removed in the Nilsson calculation one can put two nucleons in each Nilsson state. If the deformation is small, the single particle states are simultaneous eigenstates of N, ℓ, j and Ω where N is the total number of oscillator quanta. As the deformation increases, ℓ and j cease to be good quantum numbers and states of the same Ω are distinguished by the asymptotic quantum numbers $[N, n_3, \Lambda]$ (Alaga (1955)) where n_3 is the number of oscillator quanta along the symmetry axis and Λ is the projection of the orbital angular momentum on this axis. These asymptotic quantum numbers characterize the state in the limit of infinite deformation but are not good quantum numbers for finite distortions. Single particle wave functions are given by $\psi_{a\Omega} = \Sigma\, a_{\ell\Lambda} \mid N\ell\Lambda\Sigma\rangle$ where $\Sigma = \pm\frac{1}{2}$ and $\Lambda + \Sigma = \Omega$. Values of $a_{\ell\Lambda}$ have been tabulated by Nilsson (1955, 1959) in extensive tables.

The order of filling of Nilsson levels (two to a level) is clearly indicated by his charts and it is a simple matter to decide which level must be the ground state for any odd A nucleus. For given A, the Nilsson level representing this state is a function of β. Excited states are produced by promoting the odd particle to higher energy levels, by breaking a pair in a lower energy state and pairing

one of the members with the odd particle or by promoting a pair of particles to a higher energy state. Alaga (1955, 1957) has listed selection rules for the N, n_3, Λ and K. It is found that transition rates are faster between members of a band than between particle states because of the collective motions in the band.

The equilibrium shape of a nucleus of given A can be obtained by adding up the energies for all the filled single particle states for a series of β values and then plotting the total energy as a function of β. The equilibrium distortion corresponds to the minimum in this total energy versus β curve. Deformation parameters obtained by this method agree well with deformations predicted from experimental electric quadrupole moments.

CHAPTER III

INSTRUMENTATION AND TECHNIQUE

INTRODUCTION

In order to build up a level structure of a nuclide, knowledge of transitions between the nuclear states is a necessity. The energy of the transitions associated with radioactive decay can be determined from the energy the radiations lose when interacting with suitable materials or, in the case of charged particles, by the deflection they experience in a magnetic field. For complex level systems it is not enough to obtain transition energies; additional information such as time related events may also be needed to give a unique solution.

This chapter deals not only with the type of instruments used in the study of the decay of ^{105}Ru but also with the methods of reduction of the experimental data. Each of the instruments used will be described in turn.

3.1 The Siegbahn $\pi\sqrt{2}$ Spectrometer

The Siegbahn spectrometer, illustrated in Figure 1, is a "flat-type" magnetic spectrometer. The term "flat" is used because the electrons travel essentially in a plane perpendicular to the magnetic field lines. The magnetic field, B, necessary to make an electron travel in an orbit of radius ρ, is given by $B\rho = \frac{mv}{e}$. Since the radius of the instrument is fixed, the magnetic field determines the momentum of the electrons focused at the detector. For a uniform magnetic field the electrons experience one dimensional focusing at a deflection angle of 180°. By shaping the pole faces, it is possible

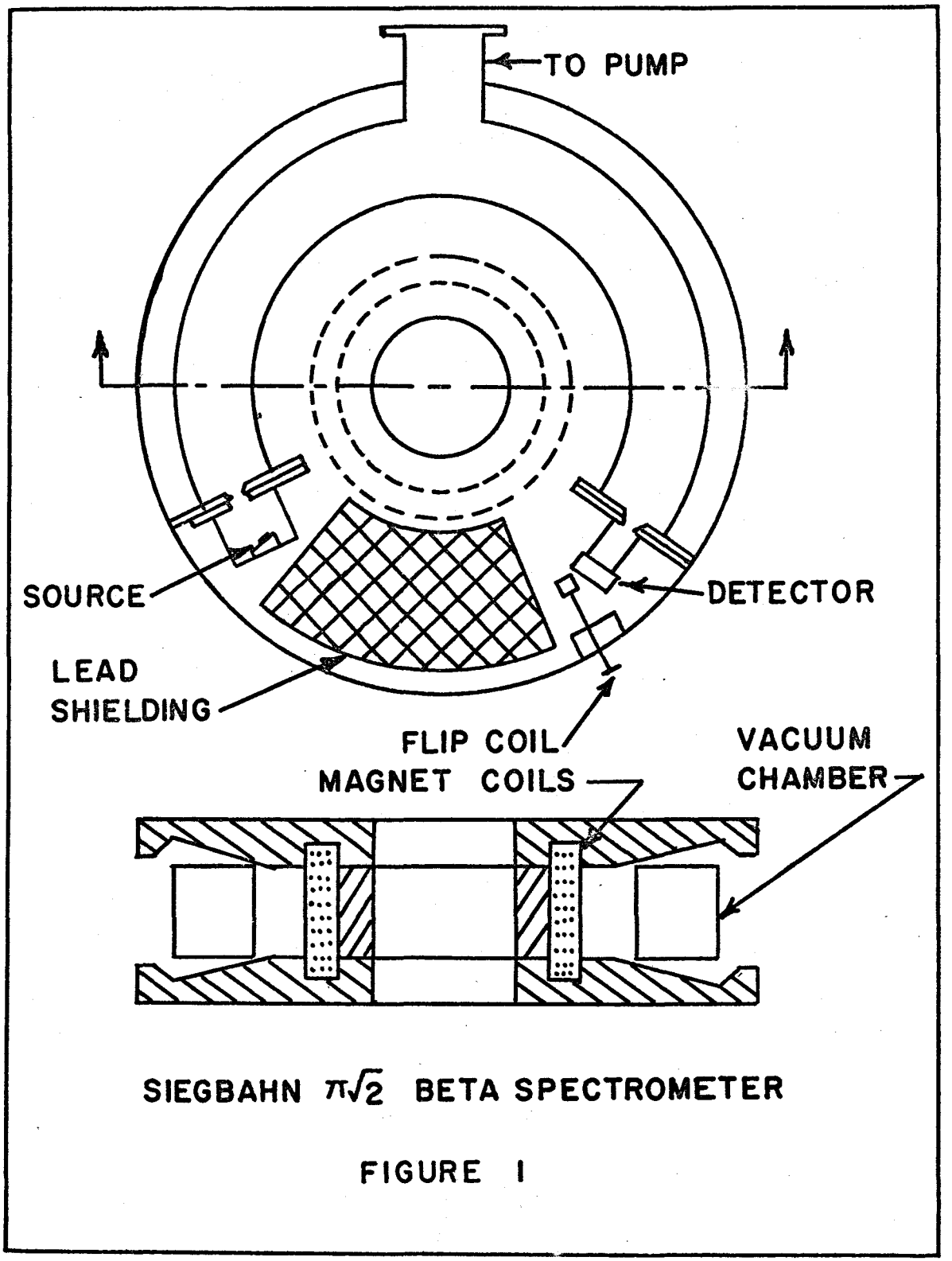

SIEGBAHN $\pi\sqrt{2}$ BETA SPECTROMETER

FIGURE 1

to attain two dimensional focusing with a consequent gain in transmission. The field shape in the Siegbahn instrument gives this focusing at a deflection angle of $\pi\sqrt{2}$ radians. In this sense the instrument is known as a double focusing magnetic spectrometer. The construction of this instrument, based on a concept of Siegbahn and Svartholm (1946), has been described by Johns et al (1953).

The spectrometer pole faces are constructed of Armco iron shaped to give a field which falls off radially as $1/\sqrt{r}$ over the region of interest. The magnet coils consist of eight sections totalling 10,000 turns of No. 18 Formex wire and are energized by a power supply delivering 800 ma at 750 volts with a current stability of 0.01%. The aluminum vacuum chamber fits between the pole faces and is closed at both ends with sliding brass plates. These plates allow one to change either sources or detectors without disturbing the vacuum in the main part of the chamber. The pressure in the chamber is maintained of the order of 0.1 to 1 microns by a 100 liters per second oil diffusion pump and forepump assembly.

The magnetic field is determined by a search coil which can be flipped through 180°. The charge set in motion by this process is measured by a Leeds and Northrup type R galvanometer. The deflection of the galvanometer is observed on a 100 cm. scale placed 2 meters from the galvanometer, and permits the field measurement to be made with an accuracy of 0.1%.

Sources are introduced into the spectrometer by a vacuum tight source holder attached to the sliding brass plate. For external conversion measurements, the source holder consisted of a steel cylinder which

served as a vacuum seal, a beta stopper, and the support for the high Z radiator foil. This made it possible to change gamma sources without disturbing the vacuum.

The detector assembly consists of an anthracene crystal optically coupled to a Dumont 6291 photomultiplier by the use of Dow Corning 200 Silicon Fluid. Anthracene crystals of dimensions 2.5 cm. by 1 cm. and either 0.2 or 0.4 cm. thick were used. The thicker crystal, which was used for detecting conversion electrons greater than approximately 500 keV, had a lucite coating to protect the anthracene from subliming in the vacuum. Electrons passing through the anthracene crystal create fluorescent radiation which is transmitted to the photocathode of the photomultiplier. The photo-electrons from the photocathode are amplified by the dynode structure to give a voltage pulse proportional to the electron energy. A lower level discriminator permits one to reject noise pulses. The output pulses were amplified, shaped and fed to an appropriate scaler.

3.1.1 The Analysis of the Beta Spectra

The method of preparing beta sources is described in Chapter IV. The source and the detector positions for best transmission were determined by measuring the counting rate as a function of the radial distances of the source and detector from the axis of the instrument. In this manner the rectangular 2.0 cm x 0.5 cm beta sources were accurately placed in the spectrometer. The beta spectra were obtained by determining the counting rate as a function of the momentum of the focussed electrons.

The response function for monoergic electrons is a peak with a

resolution , $\Delta p/p$, where Δp is the full width of the peak at half maximum height and p is the momentum corresponding to the peak position. The resolution is a function of the source and detector widths and the aberrations of the "flat" lens. In these experiments, the resolution was 0.49%. The effective solid angle or transmission of the instrument was approximately 0.2%.

If one assumes 100% detection efficiency for detecting focused electrons, the count rate, N, for the spectrometer set to focus electrons of momentum p will be

$$N(p) = \int_0^\infty N_o \, \omega \, \varphi(q) \, g(p,q) dq \qquad 3.1$$

where N_o is the source strength, ω is the transmission of the instrument, $\varphi(q)$ is the probability that an emitted electron will have a momentum q and $g(p,q)$ is the probability that an electron of momentum q will be detected when the instrument is set to focus a momentum p. Since the emitted electron must have some momentum,

$$\int_0^\infty \varphi(q) dq = 1 \qquad 3.2$$

The function $g(p,q)$ is an expression for the resolution of the instrument, and hence vanishes except when q is within a few percent of p. As long as the magnetic field shape remains constant for all momenta, the expression $g(p,q)$ will be proportional to $Z = q/p$. Under these conditions

$$\int_0^\infty g(p,q) dq = p \int_0^\infty g(p,z) dz = \eta p \qquad 3.3$$

where η is a constant. For the $\pi\sqrt{2}$ spectrometer η is independent of

p except for very low energy electrons. In equation 3.1 replacing $\varphi(q)$ by $\varphi(p)$ since $p \simeq q$ for the range in which $g(p,q) \neq 0$ and assuming that $\varphi(p)$ varies very slowly with p we obtain from equation 3.1 using equation 3.3 that

$$N(p) = N_o \varphi(p)\, \omega \eta p \qquad 3.4$$

The area under the graph of N/p versus p gives

$$\int_0^\infty \frac{N(p)}{p}\, dp = N_o \eta\, \omega$$

using equations 3.2 and 3.4. This area is simply related to the source strength by the fixed parameters of the spectrometer, η and ω.

3.1.2 The Analysis of the Internal Conversion Spectra

Because of the finite resolution of the spectrometer, a conversion electron group of momentum p will be recorded as a peak, described by the function g(p,q). The flip reading corresponding to the peak position is used to calculate the momentum of the conversion line. The instrument was calibrated by using conversion lines of known energy, such as the 411.795 ± 0.003 keV line of ^{198}Au or well known lines in the source itself.

If the transition probability for the i^{th} gamma ray in the decay of a nucleus is δ_i and if the probability for internal conversion in the ℓ^{th} electron shell for this transition is $\alpha_{i\ell}$, then the number of conversion electrons emitted per second will be $N_o \delta_i \alpha_{i\ell}$. The counting rate observed, when the spectrometer is set to focus a momentum p, due to the electrons of momentum q will be $N_{i\ell}(p) = N_o\, \delta_i\, \alpha_{i\ell}\, \omega\, g(p,q)$.

The area under the peak in a N/p versus p plot will be

$$\int_0^\infty \frac{N_{i\ell}(p)}{p}\, dp = N_o \delta_i \alpha_{i\ell} \omega \int_0^\infty \frac{g(p,q)}{p}\, dp \quad \text{or} \quad N_o \delta_i \alpha_{i\ell}\, \omega \eta$$

The intensity of a conversion line is the ratio of the area under the conversion peak to the area of the total beta spectrum. In terms of the above analysis, the intensity is $\alpha_{i\ell}\delta_i$; thus, if δ_i is known, a measurement of the conversion line area will yield $\alpha_{i\ell}$.

If the internal conversion coefficient of one line is known, one can determine the conversion coefficients of other lines in the spectrum without using the area of the beta continuum. The relevant equation is

$$\frac{N_{i\ell}}{N_{j\ell}} = \frac{N_o\ \delta_i\ \alpha_{i\ell}\ \omega\eta}{N_o\ \delta_j\ \alpha_{j\ell}\ \omega\eta} = \frac{\delta_i\alpha_{i\ell}}{\delta_j\alpha_{j\ell}}$$

Since, in this case η cancels out, one can simply compare peak heights and obtain $\alpha_{j\ell}$ directly, as follows.

$$\alpha_{j\ell} = \alpha_{i\ell}\ \frac{\delta_i\ P_{j\ell}}{\delta_j\ P_{i\ell}}$$

In the same manner one can obtain K/L or $L_1/L_2/L_3$ ratios.

3.1.3 The Analysis of the External Conversion Spectra

Gamma ray energies and intensities can be determined with a magnetic spectrometer by the use of the external conversion process. In this process the photoelectrons produced by the photoelectric interactions of gamma rays upon suitably thin radiators are focused on the detector. The radiator should be of a high Z material so that the photoelectric interaction cross-section will be large, and should be thin enough to avoid electron straggling in the radiator itself. The foils used in this experiment were 3 cm. in length by 0.8 cm. wide, composed of Sb (1.8 mg/cm^2) Au (3.6, 6 mg/cm^2) and U (6 mg/cm^2).

External conversion peaks from γ_i will appear in the spectrum at energies $E_i - B_j$ where B_j is the binding energy of the j^{th} shell of the radiator material.

The measurement of the energy of a peak is obtained from the flip coil measurement corresponding to the inflection point of the high energy side of the peak. The inflection point is used in preference to the highest part of the peak because it is less sensitive to radiator thickness. The instrument was calibrated for each radiator, using the well known gamma rays of ^{198}Au, ^{192}Ir, and ^{60}Co as standards.

The measurement of relative photon intensities was obtained using the semi-empirical expression

$$I_\gamma = \frac{k\ n}{\tau p\beta^3} \sqrt{C^2 + (Rp\beta^3/t)^2} \qquad 3.5$$

where k is an instrumental constant, n is the height of the peak, τ is the photoelectric cross-section for the radiator, p is the electron momentum, β is v/c for the electrons, R is the instrumental resolution, t is the thickness of the radiator and C is a function of β and t related to the stopping power of electrons in the radiator material. Empirical curves for $\left[C^2+(Rp\beta^3/t)^2\right]^{\frac{1}{2}}$ for the Au and U radiators used in these experiments were determined by Artna (1961) and by Stavely (1961) and were used with equation 3.5 to obtain relative values of I_γ.

3.2 The Scintillation Spectrometer

The most efficient means of detecting gamma rays is by the use of NaI(Tℓ) scintillation detectors. The NaI(Tℓ) detector is widely used because it has a high photoelectric absorption cross-section, a

high density, a response function nearly linear with energy, and is readily available in large crystals. Gamma rays are absorbed in such a crystal by the processes described in Chapter I. The absorbed energy produces fluorescent radiation which falls on the photocathode of the photomultiplier optically coupled to the crystal. The electrons are multiplied by the dynode chain to yield a pulse of current which is proportional to the number of light quanta that struck the photocathode. This pulse is amplified by a charge sensitive preamplifier. Since the electronic pulses from the preamplifier are not usually of a suitable height or suitable shape for analysis, they are fed to a linear amplifier and then to a pulse height analyzer.

The production of the fluorescent radiation and subsequent electron multiplication are governed by probability processes which lead to a pulse distribution corresponding to the full absorption of the gamma ray instead of the delta function response of an "ideal" detector. Typical resolutions for the ^{137}Cs peak are of the order of 8%; the best crystal available had a resolution of 7.1%.

The NaI(Tℓ) spectra of the ^{137}Cs gamma ray are shown in Fig. 2 for conditions of good or bad geometry. Both of these show the characteristic full energy peak, and a Compton distribution extending from zero energy up to the base of this peak. This distribution arises from events in which the Compton scattered radiation escapes from the detector . The peak at about channel 60 in the case of "good geometry" is caused by radiation Compton-scattered from material around the detector or source. Small angle scattering has filled the valley between the photopeak and Compton for the case of "poor geometry" typical of that

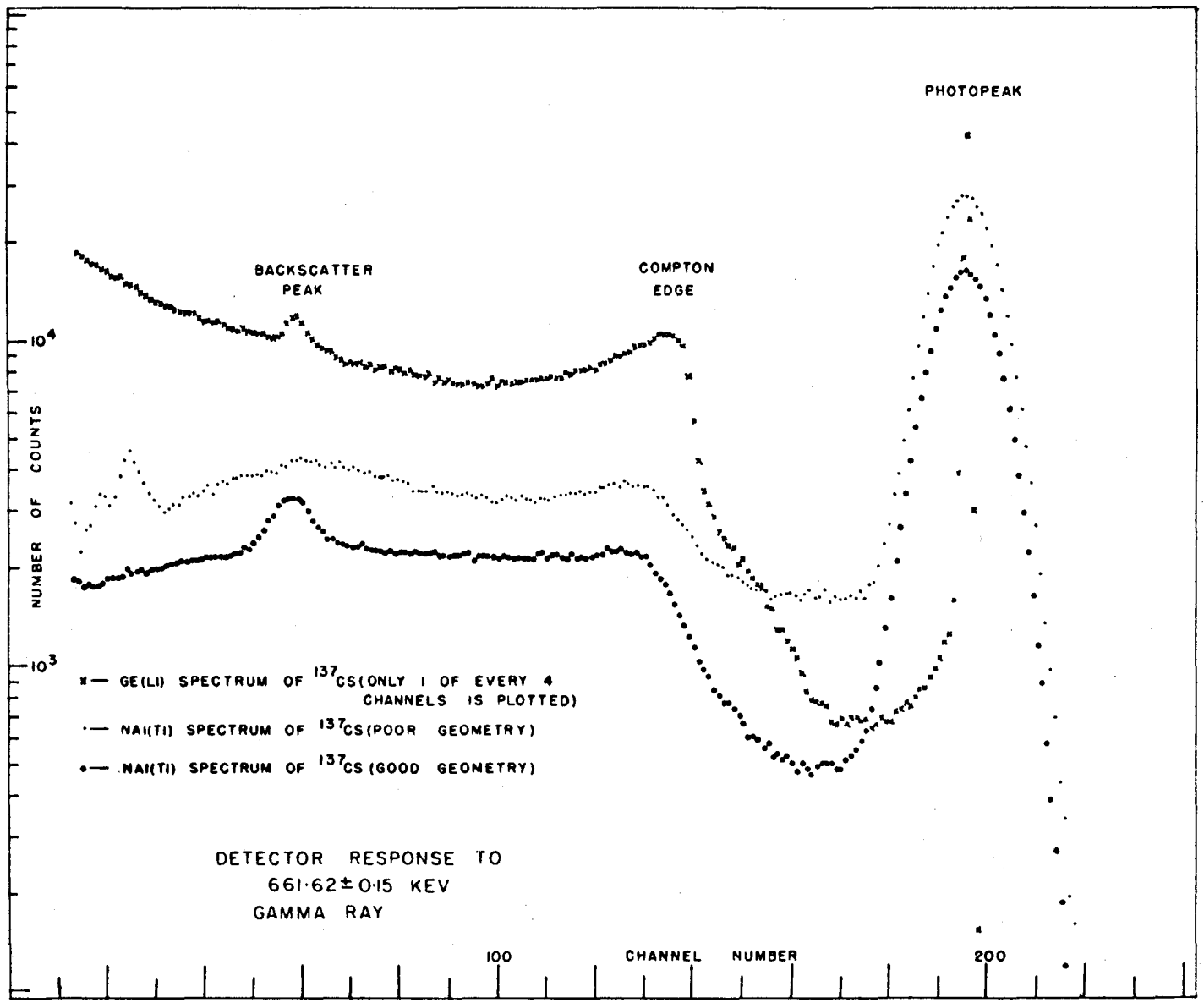
PHOTOPEAK
BACKSCATTER PEAK
COMPTON EDGE
10^4
10^3
NUMBER OF COUNTS
GE(LI) SPECTRUM OF ^{137}CS(ONLY 1 OF EVERY 4 CHANNELS IS PLOTTED)
NAI(TI) SPECTRUM OF ^{137}CS(POOR GEOMETRY)
NAI(TI) SPECTRUM OF ^{137}CS (GOOD GEOMETRY)
DETECTOR RESPONSE TO
661·62 ± 0·15 KEV
GAMMA RAY
100
CHANNEL NUMBER
200

FIGURE 2

within the Gerholm spectrometer. For gamma rays above one MeV the pair production cross-section can lead to first and second escape peaks at energies $E - m_o c^2$ and $E - 2m_o c^2$, respectively. These were unimportant in the present study.

The spectrometer was calibrated by using gamma rays of known energy from a number of "standard sources". The relative intensities of the gamma rays were determined by using the efficiency curves published by Heath (1957) and the total areas under the gamma ray response functions.

The 3" x 3" NaI(Tℓ) crystals used in this investigation were optically coupled to Dumond 6363 photomultipliers. The combined assemblies were selected for minimum gain shift with count rate and for good resolution. The detectors were shielded from beta rays by a lucite disc 1 cm. in thickness. The preamplifier and amplifier were of the Chase design (1960), in which a bipolar output pulse with equal positive and negative portions is produced. These pulses were fed into a 512 channel analyzer to record the entire spectrum at once.

In the spectra obtained from a scintillation spectrometer, one can observe coincidence summing and random summing effects as well as the true singles spectra. The coincidence summing distribution is due to the acceptance of two or more time related events by the detection system and the random summing contribution arises from summing between events which are not truly time related but just happen to sum within the resolving time of the system. Methods of removing these contributions are discussed by Kennett and Prestwich (1964). Under the conditions of the present experiments, neither of these effects seriously distorted the data.

3.2.1 The Analysis of the Singles Scintillation Spectra

As has been mentioned, the response to a gamma ray is not a simple function but has a complicated spectral distribution. The first step in the analysis of a spectrum involving many gamma rays is the determination of the response function (line shape) of each of the components of the spectrum. These line shapes must be obtained in the geometry of the experiment and from sources of monoergic gamma rays with as nearly the same physical dimensions as the unknown source whose spectrum is to be analyzed. In practice, one cannot find sources of monoergic radiations corresponding to the gamma rays required in the analysis and must resort to interpolation using such sources as are available. In this study, line shapes were obtained from the following sources, the energy of the transition in keV being shown in brackets:

^{60}Co (58.7 ± 0.7), ^{141}Ce (145.5 ± 0.4), ^{203}Hg (279.12 ± 0.05), ^{198}Au (411.795 ± 0.009), ^{64}Cu (511.0003 ± 0.005), ^{137}Cs (661.62 ± 0.15), ^{54}Mn (835.0 ± 0.3), ^{46}Sc (892 ± 3 by coincidence studies with the 1118 ± 3 photopeak), ^{65}Zn (1115.6 ± 0.4), ^{60}Co (1173.226 ± 0.040 by coincidence studies with the 1332.483 ± 0.046 photopeak) ^{22}Na (1274.6 ± 0.3), ^{24}Na (1368.526 ± 0.044), ^{42}K (1520 ± 10) ^{52}V (1434.2 ± 0.5), ^{28}Al (1794 ± 10) and ^{51}Cr (319.8 ± 0.3). The energies quoted are from the literature (Marion (1960), Robinson et al (1964), Murray et al (1964) and Nuclear Data Sheets (1966)).

The measured spectrum $\overrightarrow{M(i)}$ may be thought of as an "n" component vector whose component M(i) represents the number of counts in channel "i". In the same way $\overrightarrow{S(j)}$ is the vector whose "j^{th}" com-

ponent represents the total number of counts in the measured spectrum due to the "j^{th}" gamma ray. The two vectors are connected by means of the equation

$$\overrightarrow{M(i)} = R(i,j) \times \overrightarrow{S(j)} \qquad 3.6$$

where R(i,j) is the response matrix which expresses the contribution of each component "j" to each channel "i" of the spectrum. The components of the vector $\overrightarrow{S(j)}$ can be obtained by solving the equation

$$\overrightarrow{M(i)} \times R(i,j)^{-1} = \overrightarrow{S(j)} \qquad 3.7$$

where $R(i,j)^{-1}$ is the inverse matrix. One method of solving the problem is to invert the matrix R(i,j).

A less elegant method of solving equation 3.6 which has been used considerably involves using the equation as it stands and expressing the response matrix explicitly in the form of line shapes $\overrightarrow{L_j(i)}$. If the number of counts in each line shape is normalized to unity the response function $\overrightarrow{L_j(i)}$ satisfies the equation

$$\sum_{i=1}^{n} L_j(i) = 1$$

Then one can write

$$M(i) = \sum_{j=1}^{m} S(j)\, L_j(i)$$

where m is the total number of gamma rays. Since $m < n$ we have an overdetermined set of n linear equations. In this approach, the S(j)'s are determined by a graphical method; successively "stripping" or "peeling" gamma ray components from the total spectrum. First one adjusts the amplitude of the highest energy line shape to fit the highest energy photo peak in the data and then subtracts its contribution from the spectrum. The residual spectrum is re-

analyzed in the same way and the process repeated until all the components have been determined. Using this method, the "stripper" can put in his "biased feelings" since he is controlling the process. However, the errors are cumulative and the method inevitably misses weak peaks.

An alternative method for obtaining the components of $\overrightarrow{S(j)}$ is to solve equation 3.7, applying a weighted non-linear least squares analysis to it. Using this method one solves for all the components of $\overrightarrow{S(j)}$ simultaneously. One makes first guesses at the energies and intensities of the components which are subsequently corrected by a least squares iterative procedure. This method has the advantages that it removes the "stripper's" bias, it leads to intensity values with least squares errors attached, and it yields a goodness of fit parameter, χ^2. Moreover, by making use of the computer, it avoids the tedious and time consuming labor of the stripping method.

Both methods are limited in precision by errors in the line shapes. For the hand stripping method the line shapes are graphically interpolated from the standard lines. For the computer based method, each standard line shape is expressed in a mathematical form by means of a Gaussian which represents the photopeak and a series of Fourier coefficients which describe the Compton distribution. The line shapes for the gamma ray energies of interest are then calculated from curves fit to the coefficients (Kitching (1966)). The method has been described in detail by Heath (1962) and will not be discussed further here.

3.3 The Solid State Spectrometer

The development of the solid state Ge(Li) detector has made possible simple, high resolution studies of gamma ray spectra (Freck and Wakefield (1962), Tavendale and Ewan (1963)). At present, using this type of spectrometer, one can achieve a resolution of approximately 0.3% for the ^{137}Cs gamma ray. The best detector used in this work produced the ^{137}Cs peak, shown in Fig. 2, with a full width at half maximum of 2.2 keV as compared to the 7.1% resolution obtained with the NaI(Tℓ) detector. Because large crystals are not obtainable, the detection efficiency is not as good as that of NaI(Tℓ) crystals. The advantages of the Ge(Li) detectors are their excellent resolution and their strictly linear relationship between output pulse height and gamma ray energy. They are somewhat inconvenient to use since they must be kept at liquid nitrogen temperatures. Moreover, at the present time these detectors have a relatively short useful lifetime.

The Ge(Li) detector is produced from a block of high grade p-type germanium. One face of the block is coated with lithium which is diffused in at high temperatures to make an n type region near this face. The lithium is then drifted inward to create a large "depletion depth" which is intrinsic in character. Detectors may be made in a variety of shapes and sizes, with depletion volumes ranging up to 30 cc.

The depletion layer acts like an ionization chamber in which electron-hole pairs created by the gamma ray are swept out to the n and p terminals by an applied reverse bias. Electron-hole pairs may

be lost by recombination or by trapping of the carriers at imperfection centers in the crystal. Since these crystals are semiconductors, large leakage currents will flow unless the detector is kept cold. Moreover, the lithium will drift and alter the depletion layer if the detector is not kept at a low temperature.

The number of electron-hole pairs produced is proportional to the energy imparted to the detector. The average energy required to produce an electron-hole pair in Ge is 2.85 eV (Ewan and Tavendale (1964)) and hence the absorption of a 1 MeV photon in the crystal will result in 3.5×10^5 pairs. Assuming that the number of pairs produced has a Gaussian distribution associated with it, the statistical fluctuation will be approximately 6×10^2 pairs. Stated differently, a 1 MeV photopeak should have a FWHM (full width at half maximum) of 1.8 keV. Fano (1947) has shown that for the case where the total energy of the radiation is absorbed in the detector, it is not entirely correct to treat the production of electron-hole pairs as a sequence of independent events since exactly the same total energy is given up to the crystal. As a result, the distribution in the number of electron-hole pairs is no longer strictly Gaussian and the mean square deviation of the number of pairs should be reduced by the Fano factor, F. The value of F is not known very well at present but it appears that the limiting resolution for a 1 MeV gamma ray could be as low as 0.5 keV.

Increasing the field on the detector reduces the possibility of recombination and trapping and therefore improves the resolution of the instrument. Also the charge collection time is shortened.

However since noise is due to fluctuations in reverse current and this increases with increasing field, an optimum field exists for best performance of the detector.

The best system used in this investigation consisted of a combined assembly (Nuclear Diodes) of a Ge(Li) detector of 1.5 $cm.^2$ area by 0.4 cm. thick depletion region coupled to a cooled field-effect transistor which provided the first stage of a Tennelec field-effect preamplifier. Further amplification was achieved using a Tennelec TC200 amplifier which fed a multichannel analyzer. All the detectors used for singles spectra were of the planar type.

3.3.1 The Analysis of the Singles Solid State Spectra

The energies of the stronger gamma rays were obtained from composite sources of ^{105}Ru and various standards. These stronger gamma rays were then used as internal standards to determine the energies of the weaker ^{105}Ru photons. The nonlinearities of the 1024 and 512 channel analyzers were obtained by using a pulse generator and by the use of a mixture of calibration sources. In addition to the sources listed in section 3.2.1, ^{207}Bi (569.5 $\pm$ 0.2, 1063.7 $\pm$ 0.2 and 1772.2 $\pm$ 2.5 keV) was used in this work.

In order to determine the relative intensities of the gamma rays in the spectrum, it was necessary to measure the efficiency of the Ge(Li) detector as a function of energy. This was done by comparing its efficiency with that of a NaI(Tℓ) detector whose efficiency as a function of energy has been tabulated by Heath (1957) and confirmed by experiments carried out in this laboratory and elsewhere. Spectra of calibration lines were taken with both detectors,

in standard geometries appropriate to the two. It can easily be shown that the efficiency associated with the peak area of the Ge(Li) detector for the K^{th} gamma ray is given by

$$\epsilon_{GK} = \frac{N_{GK}}{N_{NK}} \cdot \frac{(\epsilon\omega)_{NK}}{\omega} \cdot \frac{T_{NK}}{T_{GK}} \cdot (P/T)_{NK}$$

where N_{GK} and N_{NK} are the number of counts recorded in the photopeak of the germanium and NaI(Tℓ) spectra in times T_{GK} and T_{NK} respectively, $(\epsilon\omega)_{NK}$ is the solid angle plus efficiency taken from Heath's tabulation and ω is the solid angle subtended by the germanium detector at the source, and $(P/T)_{NK}$ is the photopeak to total spectrum ratio for the NaI(Tℓ) detector.

Alternatively, one may obtain the desired efficiency curve by using a single source such as ^{207}Bi emitting several lines whose relative intensities are known, and plotting the relative efficiencies using the theoretical photoelectric cross-sections for Ge(Storm et al (1958)) as a guide.

3.4 The Gamma-Gamma Coincidence Spectrometers

The γ-γ coincidence measurements were carried out with a two dimensional analyser (32 by 32 channels) while the β-γ measurements were performed with a 512 channel analyzer. A block diagram of the coincidence circuit as used for the γ-γ work is shown in Fig. 3. Two NaI(Tℓ) crystals, mounted in the geometry shown in the figure and shielded from each other by a lead plate, were used as detectors. The pulses from the detectors were amplified and transformed into bipolar pulses. Each of the double-delay-line amplifier units produced a broad flat-topped bipolar output pulse whose height could be

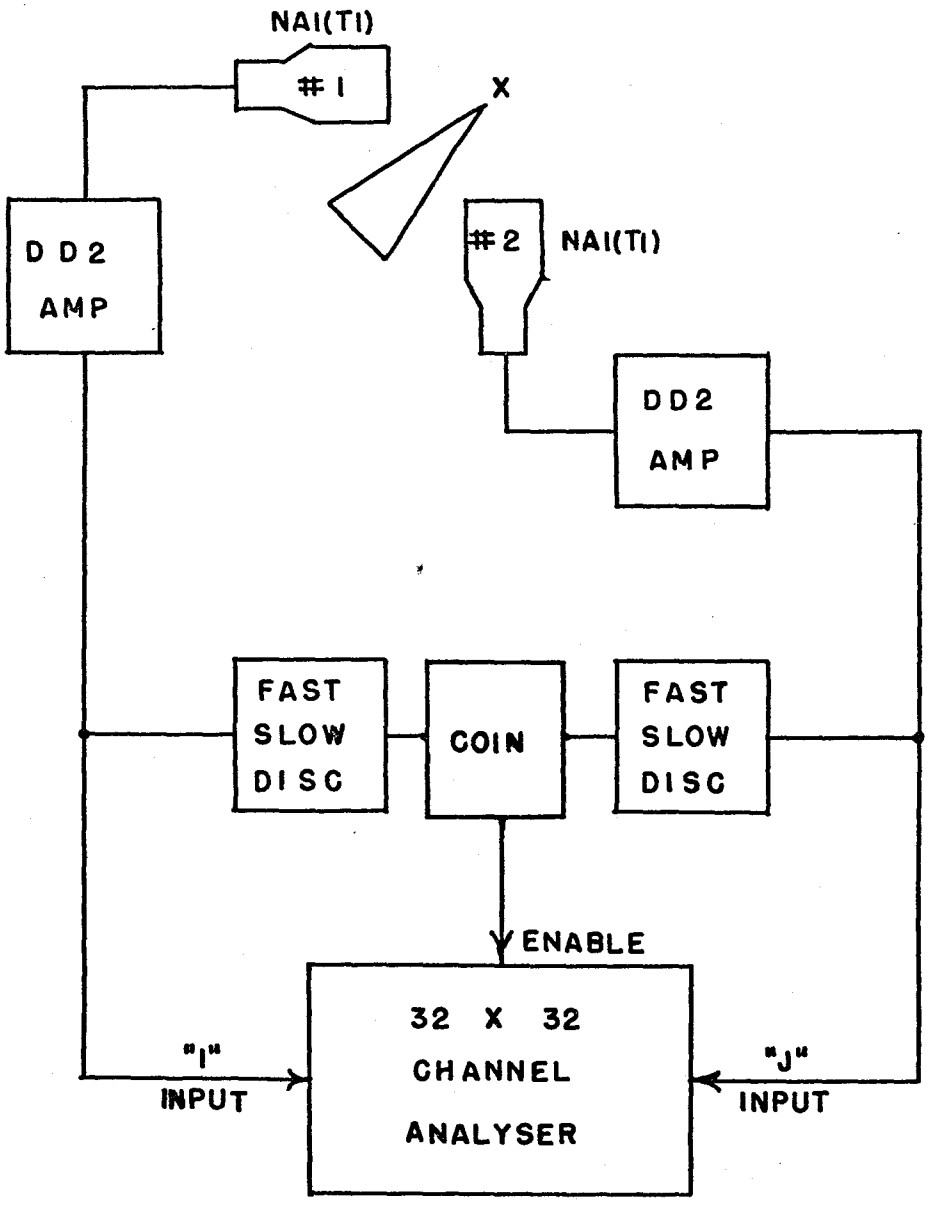

TWO DIMENSIONAL
COINCIDENCE SPECTROMETER
USING NAI(TI)— NAI(TI)

FIGURE 3

used as a measure of the gamma ray energy. The fast-slow discriminator output consisted of a "fast" marker pulse derived from the crossover point of the bipolar pulse and a slow "logic" pulse which only appeared if the input pulse height fell within the lower and upper levels of the discriminator. In order to preserve a constant coincidence efficiency, it was important that the time interval between the arrival of a gamma ray at the detector and the production of the timing pulse should be independent of gamma ray energy. For the experiments described here, the "walk" in the timing marker was found to be negligible for pulses between 0.2 and 8 volts (the maximum possible output from the DD2 amplifier) when the coincidence unit was set to a resolving time of approximately 40 nanoseconds. The effect of the "walk" in the timing marker was examined by observing the 892 keV-1118 keV coincidence spectrum of ^{46}Sc with the gate in one fast-slow discriminator set on the 1118 keV photopeak. Any change in coincidence efficiency as a function of energy would then reveal itself through a distortion of the coincidence spectrum of the 892 keV transition. The slow logic pulses were not needed for experiments involving the two dimensional analyser but were used in other experiments to be described.

The fast pulses from the two discriminators were fed to a coincidence circuit which would send a logic pulse to the analyzer whenever two pulses arrived within the resolving time of the circuit. This logic pulse enabled the analyzer to accept the pair of coincident pulses arriving from the two detectors and stored the event in the

matrix position (i,j) where channel i was proportional to the pulse height from crystal 1 and channel j was proportional to the pulse height received from crystal 2. Thus the analyzer stored information, in the form of a matrix, concerning all the coincident events recorded by the two detectors during the course of the experiment. Included in these events were chance coincidences which were due to the finite resolving time of the coincident circuit. It can be shown that the ratio of the number of chance events to the number of true coincidences is given by $2\tau N_o$; this indicates that for a given value of the resolving time, τ, there is an upper usable limit for the source strength. In these experiments, the sources used were sufficiently weak that $2\tau N_o$ was less than 0.1.

As has already been pointed out, the spectrum can be distorted by random or coincidence summing in either of the detectors. The effect of this process on the data is to transfer events from a position (i,j) in the matrix to location (i + k, j + l) where k and l are related in a rather complicated fashion to the strong gamma rays found in the spectrum. The number of events misplaced in this manner was very small under the conditions of these experiments, but the possibility of weak effects being due to this process was kept in mind in interpreting the data.

3.4.1 The Analysis of the Coincidence Data Using Two NaI(Tℓ) Detectors

In order to display all the γ-γ coincidence data from the NaI(Tℓ) detectors on a single two dimensional grid for a nucleus like ^{105}Ru, an analyzer with a 56 x 56 channel capacity was required. Since the instrument available had a capacity of 32 x 32 channels,

it was necessary to carry out the experiment four times, once for each of the four quadrants of a 56 x 56 channel grid.

The number of counts recorded in position (i,j) is given by

$$M(i,j) = \sum_{m=1}^{A} \sum_{n=1}^{A} B_{mn} L_m(i) L_n(j)$$

where A is the total number of gamma rays in the spectrum; B_{mn} is the number of recorded coincidences between gamma rays m and n, and $L_m(i)$ and $L_n(j)$ are the i and j components of the vectors which represent the line shapes of the m^{th} and n^{th} gamma rays.

The reduction of the matrix to coupling coefficients between pairs of gamma rays was carried out by the hand stripping technique. Since each row or column of the matrix represents the spectrum in coincidence with a "one-channel" gate set on the output of the other detector, the result of stripping in the i-direction is to reduce the problem to a set of m equations of the form

$$M_m'(j) = \sum_{n=1}^{A} B_{mn} L_n(j)$$

where $M_m'(j)$ represents the number of counts in channel j belonging to coincidences with the m^{th} gamma ray. Further stripping of this data along the j direction results in the coefficients B_{mn}. If the apparatus was working satisfactorily and if the data had been reduced satisfactorily, the coefficients B_{mn} should form a symmetric matrix, since B_{mn} must be equal to B_{nm}.

The B_{mn} coefficients may be used to obtain the coincidence probabilities δ_{mn} through the equation

$$B_{mn} = N_o \delta_{mn} (\varepsilon\omega)_m (\varepsilon\omega)_n$$

where N_o is the total number of radiations emitted by the source, and $(\varepsilon\omega)_m$ and $(\varepsilon\omega)_n$ are the respective solid angle and efficiency factors for the two crystals. Since the value of N_o could be easily found from a singles run taken in either the i or j dimension of the analyzer, and since the efficiency factors were known from Heath's tables (1957), the values of δ_{mn} are readily obtained from this equation.

3.4.2 The NaI(Tℓ) - Ge(Li) Detector Coincidence Experiment

Despite the very low efficiency of the Germanium detector, it was possible to carry out a γ-γ coincidence experiment using a 10 c.c. coaxial type Ge(Li) detector in coincidence with a standard 3" x 3" NaI(Tℓ) detector. The inherently high resolution of the Ge(Li) detector demanded a much larger two dimensional analyzer to handle the data, than was available. Thus, it was necessary to record each coincident event on tape by its (i,j) address, and then to sort the data in the IBM 7040 computer at a later time. The experimental set up is shown in Fig. 4. The channel numbers (i,j) of the coincident pair were first stored in a buffer storage. After 2044 events had been so recorded, the information was dumped on magnetic tape and the buffer storage system was released to file further information. In all, five tapes which included information about 6×10^6 coincident events were used in the experiment. These tapes were then fed to the computer which sorted them to yield a 512 x 256 channel matrix of the type discussed in the last section. In addition to punching out the information in each channel, projections of the data in both directions were punched out corresponding to

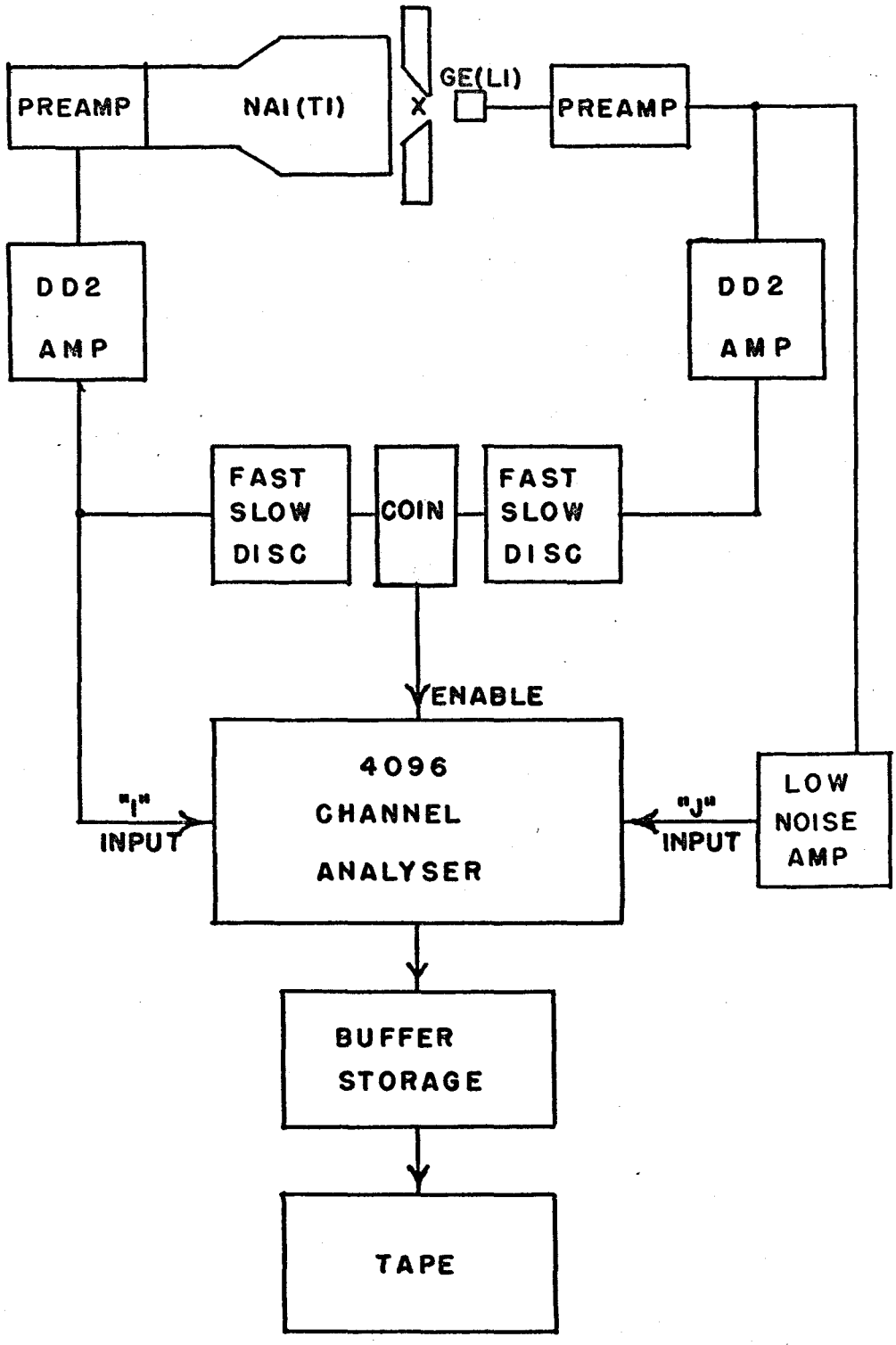

TWO DIMENSIONAL
COINCIDENCE SPECTROMETER
USING NAI(TI) — GE(LI)

FIGURE 4

$M(i) = \sum_{j=1}^{n} A(i,j)$ where $A(i,j)$ is the number of counts in position (i,j), $M(i)$ is the sum of all such terms in the j direction and n is the number of channels in the j direction.

The coincidence experiment was performed in a 180° geometry with the source mounted in an anti-Compton shield to prevent either detector "seeing" radiation scattered from the other. The pulses from the Ge(Li) detector were amplified by a Tennelec charge sensitive tube preamplifier and a TC200 amplifier for the analyzing side while the logic pulses were generated, using equipment similar to that described for the sodium iodide gamma coincidence work.

3.4.3 The Analysis of the NaI(Tℓ) - Ge(Li) Coincidence Data

Since the response to a gamma ray by a Ge(Li) detector produces a sharp peak whose area represents a very small fraction of the total area of the response function but which protrudes significantly from the rest of the spectrum, it was convenient to determine the spectrum in coincidence with this peak and reject the spectrum in coincidence with the Compton background. The Ge(Li) projection spectrum was observed for the photopeaks of all the gamma rays which had been identified in earlier experiments. Since most of these peaks sit on a Compton distribution from higher energy peaks a large fraction of the counts in the spectrum will be due to events coincident with these gamma rays. This contribution was removed at each channel along the NaI direction by subtracting the Compton background in the following manner. For a peak covering 2n channels along the germanium axis (n being of the order of 2 or 3), a good measure of the NaI spectrum in coincidence with this peak was obtained by summing

the counts in these channels and subtracting from this sum the counts accumulated in the adjacent n channels above and n channels below the peak. Since some of the peak area is removed by this method, the number of counts in the coincidence spectrum must be scaled upward in the ratio of the total peak area to the measure of the peak area found above.

In this manner the NaI(Tℓ) spectrum in coincidence with the photopeak alone is obtained. An analysis of these spectra yield the number of coincidence events between a Ge(Li) photopeak and the NaI(Tℓ) photopeak as before, in the form

$$B_{mn} = N_o \ \delta_{mn} \ (\varepsilon\omega)_p \ (\varepsilon\omega) \ (P/T)$$

where $(\varepsilon\omega)_p$ is the photopeak efficiency and solid angle factor for the Ge(Li) detector. Knowing these factors and N_o allows one to get the $\delta_{mn's}$.

3.5 The Gerholm Lens Type Spectrometer

The other type of magnetic spectrometer used in this investigation was the double lens type spectrometer built in this laboratory (Habib (1959)) after the design of Gerholm (1956). Since only one section of the instrument was used to detect betas, this discussion will be limited to considering only one half of the spectrometer. A sectional drawing of the instrument is found in Fig. 5. The instrument is a hollow Armco iron cylinder with the inner coils producing an axial field inside the 6" diameter vacuum chamber. This axial field rises almost linearly from a value of zero at the source end to a maximum just in front of the detector. Electrons from the source spiral around the axis to be focussed in a ring focus at the

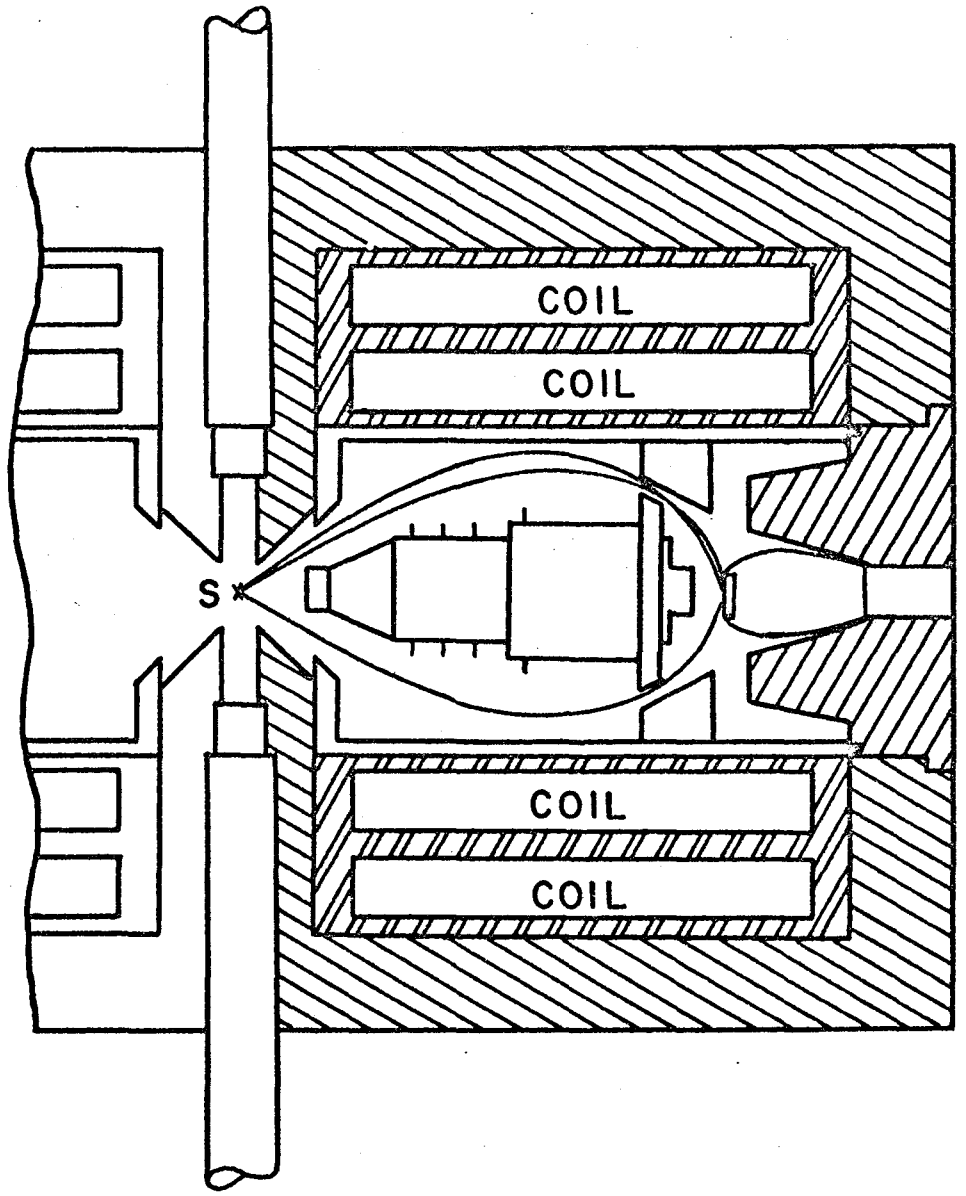

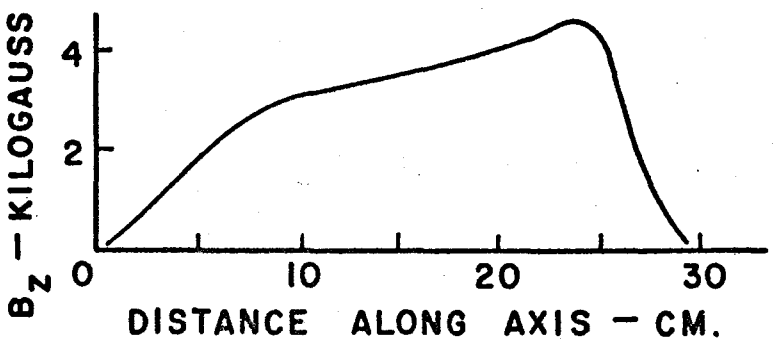

DOUBLE LENS COINCIDENCE SPECTROMETER

FIGURE 5

exit baffles. The current to the coils is supplied by a 5 kw D.C. generator and is stabilized to 0.05% by a chopper amplifier feedback system. At maximum current the instrument can focus 4.5 MeV electrons.

The electrons were detected by an anthracene crystal (2.5 cm. diameter x 2 mm. thick) optically coupled by means of a lucite light pipe to a 56 AVP photomultiplier. Pulses from the photomultiplier were amplified and could be used to obtain time markers in coincidence experiments or simply counted by suitable scaling equipment.

A lead plug on the axis of the spectrometer shielded the detector from direct radiation. Radial fins located along this plug served to reduce multiple scattering of electrons from the walls to the detector (Burke (1963)). With a 0.2 cm. diameter source, one can obtain 1% resolution at a transmission of 1%. With the baffles wide open, both the resolution and transmission become 3.5%.

Since the magnetic field is closely proportional to the current through the coils, the instrument is current stabilized , rather than field stabilized, and the voltage developed across a standard resistance in series with the magnetic coils is used as a measure of the focussing field. The instrument was calibrated using the well known conversion lines from ^{198}Au and ^{137}Cs.

3.5.1 The Analysis of the Beta Spectra

In section 3.1.1, it was shown that the area under a N/p versus p plot gave $N_o \eta \omega$. In order to determine if the spectrum contained more than one component, a Fermi analysis of the data was made by plotting $\sqrt{\frac{N(p)}{p^2 F}}$ against electron energy. In this expression

N(p) is the number of recorded counts per unit momentum interval; and is proportional to the number of recorded events at momentum p divided by p. The Fermi functions have been tabulated for all Z and for all electron energies (Fermi Functions (1952)). If the spectrum contained more than one beta group, it could be resolved into its components by successively peeling off the highest energy group. An N/p versus p graph was then made for each beta group and the areas under the curves determined to yield values of $N_o \delta_i \eta \omega$ where δ_i corresponds to the beta branching ratio. Dividing this by the area under the entire beta continuum, $N_o \eta \omega$ yields the branching ratio δ_i for the i^{th} beta group. From this one could also obtain the $\log_{10} ft$ value for the i^{th} beta transition using the half-life of the nuclide under study.

As well as determining the separate groups by a subtractive fitting process, the data were analyzed using a weighted non-linear least squares fit to the data in the quadratic form

$$\frac{N(E_i)}{pf(E_i)} = \sum_{j=1}^{n} (M_j E_i + D_j)^2$$

where M_j and D_j are adjustable parameters. It is clear that M_j represents the slope of the normal Fermi plot for the j^{th} beta group and $-D_j$ is equal to this slope multiplied by the end-point of the j^{th} group. First guesses were made, postulating the number of beta groups together with their intensities and end points and an iterative program was used to fit the data by successive approximations. The analysis was first carried out restricting the values of D_j by the

condition that $W_j = W_o - E_j$ where W_o and W_j are the end points of the ground state and j^{th} beta groups and E_j is the excitation energy of the level fed by the j^{th} groups. E_j can be considered as known to high precision from the gamma ray measurements. The analysis was then repeated, using the estimates from the above analysis as a starting point, but removing the conditions on the D_j's. In some cases this improved the fit and showed that some of the weaker beta groups fed into the original computations were not real. The program was written to yield the areas of the partial beta spectra by numerical integration using stored F(Z,E) functions and to give these results with standard deviations.

3.6 The Beta-Gamma Coincidence Spectrometer

The arrangement for obtaining beta-gamma coincidences is shown schematically in Fig. 6. The NaI(Tℓ) detector is encased in a soft iron holder which shields the photomultiplier from stray fields and from radiation scattered from the spectrometer walls. The pulses from the beta detector were fed to a double-delay-line amplifier and a fast-slow discriminator. A coincidence required the simultaneous arrival of a fast logic pulse from each detector and a slow pulse from the beta detector. The slow gate was placed over the peak in the beta response to reduce any possibilities of obtaining coincidences with scattered electrons. It was found that without this requirement, electrons scattered from the walls of the vacuum chamber produced a distortion of the beta spectrum and created high energy tails extending beyond the true end point. Multiple sources were used in this investigation and normalization was

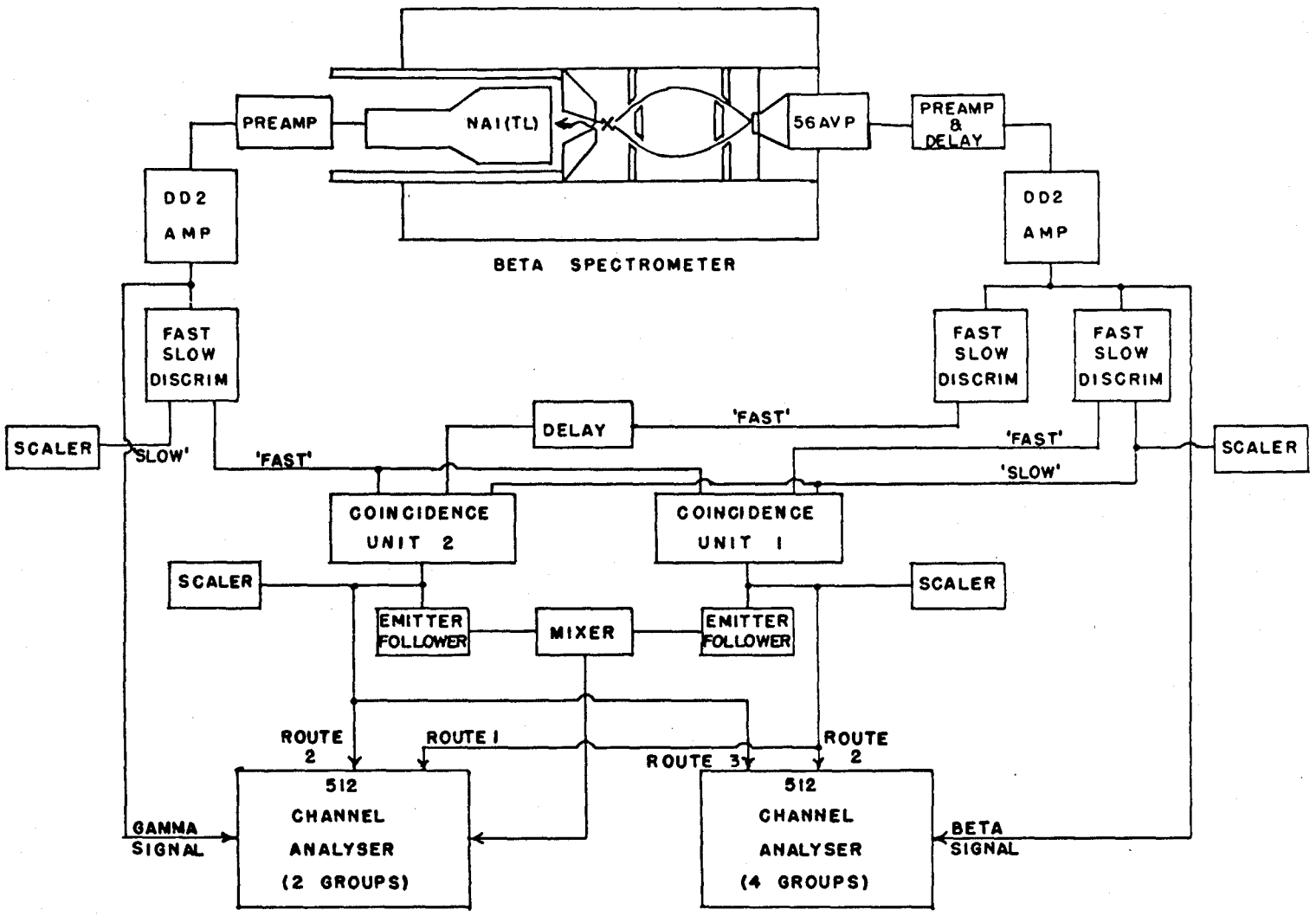

FIGURE 6

BETA-GAMMA COINCIDENCE SPECTROMETER

achieved by scaling the counts from a window placed over a prominent gamma ray transition. The gamma rays in coincidence with a momentum p selected by the magnetic spectrometer were recorded in 256 channels of a 512 channel analyzer. At the same time, the other half of the analyzer was used to record the chance spectrum. This spectrum was obtained by delaying the logic pulse feeding coincidence circuit two. The resolving time of the two coincidence circuits were set to be equal so that the chance spectrum recorded was applicable to that involving coincidence circuit one. A second 512 channel analyzer was used to record the distribution of pulses from the beta detector. The true and chance coincidence beta pulses passed by the window were routed to two quadrants of the analyzer and the remainder to the first quadrant. This made it very simple to obtain peak to total ratios for each beta momentum value. The number of betas passed by the window was also recorded independently. Data were accumulated in the manner described above for a large number of momentum settings over the entire beta spectrum. These data were then analyzed in the fashion described in the next section.

3.6.1 The Analysis of the Beta-Gamma Data

The gamma ray coincidence spectrum for each beta momentum setting was analyzed using the computer program described in section 3.2.1. The use of this program required a knowledge of line shapes for the NaI(Tℓ) detector in the spectrometer geometry. The line shape for the Cesium line obtained in this geometry is shown in Fig. 2; it is clearly different from the line shape obtained in an open-air geometry. From the library of experimental response functions, line

shapes were computer calculated for all the transitions observed in ^{105}Ru. The absolute efficiency of the NaI(Tℓ) detector in this geometry was measured as a function of energy by means of beta-gamma coincidence experiments with sources of ^{198}Au (411.795 keV), ^{192}Ir (316.468 keV), ^{56}Mn (845 keV) and ^{52}V (1434 keV). The values of $\epsilon\omega$ for these transitions were derived from the expression

$$\frac{N_{\beta\gamma}}{N_\beta} = \frac{N_o \varphi(p)\, \omega\eta p\, \delta_\beta}{N_o \varphi(p)\, \omega\eta p\, \delta_\beta} \quad \frac{(\varepsilon\omega)_\gamma}{1 + \alpha_T} = \frac{(\varepsilon\omega)_\gamma}{1 + \alpha_T}$$

where the $\beta\gamma$ rate and the β rate can be determined at any convenient beta momentum value. δ_β is the beta branching ratio and α_T is the total conversion coefficient of the transition. These nuclides were chosen because their highest energy beta groups lead to the gamma rays of interest and there is a wide energy gap between the end point of this group and the lower energy beta groups. The efficiency curve was extended to higher energies by using the 2.754-1.368 MeV cascade in ^{24}Na, and normalizing the lower energy $(\varepsilon\omega)$ value to the Vanadium point. The efficiency of the NaI detector in this geometry (without a lucite beta stopper) was found to be essentially independent of energy up to 600 keV and to fall gradually with increasing energy above this point. With the 1 gm/cm^2 beta stopper in place, the efficiency for lower energies was reduced.

A separate beta source was used at each beta momentum setting and the gamma ray coincidence spectrum was accumulated in the manner described. The relevant expressions for the number of events recorded in the gamma monitoring gate, the beta detector window and the β-γ

coincidence spectrum are

$$N_\gamma = A\, N_{op}$$

$$N_\beta(p) = \frac{N_\gamma}{A} \sum_{j=1}^{n} \varphi_j(p)\, \omega\eta_p\, \delta_j\, W_p$$

$$M_{\beta\gamma_p}(i) = \sum_{k=1}^{\mu} N_{\beta k}(p)\, L_k(i)$$

where N_{op} is the total number of disintegrations for the source used at momentum p, A is a constant expressing the fraction of these producing a gamma pulse in the monitoring gate, and W_p is the fraction of the betas falling on the beta detector which are passed by the window when the spectrometer is set to focus electrons of momentum p. The factor $\varphi_j(p)$ is the probability that an electron of the j^{th} beta group will have momentum p and δ_j is the intensity of that group. Finally, $N_{\beta k}$ represents the number of events in the $\beta\gamma$ spectrum associated with the k^{th} gamma ray and $L_k(i)$ is the response function for that gamma ray.

Upon stripping the $M_{\beta\gamma}(i)$ spectra, using the weighted non-linear least squares fitting program already discussed one obtains values for $N_{\beta k}(p)$. These are given in terms of coincident probabilities by expressions of the form

$$N_{\beta k}(p) = \frac{N_\gamma}{A} \sum_{j=1}^{n} \varphi_j(p)\, \omega\eta_p\, \delta_j\, W_p\, f_{jk}\, (\varepsilon\omega)_k$$

where f_{jk} is the probability that the k^{th} gamma ray will follow emission of a beta ray from the j^{th} group. This family of equations represents the coincidence beta spectrum associated with each of the

k gamma rays. Upon analyzing each of these by the method described in section 3.5.1, one arrives at areas for the j^{th} beta group in coincidence with the k^{th} transition

$$N_{\beta jk} = \frac{N_\gamma}{A} \delta_j f_{jk} \eta\omega (\varepsilon\omega)_k$$

Since the total area of the beta singles spectrum is given by

$$N_\beta = \frac{N_\gamma}{A} \eta\omega$$

the absolute intensities of the various beta groups are given by

$$\delta_j f_{jk} = \frac{N_{\beta jk}}{N_\beta (\varepsilon\omega)_k}$$

The analysis of the coincidence beta spectrum proves to be much cleaner than the analysis of the beta singles because there are fewer beta groups in the spectrum.

CHAPTER IV

SOURCE PREPARATION

Sources for the external conversion investigation consisted of groups of sealed quartz capsules which would fit easily into the source holder described in Chapter III. When natural ruthenium is irradiated with neutrons, the following radioactive nuclides are produced with their half-lives indicated in brackets:

$$^{97}_{44}Ru_{53} - (2.9 \text{ days}) \rightarrow {}^{97}_{43}Tc_{54} - (2.6 \times 10^{6} \text{ years}) \rightarrow {}^{97}_{42}Mo_{55} \quad ;$$

$$^{103}_{44}Ru_{59} - (40 \text{ days}) \rightarrow {}^{103}_{45}Rh_{58} \quad ; \qquad \text{and}$$

$$^{105}_{44}Ru_{61} - (4.5 \text{ hours}) \rightarrow {}^{105}_{45}Rh_{60} - (35 \text{ hours}) \rightarrow {}^{105}_{46}Pd_{59} \quad .$$

After an irradiation of eight hours in the reactor at a flux of 10^{13} neutrons/cm^2-sec the following activities will be obtained from 900 mg. of this material;

^{105}Ru (130 mc), ^{103}Ru (3.6 mc), ^{97}Ru (1.3 mc) and ^{105}Rh (11.8 mc)

Since the quartz capsules did not have to be broken during their use in the $\pi\sqrt{2}$ spectrometer, the capsules were re-irradiated for further investigations after they were allowed to "cool" for a suitable period of time.

All other sources used in the study of this nuclide were made from stable ruthenium enriched in the 104 isotope. This material was obtained from Oak Ridge National Laboratory with the following isotopic percentages; 104 ($99.7 \pm 0.1\%$), 102 ($0.3 \pm 0.1\%$) and other ruthenium isotopes ($< 0.1\%$) .

Impurities detected by a spectrographical analysis of the material conducted by the supplier were iron (0.03%), magnesium (0.01%), sodium (0.01%) and silicon (0.05%). Upon irradiation of 100 μg of this material for eight hours in the reactor, the following activities would be produced; ^{105}Ru (78 uc), ^{103}Ru (0.004 uc), ^{97}Ru (0.002 uc) and ^{105}Rh (7.1 uc).

The quartz capsule containing the irradiated ruthenium powder was broken in a three milliliter solution of equal parts of 1N sodium hydroxide and sodium hypochlorite. This solution was heated to boiling for at least five minutes in order that all the ruthenium would dissolve. To this boiling solution was added ten milliliters of a saturated solution of sodium persulfate. With the addition of this material ruthenium tetroxide was bubbled out of the solution with the aid of an air stream which passed through a trap of three millilitres of 1/4N sodium hydroxide solution. The ruthenium tetroxide dissolved in this solution provided source material which was initially free of any rhodium activity.

Sources used in the study of the gamma radiations were obtained by adding ethyl alcohol to the sodium hydroxide solution causing the ruthenium to precipitate out of the solution as a black powder. The solution and precipitate were allowed to pass through a filter paper which was subsequently dried and used as the source.

By electroplating samples, uniform sources were easily obtained. The plating period controlled both the source strength and source thickness and yielded sources suitable for beta ray studies. The 129.7 keV transition which is highly internally converted was used to give an indication of source thickness effects. When a source was too thick, electron straggling in the source resulted in a broadening of this conversion line on the low energy side.

Sources for the lens spectrometer and internal conversion studies were prepared by adding three millilitres of a plating bath to the sodium hydroxide solution which contained the ruthenium. This bath was composed of 20 g. ammonium phosphate, 90 g. sodium phosphate and 5 g. sodium chloride per 1000 ml. of solution (Mitchell and Martin (1956)). Circular sources of 4 mm. diameter for the lens spectrometer were then plated onto copper foil (0.0002 inches thick) at a current of 200 ma for five minutes. Rectangular sources of dimensions 2 cm. x 0.5 cm. for the internal conversion study were plated onto the same thickness copper foil at a current of 800 ma for 10 to 30 minutes.

CHAPTER V

EXPERIMENTAL RESULTS

5.1 Historical Introduction

The decay of ^{105}Ru has been investigated by many workers (Duffield and Langer (1951), Coryell and Irvine (1955), Saraf et al (1960), Ricci et al (1960), Brandhorst (1961), Arya (1963) and Neeson and Arns (1965)). Both Duffield (1951) and Coryell (1955) measured the life time of the 130 keV isomeric state in ^{105}Ru determining it to be 30 sec, using fast chemical separation techniques. The results of Saraf et al, Ricci et al, Brandhorst and Neeson and Arns are summarized in Table I. In this table the transition energies are listed in keV and the transition intensities are either given relative to the 725 keV gamma ray or in photons per decay.

Saraf and co-workers carried out gamma-gamma coincidence experiments using 1.5 in. diameter by 2 in. thick NaI(Tl) detectors and beta-gamma coincidence experiments using a 1.5 in. diameter by 0.5 in. thick anthracene crystal as a beta detector. They established levels in ^{105}Rh at 0, 130, 395, 475, 725, 795, 960, 1350 and 1750 keV with a beta transition of approximately 1% intensity to either the isomeric or ground state. The total energy available for the decay was determined to be 1875 keV.

Ricci et al determined the 130 keV isomeric transition to be E3 in nature by measuring its internal conversion K/L ratio with a magnetic

TABLE 1

Results of Previous Investigations

Saraf et al		Ricci et al		Brandhorst		Neeson and Arns	
Energy	Intensity*	Energy	Intensity	Energy	Intensity	Energy	Intensity*
130	5	130	11	130	11.6	130	27.4
						148	2.5
						150	1.9
						188	2.1
		210	10	210	<1	210	1.7
265	3.5	260	13	265	14.0	263	9.5
320	7.5	317	26	320	21.3	315	9.9
						317	2.5
						393	3.5
400	3.5	400	14	400	12.2	413	2.1
475	19	475	42	475	30.4	470	19.4
485	5.7					485	2.8
						575	1.2
						650	2.4
665	19	670	26	665	38.2	677	5.6
725	51	725	100	726	100	725	44.5
						870	1.0
875	5.8	870	8	875	4.7	875	2.1
						920	2.1
960	5.3	970	5	960	3.1	955	1.0
1350	1.0			1350	0.6	1345	0.1
						1375	< 0.1
						1578	<0.1
1750	0.2			1720	0.1	1730	<0.1

* Gamma Transition Probability per 100 Disintegrations

spectrometer. Gamma-gamma coincidence measurements were carried out with 2 in. by 2 in. NaI(Tl) detectors. The beta singles spectrum was obtained by making use of a stilbene crystal. They proposed levels for ^{105}Rh at 0(7/2+), 129(1/2-), 475(7/2-,9/2-),390 or 530(1/2-,3/2-,5/2-), 685, 725(7/2+,5/2+),790(3/2-,5/2-),1100 and 1345 keV with a half-life for the decay of 4.44 $\pm$ 0.02 hours. The total decay energy was determined to be 1905 $\pm$ 25 keV and no beta transitions to levels with an energy less than 725 keV were found.

Brandhorst determined the half life to be 4.43 $\pm$ 0.02 hours, carried out gamma-gamma coincidences with 3 in. by 3 in. NaI(Tl) crystals, and beta-gamma coincidence studies employing a hollow plastic scintillation crystal as the beta detector. His decay scheme proposed levels at 0, 130, 395 or 530, 475, 685, 726, 795, 960, 1350 and 1720 keV with a beta transition intensity to the ground state of 10.6% and a total decay energy of 1875 keV.

Inasmuch as no high precision measurements of the gamma ray spectrum had been made, it was decided to obtain more precise energy measurements using the external conversion method with the hope that the decay scheme could be tested more rigorously. In particular, it was hoped to resolve the discrepancy concerning the ground state beta transition by making use of a magnetic spectrometer. Preliminary measurements showed that all the previous workers had missed salient features of the decay and led to the long series of experiments described below. While this work was in progress Neeson and Arns published the results of their gamma-gamma angular correlation studies. These workers had free access

to all of the data accumulated at McMaster and used the portion of this data that they felt was relevant to their work. As will appear later, their conclusions are not in agreement with the results of this thesis. They obtained levels at 0, 130, 150, 393, 470, 618, 658, 725, 785, 806, 935, 955, 1020, 1345, 1375, 1578 and 1730 keV.

5.2 The Gamma Ray Spectrum

The measured gamma ray energies and intensities are presented in Table II. This table embodies data accumulated from external conversion measurements, internal conversion measurements, Ge(Li) detector measurements and beta-gamma and gamma-gamma coincidence studies.

The first four columns show the results of energy measurements obtained from external conversion, gamma-gamma coincidence, internal conversion and Ge(Li) detector methods, respectively. The next four columns list the corresponding absolute intensities of the transitions. The photon intensities were initially measured relative to the strong 725 keV radiation, and adjusted to represent absolute photon intensities using the results of the beta-724.5 keV coincidence experiment and the decay scheme to be described. It should be noted that the intensity entries in the β-γ column refer to the intensities of the beta rays directly feeding the gamma ray in question. As such, these values should be equal to or less than the photon intensities in the first three intensity columns. The second last column indicates the location of each gamma ray in the decay scheme. The energy of each level in the decay scheme was determined by a weighted average of the transition energies involved in the various paths of de-excitation to the ground

TABLE II

Gamma Rays in the Decay of ^{105}Ru

Energies in keV				Intensities in %					
E.C.	NaI(Tl)	I.C.	Ge(Li)	E.C.	Ge(Li)	NaI(Tl)	β-γ	Classification	$E_{calc.}-E_{exp.}$
			63.6 ± 0.5		0.021 ± 0.002			455.9 → 392.6	-0.3
			73.0 ± 0.3		0.009 ± 0.002				
			75.3 ± 0.3		0.016 ± 0.002				
			82.0 ± 0.3		0.026 ± 0.003			806.1 → 762.0	+0.1
			85.9 ± 0.3		0.032 ± 0.002			724.5 → 638.7	-0.1
			87.9 ± 0.3		0.040 ± 0.003				
			90.0 ± 0.3		0.027 ± 0.003				
			92.0 ± 0.4		0.023 ± 0.002				
			95.8 ± 0.2		0.023 ± 0.002				
			99.6 ± 0.2		0.013 ± 0.002				
		129.2 ± 0.4	129.7 ± 0.2	4.9 ± 1.0	5.0 ± 0.2			129.7 → 0	0
			139.6 ± 0.4		0.030 ± 0.007			638.7 → 499.2	-0.1
149.0 ± 0.3			149.2 ± 0.2	2.1 ± 0.5	1.67 ± 0.05			149.2 → 0	0
		162.5 ± 0.7	163.6 ± 0.2		0.140 ± 0.007			969.5 → 806.1	-0.2
			183.6 ± 0.2		0.100 ± 0.007			969.5 → 785.9	0
			225.0 ± 0.2		0.150 ± 0.009			724.5 → 499.2	+0.3
			245.6 ± 0.4		0.029 ± 0.008			1215.2 → 969.5	+0.1
			255.1 ± 0.2		0.062 ± 0.006			724.5 → 469.4	0
262.6 ± 0.2		262.3 ± 0.4	262.9 ± 0.2	7.4 ± 0.5	7.2 ± 0.3		0.10 ± 0.03	392.6 → 129.7	0
316.4 ± 0.2		316.6 ± 0.5	316.5 ± 0.2	11.5 ± 1.2	11.7 ± 0.4		10.7 ± 0.4	785.9 → 469.4	0
		326.7 ± 0.5	326.1 ± 0.2		1.18 ± 0.06			455.9 → 129.7	+0.1
		331.3 ± 0.5	330.9 ± 0.2		0.79 ± 0.04			969.5 → 638.7	-0.1
350.5 ± 0.6		350.2 ± 0.4	350.2 ± 0.2	1.6 ± 0.5	1.48 ± 0.07	1.1 ± 0.1	2.2 ± 0.4	806.1 → 455.9	0
	350 ± 5					0.3 ± 0.1		499.2 → 149.2	-0.2
	351 ± 5					0.08 ± 0.02		1321.3 → 969.5	+0.8
			369.2 ± 0.3		0.062 ± 0.018			762.0 → 392.6	+0.2
393.4 ± 0.3			393.4 ± 0.2	4.8 ± 0.6	4.2 ± 0.2		2.7 ± 0.6	785.9 → 392.6	-0.1
			407.5 ± 0.3		0.18 ± 0.02			1377.1 → 969.5	+0.1
413.6 ± 0.3			413.5 ± 0.2	3.0 ± 0.6	2.48 ± 0.12		3.3 ± 0.6	806.1 → 392.6	0
469.3 ± 0.3			469.4 ± 0.2	18.3 ± 1.0	18.8 ± 0.7	17.5 ± 1.0	1.4 ± 0.1	469.4 → 0	0
	470 ± 10					1.3 ± 0.2		969.5 → 499.2	+0.3
			489.6 ± 0.2		0.59 ± 0.03			638.7 → 149.2	-0.1
497.7 ± 0.3		499.7 ± 0.4	499.2 ± 0.2		2.40 ± 0.12			499.2 → 0	0
			500.4 ± 0.4		0.30 ± 0.05			969.5 → 469.4	-0.3
			513.7 ± 0.2		0.36 ± 0.04			969.5 → 455.9	-0.1
			539.2 ± 0.3		0.13 ± 0.04			1345.2 → 806.1	-0.1

TABLE II (cont'd)

Gamma Rays in the Decay of ^{105}Ru

Energies in keV				Intensities in %					
E.C.	NaI(Tl)	I.C.	Ge(Li)	E.C.	Ge(Li)	NaI(Tl)	β-γ	Classification	$E_{cal.}-E_{exp.}$
			559.5 ± 0.3		0.087 ± 0.016			1345.2 → 785.9	-0.2
576.2 ± 0.7		575.5 ± 0.5	575.3 ± 0.2	1.8 ± 0.3	1.07 ± 0.05		1.0 ± 0.4	724.5 → 149.2	0
	575 ± 5					0.13 ± 0.05		969.5 → 392.6	+1.9
			591.3 ± 0.3		0.080 ± 0.016			1377.1 → 785.9	-0.1
			621.0 ± 0.3		0.080 ± 0.016			1345.2 → 724.5	-0.3
			632.3 ± 0.2		0.23 ± 0.02			762.0 → 129.7	0
			638.6 ± 0.2		0.28 ± 0.03			638.7 → 0	+0.1
			652.6 ± 0.2		0.35 ± 0.02		0.9 ± 0.4	1377.1 → 724.5	0
	656 ± 8					0.20 ± 0.05		1442 → 785.9	0
		654.9 ± 0.9	656.1 ± 0.2		2.40 ± 0.09			785.9 → 129.7	+0.1
677.2 ± 0.6		677.8 ± 0.8	676.4 ± 0.2	16.4 ± 0.8	16.7 ± 0.7		16.5 ± 0.8	806.1 → 129.7	0
724.8 ± 0.3		724.6 ± 0.5	724.5 ± 0.2	49 ± 2	49 ± 2		48.2 ± 2.5	724.5 → 0	0
			738.3 ± 0.4		0.060 ± 0.007			1377.1 → 638.7	+0.1
			786.1 ± 0.2		0.088 ± 0.008			Sum Peak (469.4 and 316.5)	
			806.2 ± 0.3		0.047 ± 0.008		0.4 ± 0.2	806.1 → 0	-0.1
						0.012±0.004		969.5 → 149.2	-1.7
	822 ± 5								
			822.1 ± 0.2		0.19 ± 0.01		0.7 ± 0.4	1321.3 → 499.2	0
			845.9 ± 0.2		0.73 ± 0.03			1345.2 → 499.2	+0.1
			852.0 ± 0.2		0.140 ± 0.008			1321.3 → 469.4	-0.1
876.4 ± 0.8			875.8 ± 0.2	3.1 ± 0.3	3.40 ± 0.14		4.0 ± 0.2	1345.2 → 469.4	0
	876 ± 10					0.11 ± 0.03		1269 → 392.6	-0.4
905.1 ± 2.0			907.7 ± 0.2	0.6 ± 0.2	0.59 ± 0.03		1.0 ± 0.3	1377.1 → 469.4	0
			952.8 ± 0.3		0.043 ± 0.014			1345.2 → 392.6	-0.2
970.9 ± 0.6			969.4 ± 0.2	2.7 ± 0.4	2.34 ± 0.09		2.1 ± 0.2	969.5 → 0	+0.1
			1017.2 ± 0.2		0.340 ± 0.017		0.39±0.04	1486.6 → 469.4	0
			1059.0 ± 0.3		0.023 ± 0.007			1697.5 → 638.7	-0.2
			1215.2 ± 0.3		0.084 ± 0.008		0.096±0.010	1215.2 → 0	0
			1221.2 ± 0.3		0.018 ± 0.001			1720.2 → 499.2	-0.2
			1250.9 ± 0.3		0.023 ± 0.004			1720.2 → 469.4	-0.1
			1321.3 ± 0.2		0.23 ± 0.01		0.31±0.03	1321.3 → 0	0
			1345.9 ± 0.5		0.022 ± 0.003			Sum Peak (469.4 and 875.8)	
			1376.8 ± 0.3		0.056 ± 0.006			1377.1 → 0	+0.3
			1697.4 ± 0.3		0.085 ± 0.005		0.15±0.02	1697.5 → 0	+0.1
			1720.2 ± 0.3		0.032 ± 0.002			1720.2 → 0	0

Note: β-γ results are uncorrected for gamma rays feeding the level.

state. The last column shows the difference between the separation of the levels involved in the transition and the actual energy measurement of the transition.

A detailed discussion of these results is given in the following sections. The experimental techniques associated with these measurements has been described in Chapters III and IV.

5.2.1 The External Conversion Measurements

A composite external conversion spectrum is shown in Figures 7 and 8. In these figures the transition energies are quoted in keV and the shell in which each peak occurred is indicated. Since these measurements were made with natural ruthenium, the peaks associated with the 215 keV transition in ^{97}Ru, and the 498 keV line in ^{103}Ru are clearly evident. The ^{105}Rh daughter of ^{105}Ru is responsible for the peaks associated with the 306 and 319 keV gamma rays. Each portion of the spectrum was studied with a suitable radiator; the antimony radiator being necessary to examine the K peak of the 129 keV gamma ray and gold or uranium radiators being used for higher energies. The energy region below the K peak of the 129.7 keV photon peak was carefully scanned for low energy conversion electrons but the only observable peaks were due to Auger electrons. It was necessary to use a 6 mg/cm^2 Au radiator to obtain the intensity required to measure the K peak of the weak 350 keV radiation.

The 499.2 keV transition is masked by the 498-K conversion peak in ^{103}Ru and the 413-L and-M conversion peaks mask the 489.6-K conversion peak. Since only about 400 gauss-cm of the spectrum could be scanned

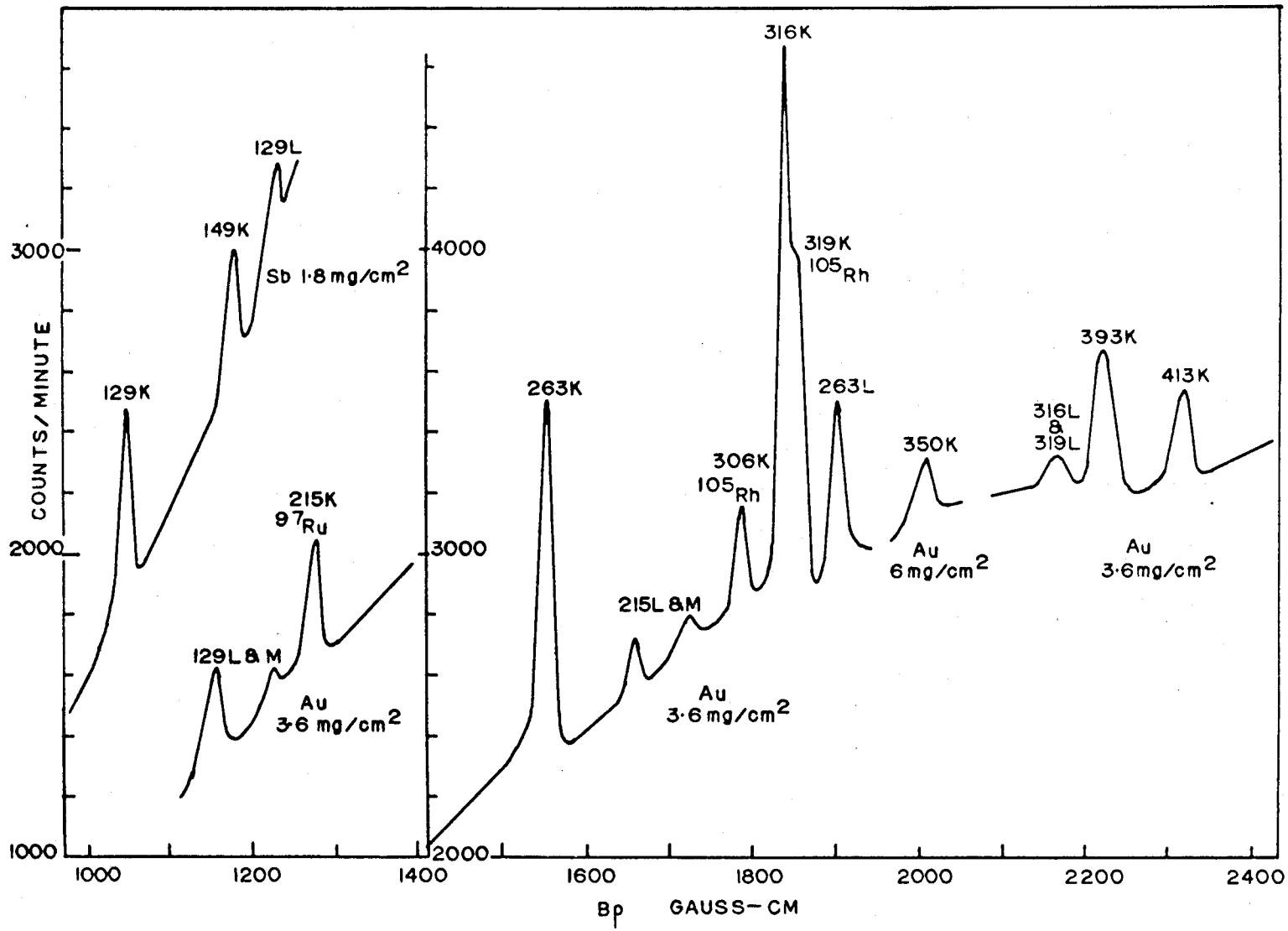

FIGURE 7

LOW ENERGY EXTERNAL CONVERSION SPECTRA

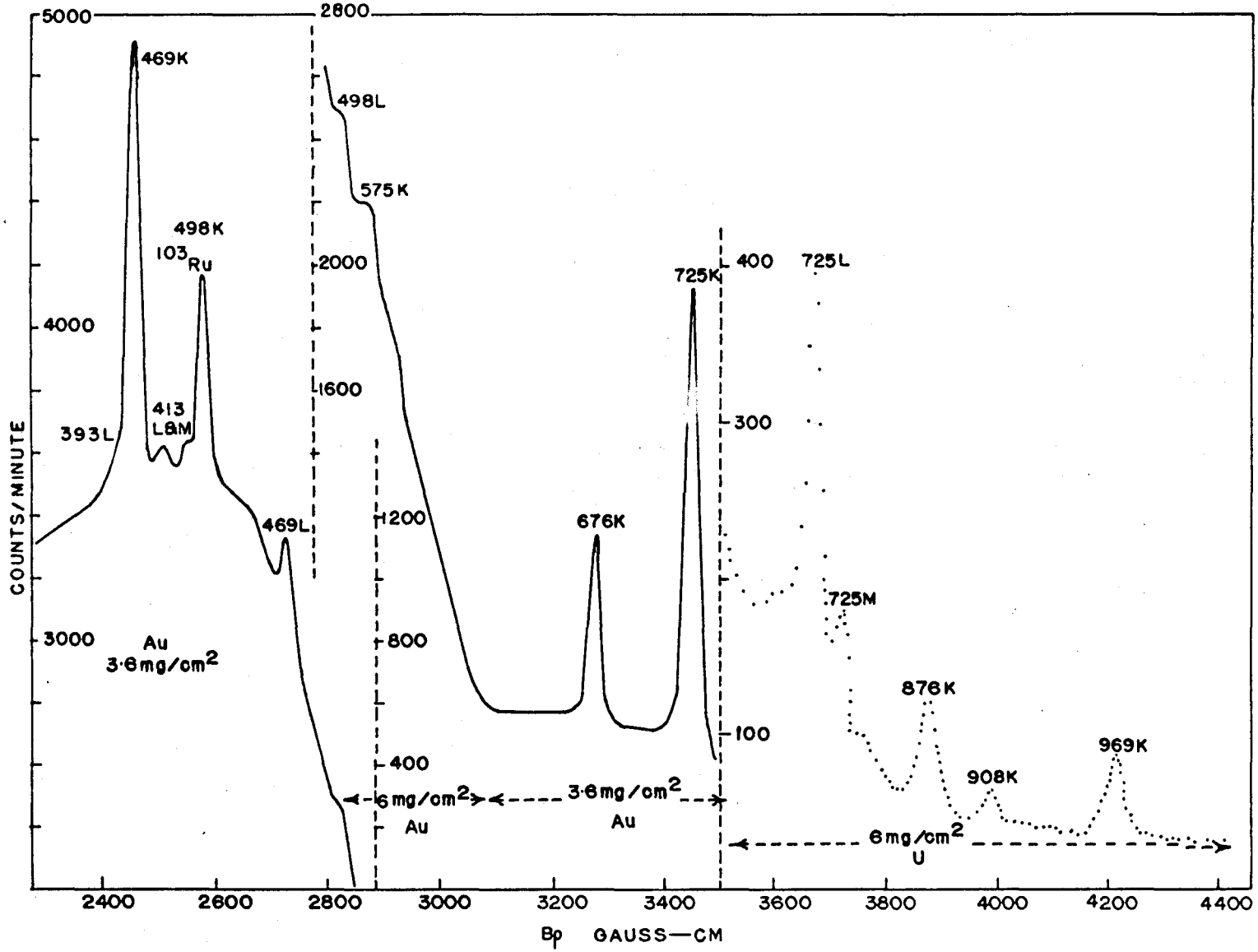

FIGURE 8

HIGH ENERGY EXTERNAL CONVERSION SPECTRA

in 8 hours, it was necessary to use a great many sources to obtain the data shown in Figures 7 and 8. The decay rate of each peak was followed to determine which ones were associated with the 4.44 hour ^{105}Ru. The intensities of the lines observed were determined relative to the 469.4 keV or the 724.5 keV transition using the semiempirical formula discussed in chapter III. The magnetic spectrometer was calibrated for each radiator used by means of known lines from the following nuclides; ^{105}Rh (318.9 ± 0.1), ^{192}Ir(295.94 ± 0.01, 308.43 ± 0.01, 316.49 ± 0.01, 468.05 ± 0.01, 604.39 ± 0.02, 612.44 ± 0.02 and 884.6 ± 0.4), ^{198}Au (411.795 ± 0.009) and ^{60}Co (1173.23 ± 0.04 and 1332.48 ± 0.05).

5.2.2 The Internal Conversion Measurements

The results of the internal conversion energy measurements are found in Table II and the internal conversion line intensities are found in columns 3, 4 and 5 of Table III. A composite of typical spectra is displayed in Figure 9. The magnetic spectrometer was calibrated using the K conversion peak of the strong 469.4 keV line as an internal standard. Since it required several hours to establish a weak conversion electron peak, a different source was needed for each conversion line. For each such source, a scan was made over one of the stronger conversion lines, 130-L, 263-K, 469-K or 725-K, to provide a relative intensity measurement. The number of conversion electrons per decay for each peak was then established by comparing the areas of these strong conversion lines to the area of the total beta continuum. Several determinations of each conversion line intensity were made. The number of counts in each conversion peak was corrected for the beta detector

TABLE III

Internal Conversion Results

Energy	Intensity %	No. of Electrons per 100 decays ($\times 10^{+2}$)			Conversion Coefficient ($\times 10^{+3}$)			Multipolarity
		N_K	N_L	N_M	α_K	α_L	α_M	
129.7	5.0	1290 ± 130***	550 ± 55	125 ± 13	2580 ± 258	1100 ± 110	250 ± 25	E3
149.2	1.67		3.2 ± 0.5	2.0 ± 0.5	**	19.2 ± 3.0	12.0 ± 3.0	M1 + E2
163.6	0.14	2.0 ± 0.9			143 ± 64			M1 + E2
262.9	7.2	11.2 ± 0.8			15.6 ± 1.1			M1
316.5	11.7	10.0 ± 1.0****	0.72 ± 0.20		8.9 ± 0.9	0.62 ± 0.17		E1
326.1	1.18	1.26 ± 0.20			10.7 ± 1.7			M1
330.9	0.79	0.82 ± 0.20			10.4 ± 2.5			M1
350.2	1.48	0.56 ± 0.10			3.8 ± 0.7			E1
393.4	4.2	2.1 ± 0.6			5.0 ± 1.4			M1 and/or E2
413.5	2.48	0.4 ± 0.3			1.6 ± 1.2			E1
469.4	18.8	9.6 ± 0.9	1.4 ± 0.2		5.1 ± 0.5	0.75 ± 0.11		M1 and/or E2
499.2 and 500.4	2.7	1.5 ± 0.3			5.5 ± 1.1			M1 and/or E2
575.3	1.07	0.3 ± 0.1*			2.8 ± 0.9			M1 and/or E2

TABLE III (cont'd)

Internal Conversion Results

Energy	Intensity %	No. of Electrons per 100 decays ($\times 10^{+2}$)			Conversion Coefficient ($\times 10^{+3}$)			Multipolarity
		N_K	N_L	N_M	α_K	α_L	α_M	
656.1	2.4	0.66 $\pm$0.15			2.8 $\pm$ 0.6			M1 and/or E2
676.4	16.7	1.56 $\pm$0.20			0.93 $\pm$ 0.12			E1
724.5	49	7.75 $\pm$0.80			1.58 $\pm$ 0.16			M1 and/or E2
875.8	3.4	0.48 $\pm$ 0.15			1.41 $\pm$ 0.4			M1 and/or E2
969.4	2.34	0.27 $\pm$0.10			1.2 $\pm$ 0.4			M1 and/or E2

* - mean of 3 determinations - each with errors of 50% and at limit of detection

** - K peak masked by 130 L's

*** - Corrected for a detector efficiency of 80%

**** - Includes a contribution from the 318.9 keV (M1) transition in ^{105}Rh

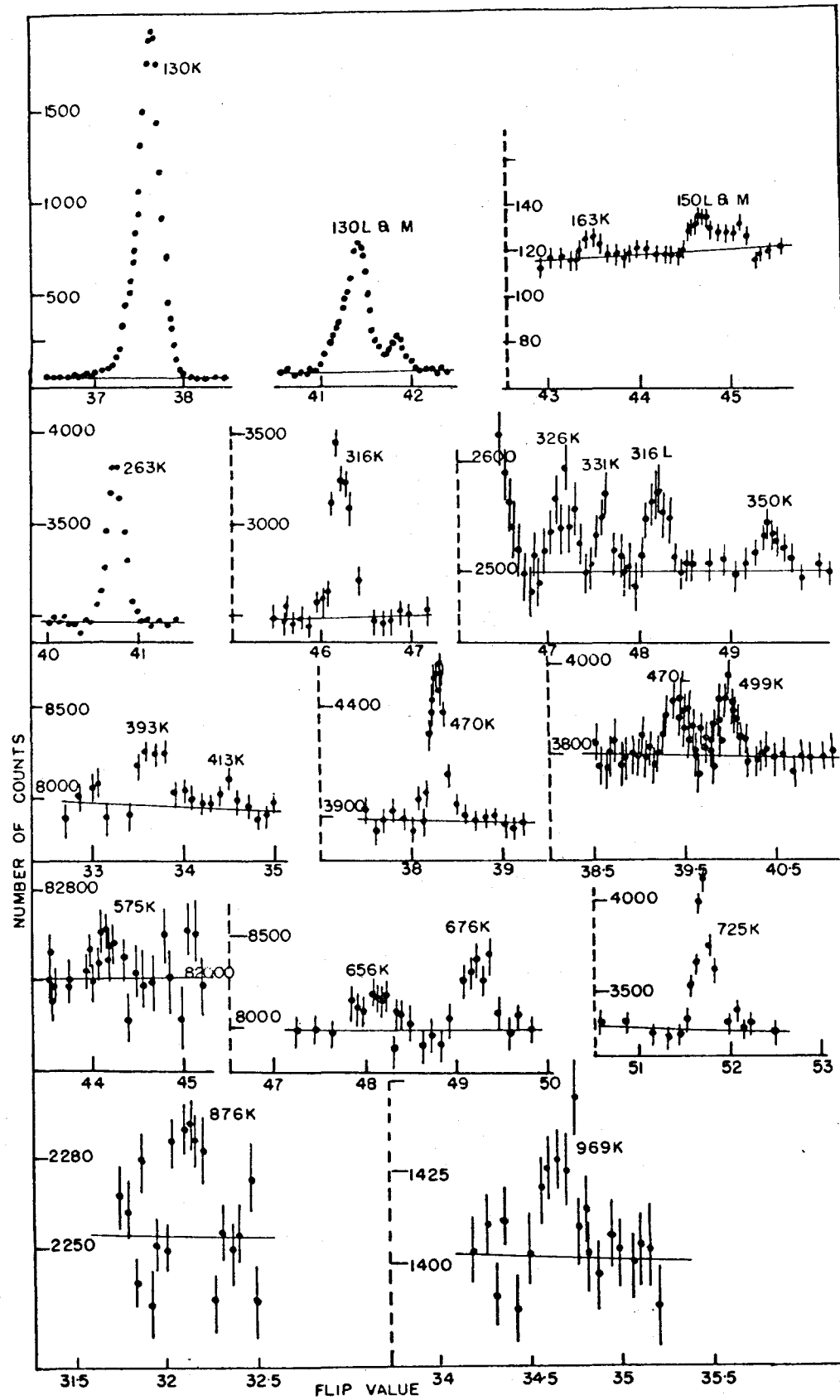

INTERNAL CONVERSION SPECTRA

FIGURE 9

efficiency to yield the true conversion line intensity.

The detection efficiency was very nearly 100% except for the K conversion peak of the 129.7 keV radiation, where it was measured to be 80%. This peak was also sensitive to source thickness, and some of the runs with thicker sources showed considerable degradation on the low energy side of this peak. The 149.2-K conversion line was completely obscured by the very much stronger 129.7-L conversion peaks. The 316.5-K peak includes some contribution from the 318.9-K peak associated with the ^{105}Rh decay. The continuum near the peaks shown in Figure 9 is not displayed in its entirety, but was carefully measured in each spectrum to provide the necessary base line.

The internal conversion coefficients in columns 6,7 and 8 of Table III were derived from the conversion electron intensities by the use of the Ge(Li) photon intensities shown in column 2. Figure 10 presents the theoretical conversion coefficients calculated by Sliv and Band (1956, 1958) for Z = 45 together with the measured coefficients of Table III. It is clear that most of the transitions are M1 and/or E2 in character but that there are a number of E1 transitions present. These conclusions are presented in the last column of Table III.

5.2.3 The Ge(Li) Gamma Ray Measurements

The gamma ray spectrum obtained with the 4 mm thick Ge(Li) detector is displayed in Figures 11 and 12. The gamma ray energies (in keV) are indicated above each peak. The weaker peaks are presented in an expanded scale in inserts at the appropriate points. The inserted region of the spectrum below 130 keV was obtained with a differ-

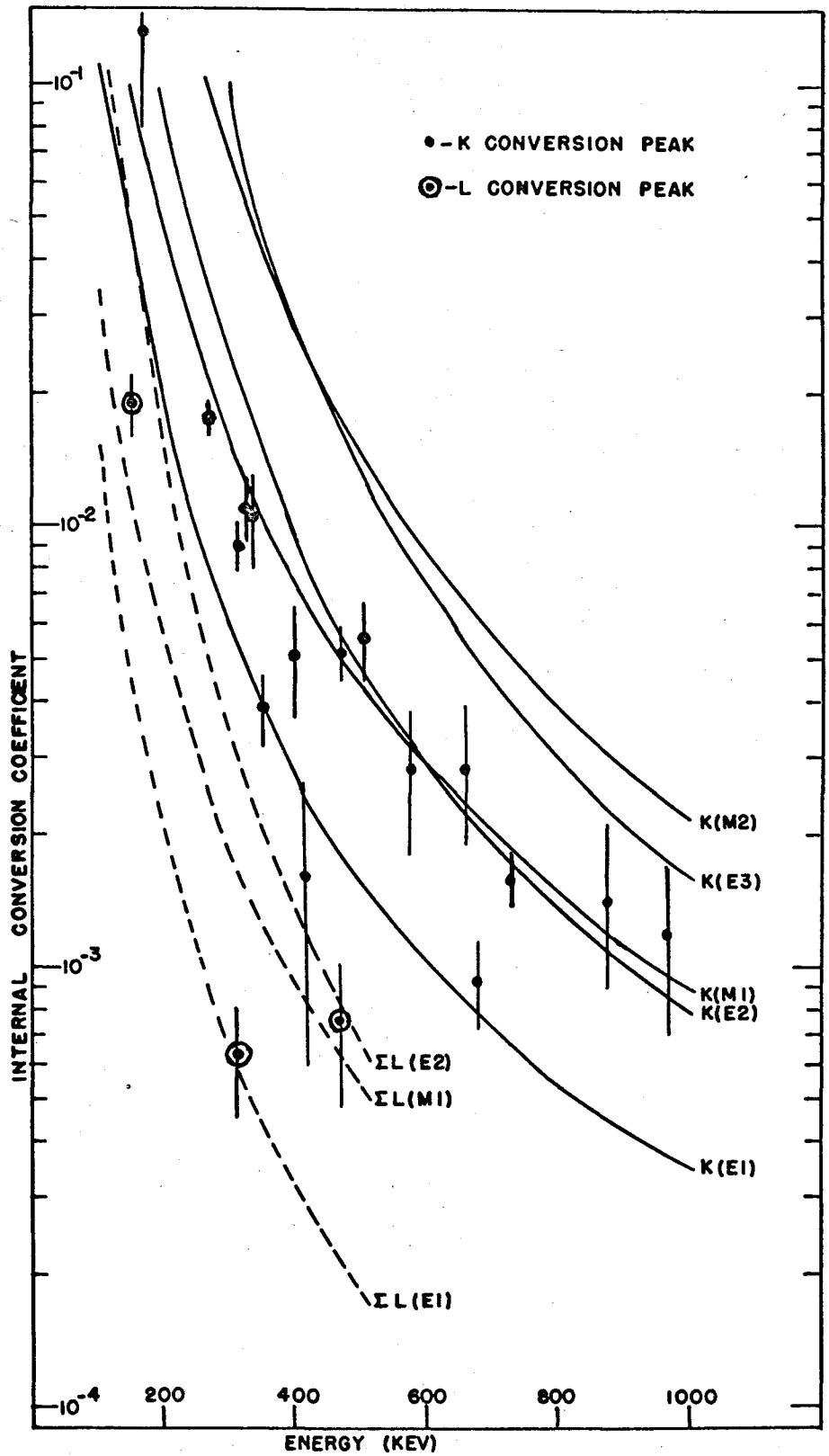

THEORETICAL AND EXPERIMENTAL
INTERNAL CONVERSION COEFFICIENTS

FIGURE 10

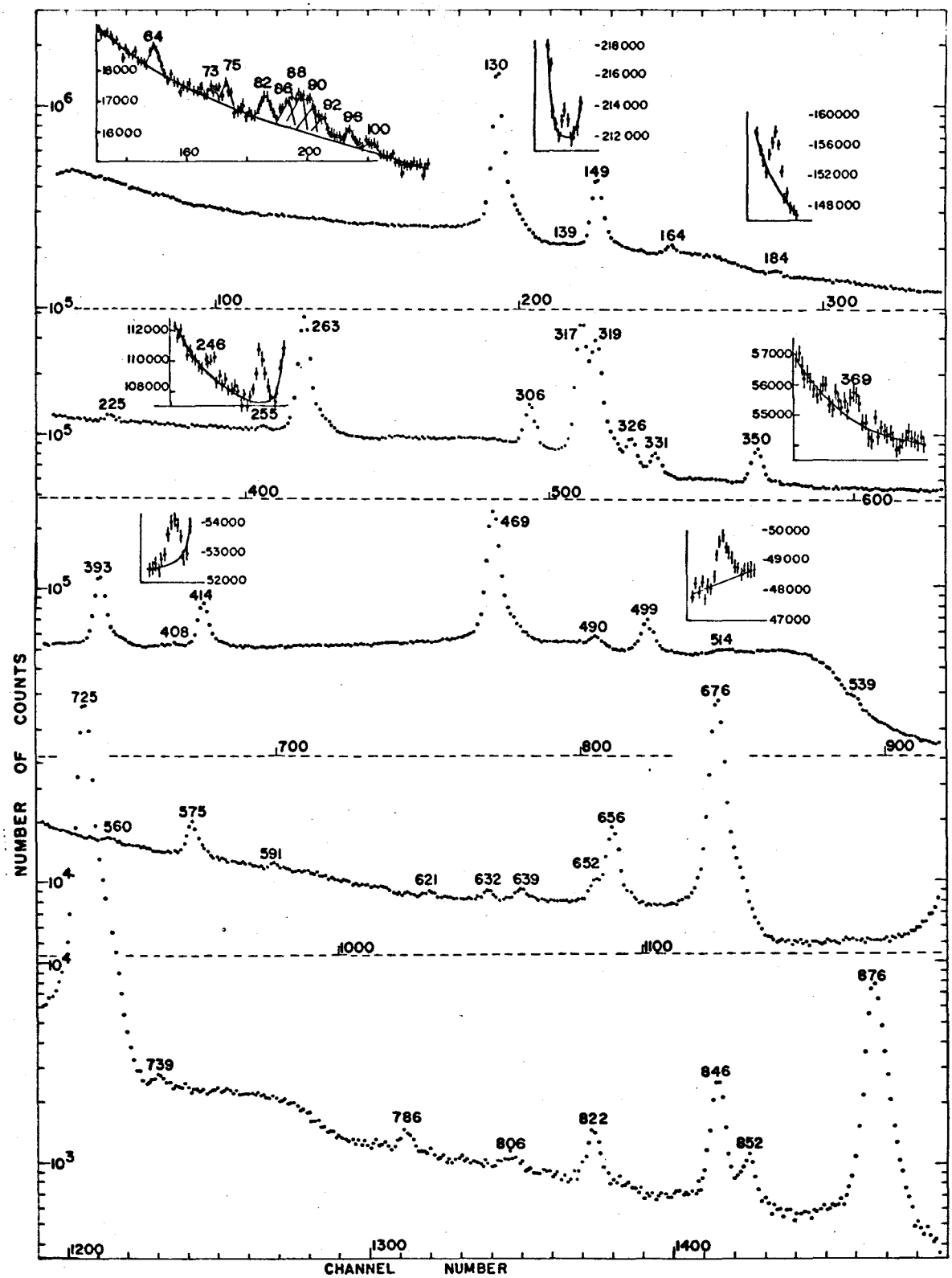

LOW ENERGY GAMMA RAY SPECTRUM
USING A Ge(Li) DETECTOR

FIGURE II

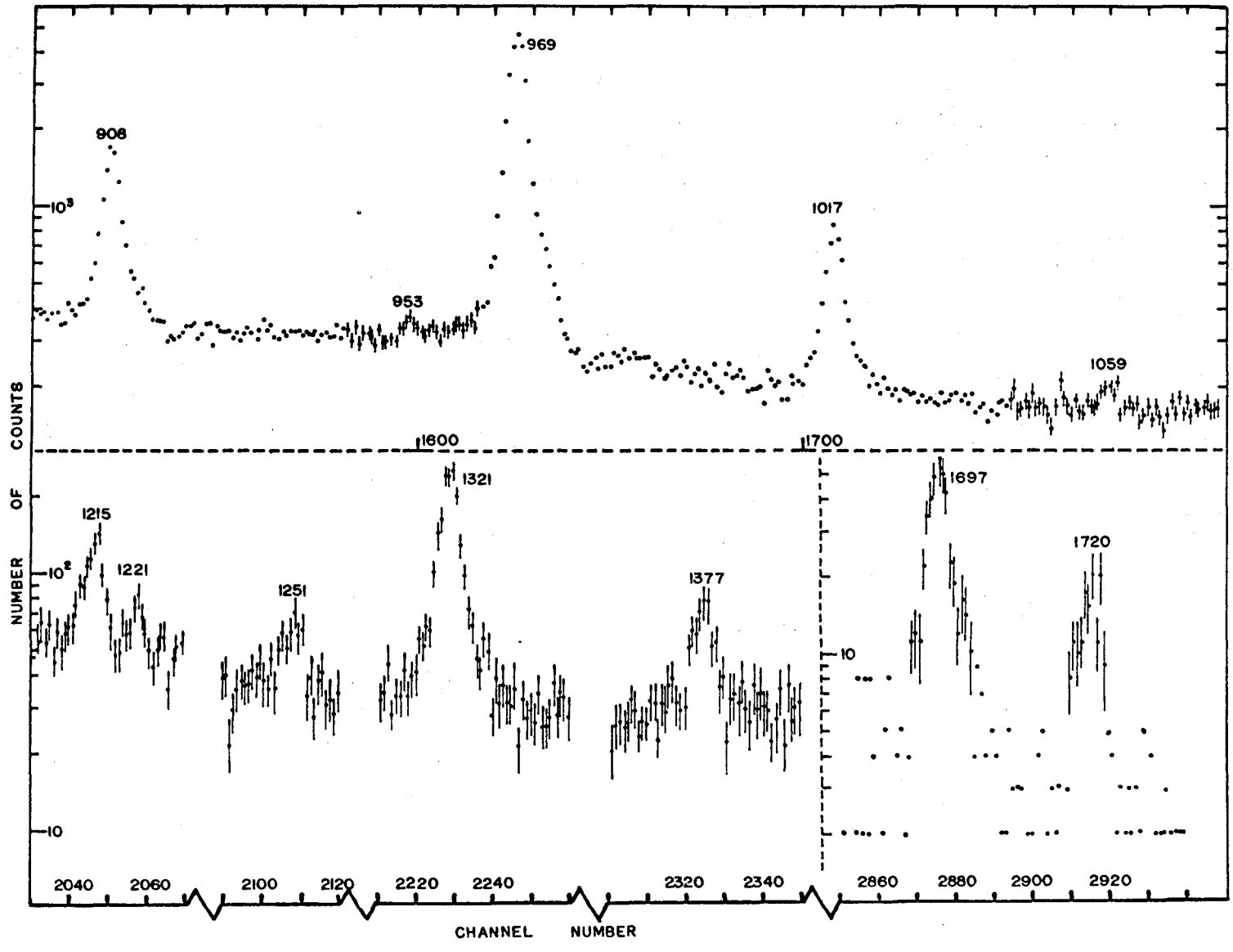

FIGURE 12

HIGH ENERGY GAMMA RAY SPECTUM USING A Ge(Li) DETECTOR

ent recording system. The peaks at 318.9 ± 0.1 and 306.1 ± 0.2 keV are associated with the ^{105}Rh decay. Two additional peaks in this decay, at 280.1 ± 0.2 and 442.8 ± 0.7 keV appear in the spectrum after the ^{105}Ru activity has died away. These four transitions all decay with the half-life of ^{105}Rh and have relative intensities of 19.5 ± 0.8, 5.2 ± 0.2, 0.168 ± 0.013 and 0.043 ± 0.005 respectively. The 497.3 ± 0.3 keV transition associated with ^{103}Ru decay and the 215.1 ± 0.3 keV transition of ^{97}Ru also appeared in ^{105}Ru sources which had been allowed to decay for two or three days. The energy and intensity measurements tabulated in Table II are the result of six experiments using the 4 mm thick Ge(Li) detector and seventeen other experiments involving detectors with six to ten keV FWHM on the ^{137}Cs peak and various analyzers. Calibration of the system and evaluation of the efficiency curves were determined by methods discussed in Chapter III. Although the high energy spectrum in many of these runs possessed much better statistical accuracy than the spectrum of Figure 12, no new peaks with intensity greater than 0.01% were discovered for the energy region above the 908 keV peak.

The energies of the more intense lines were calculated from calibration lines recorded simultaneously with the ^{105}Ru source while the energies of the weaker radiations were determined by making use of the stronger ^{105}Ru peaks as internal standards.

5.3 Results from Coincidence Measurements

The results of γ-γ coincidence studies are found in Tables IV and V while those for the β-γ coincidence measurements are found in Table VI. The method of accumulating and analysing this data has already

TABLE IV

Coincidence Probabilities from NaI-NaI Experiments

(keV) (Gate Side)

	149	164	184	225	245	255	263	317	326	331	350	393	408	414	469	490	499	514	539	560	575	591	639	653	656	676	725	738	846	876	908	953	969	1017	1059
149										(0.58)						0.23					0.7								0.16							0.01
164														0.04												0.16									
184															0.09										0.08										
225	0.03										0.03						0.2																		
255															0.11																				
263			0.03									5.22		2.55						0.2					0.05					0.14		0.03			
317			0.19												11.9						0.16														
326											0.8							0.43																	
331	0.5												0.05			0.23							0.36												
350	0.2			0.06					0.88										0.03										0.07				0.04		
393							5.19														0.06														
408	0.06														0.1		0.1						0.04										0.09		
414		0.06					2.65																												
469			0.11			0.14		12.1									1.6				0.16				0.2					3.9	0.51			0.55	
490	0.6									0.64			0.08															0.06							
499				0.21											1.7														1.85						
514																																			
539							0.05																			0.3									
560												0.04																							
575	1.07						0.18	0.13																0.07											
591																																			
639										0.25			0.04																						
653	0.07																				0.07						0.54								
656			0.03				0.06								0.09																				
676		0.21																	0.27																
725																								0.58											
738																0.07																			
846	0.27										0.17						1.26																		
876							0.07								4.0																				
908															0.4																				
953							0.06																												
969					0.02								0.16																						
1017															0.45																				
1059	0.02																																		

TABLE V

COINCIDENCE PROBABILITIES FROM Ge-NaI EXPERIMENTS

(Gate Side)

NaI Peaks (keV) \ Ge Peaks (keV)	149	164	225	263	317	326	331	350	393	408	414	469	490	499	514	575	591	639	653	676	725	822	846	876	908	969	1017	1059	1221	1251
149							0.35 0.50	0.3					0.41			0.9						0.028	0.11					0.03		
164																			0.06	0.26										
263		0.025						0.07	5.4		2.4					0.1			0.03											
317												11.4					0.1													
326								0.9							0.21															
331	0.55												0.64																	
350	0.12					1.1																0.016	0.1							
393				5.0																										
408																										0.08				
414		0.025		2.5																										
469					11.6			0.12						1.2			0.2							3.2	0.7		0.7			0.02
490	0.66						0.62																							
499			0.12									1.6										0.16	0.8						0.03	
514						0.29																								
539				0.1							0.05									0.26										
560																														
575	1.0			0.1	0.18				0.05																					
591																														
639							0.37 0.21																							
653																					0.58									
676		0.17																												
725																			0.4											
738	0.08																													
846	0.22							0.2						1.1																
876												4.2																		
908												0.7																		
953				0.04																										
969								0.04		0.11																				
1017												0.45																		
1059	0.02																	TR												

been discussed in Chapter III. The decay scheme of Figure 18 was deduced by means of **these** data and that presented in the preceding section.

5.3.1 Gamma-Gamma Coincidence Measurements

Figure 13 presents a portion of the matrix obtained when gamma-gamma coincidences between two NaI(Tl) detectors are recorded by a two dimensional analyser. The figure shows the spectra recorded along the i axis in coincidence with channels 17, 19, 21 and 23 measured along the j axis. Each spectrum thus represents the spectrum in coincidence with a "one-channel" gate of width 22 keV. The spectra displayed in Figure 13 are labelled by the median energy of the gate and show dramatic changes in character as the gate moves upward by 44 keV. The prominent peaks appearing at 150, 350, 470 and 639 keV in the 322 keV gate are due to the 330.9-489.6-149.2, the 350.2-326.1, the 316.5-469.4 and the 330.9-638.6 keV cascades. In the same way, the 366 keV gate shows evidence for the strong 393.4-262.9 and the 350.2-326.1 keV cascades, the 410 keV gate presents evidence for the 413.5 keV and the 393.4 keV photon coincidences with the 262.9 keV transition and finally the 454 keV gate shows the 316.5-469.4, the 330.9-489.6, the 500.4-469.4 and 470-499.2, the 845.9-499.2, the 875.8-469.4, the 907.7-469.4 and the 1017.2-469.4 coincident pairs. The peak at 67 keV present in all four spectra is due to lead x-rays produced from the anticompton shield.

Each of the 56 spectra of the type presented in Figure 13 were analysed into component gamma rays. The number of counts associated with each such gamma ray was then plotted as a function of the channel number along the j axis to yield coincidence spectra of the type presented in Figures 14 and 15. Because there is generally more than one gamma

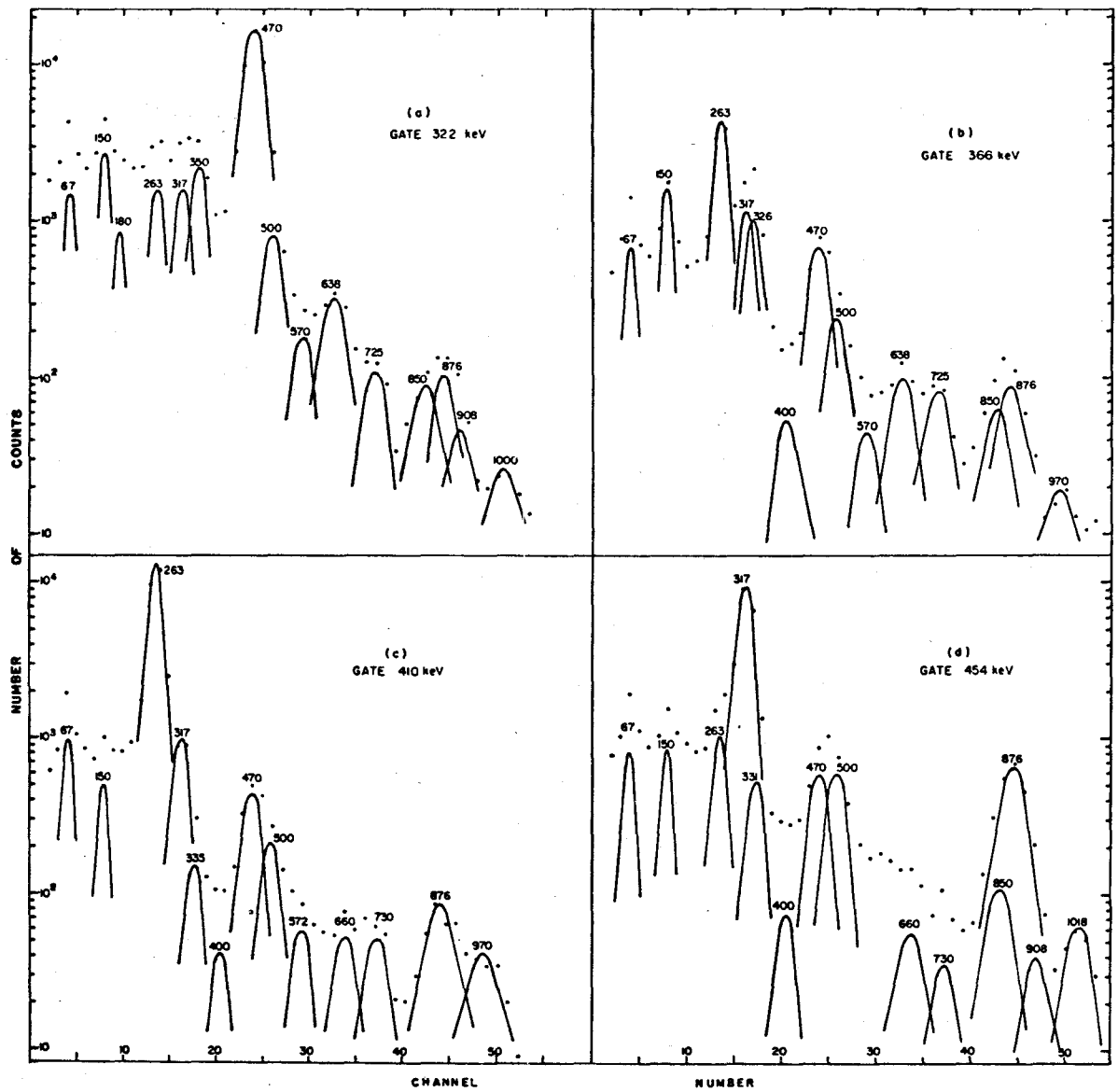

ONE DIMENSION PROJECTION OF TWO DIMENSIONAL GAMMA GAMMA SPECTRA

FIGURE 13

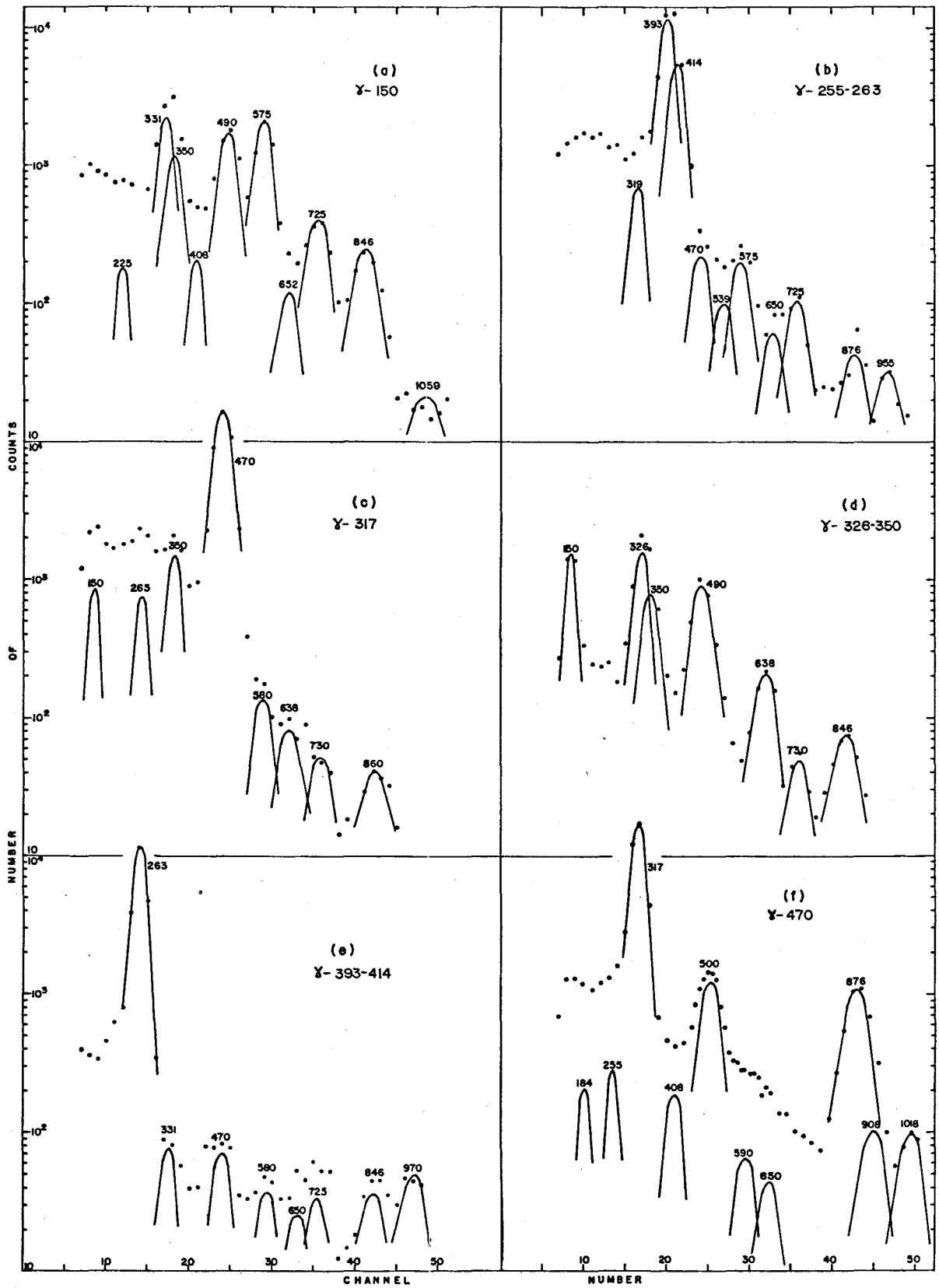

COINCIDENCE SPECTRA

FIGURE 14

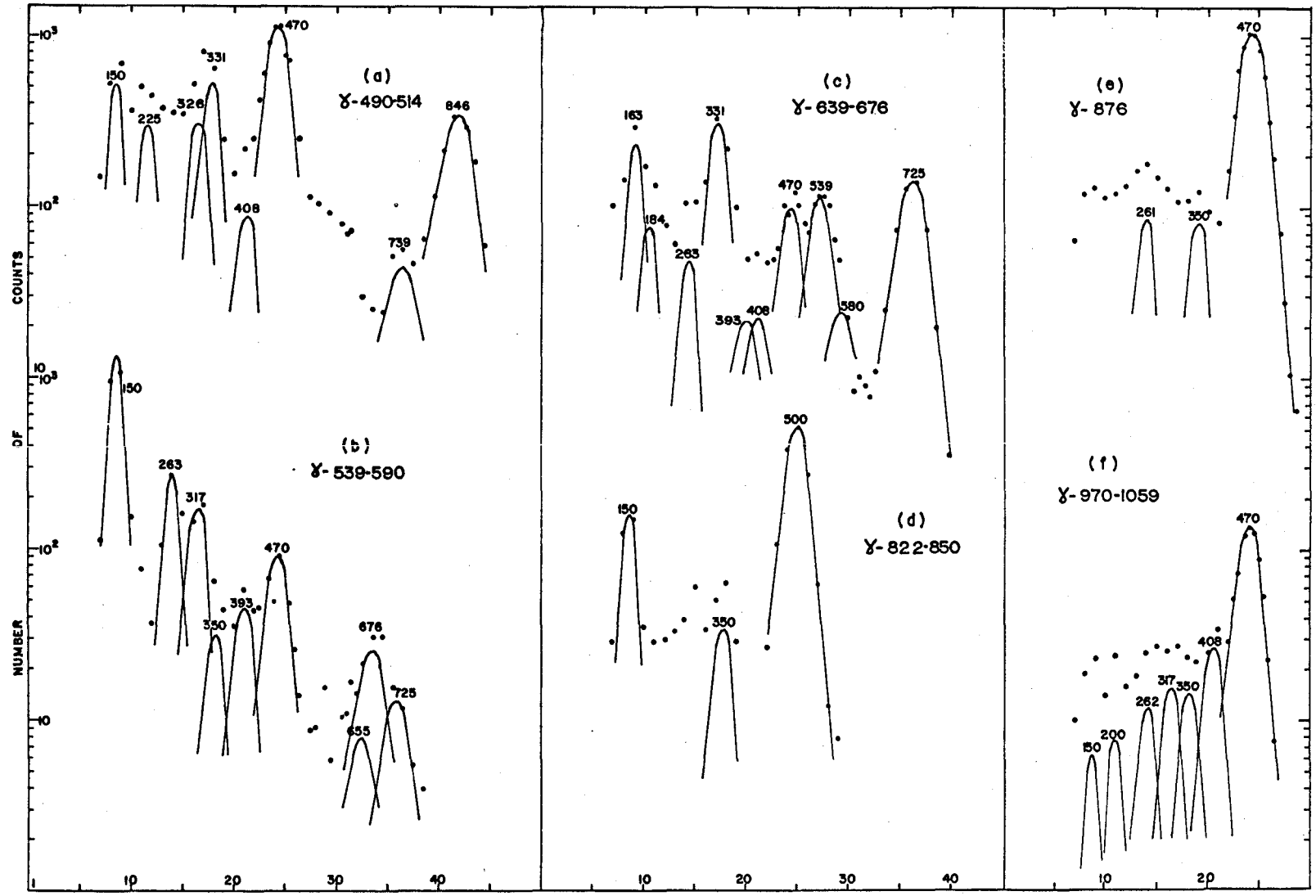

FIGURE 15

COINCIDENCE SPECTRA

ray present in any one photopeak in this spectrum , the curves of Figures 14 and 15 represent the spectra in coincidence with several adjacent gamma rays. The energies of these "gating" radiations are given in the figure. In the terminology used in Chapter III the spectra of Figures 14 and 15 correspond to $M_n'(j) = \sum_{n=1}^{A} B_{mn} L_n(j)$. An analysis of these spectra yields the coincidence probabilities presented as a matrix in Table IV.

The salient features of the spectra of Figures 14 and 15 are discussed below. In this discussion, the entry in brackets listed after each cascade represents its coincidence probability in % as deduced from the decay scheme. These entries are to be compared with the experimentally determined coincidence probabilities tabulated in Tables IV and V.

The spectrum (15f) in coincidence with gamma rays of energy 952.8, 969.4, 1017.2 and 1059.0 keV is dominated by a strong 470 keV peak associated with the 1017.2-469.4 (0.34 $\pm$ 0.02) cascade. The other peaks are almost an order of magnitude weaker and the analysis is quite sensitive to errors in the stripping process. There is evidence here and elsewhere for the 1059.0-489.6-149.2 (0.015 $\pm$ 0.007), the 952.8-262.9 (0.043 $\pm$ 0.014) and the 407.5-969.4 (0.08 $\pm$ 0.02) cascades. The 350 keV peak is probably caused by a 351.8 keV transition of intensity 0.08% which feeds the 969.5 keV level and creates a 351-969.4 (0.04) keV cascade. Evidence for this cascade also appears in the 350 keV "gate" in the Ge-NaI coincidence experiment (Table V). One can account for the 200 and 317 keV peaks by postulating a weak

211 keV transition between the 1697.5 and 1486.6 keV levels and a weak 300 keV transition between the 1269 and 969.5 keV levels but since no other evidence for these exists, they are not included in the decay scheme.

The spectrum in coincidence with gamma rays of energy close to 910 keV (not shown in the figure) reveals a strong 469 keV peak and weak peaks at 262, 315 and 400 keV. The strong peak is associated with the 907.7-469.4 (0.59 ± 0.03) cascade. The weak peaks can all be accounted for by postulating a weak gamma ray in the 900 keV region feeding the 786 keV level. Since in the stripping, along the i axis, the three low energy peaks seemed to be associated with a gamma ray peak of energy 900-950 keV, it is attractive to consider that the coincidences are due to either or both of the 912 or 934 keV radiations associated with transitions involving the 1697.5-785.9 and 1720.2-785.9 levels. The combined intensity of these two radiations would have to be 0.07% to account for the observed coincidence peak. Because there is no other evidence for these two gamma rays, they are not included in the decay scheme.

The strong 470 keV peak in figure 15e is due to the 875.8-469.4 (3.4 ± 0.2) cascade. In addition there is a weak 350 keV peak which can be accounted for by the 845.9-350 (0.08 ± 0.02) cascade, and a weak 261 keV photopeak which is believed to be associated with an 876-262.9 (0.11 ± 0.03) cascade. This 876 keV line must have an intensity of 0.11% and depopulate a level at 1269 ± 10 keV. Further evidence for this line is also shown in the reverse experiment of

Figure 14b. One might have assumed that the 261 keV peak was due to a 261-875.8 keV cascade involving the 1345.2 keV level. However, no evidence for a 260 keV peak which should appear in the Ge(Li)-NaI(Tl) experiments gated on either the 876 or 846 keV full energy peaks is seen and hence the energy has to be different from that of the 875.8 keV transition.

The following cascades are responsible for the main features of the spectrum shown in Fig. 15d; 852.0-469.4 (0.14 ± 0.01), 845.9-499.2 (0.65 ± 0.06), 845.9-350-149.2 (0.08 ± 0.02), 822.1-499.2 (0.17 ± 0.02) and the 822.1-350-149.2 (0.02 ± 0.01) keV cascades. The high point in channel 15 suggests the existence of a gamma ray of energy approximately 280 keV. However, a slight change in the i axis analysis can move the extra counts in this channel to channel 15 of Figure 15e without altering the intensity of the 261 keV line appreciably. There is thus no real evidence for a 280 keV transition.

The spectrum (not shown) in coincidence with the 724.5 keV and the 738.3 keV photons shows a strong peak at 652 keV and a weak peak at 490 keV which are associated with the 652.6-724.5 (0.35 ± 0.02) and the 738.3-489.6 (0.04 ± 0.01) cascades. This spectrum is badly distorted by random adding and chance associated with the fact that the "gate" is set on a very strong ground state transition.

Figure 15c clearly indicates the existence of the following cascades: 652.6-724.5 (0.35 ± 0.02), 539.2-676.4 (0.11 ± 0.04), 407.5-330.9-638.6 (0.03 ± 0.01), 330.9-638.6 (0.25 ± 0.03), 183.6-656.1 (0.02 ± 0.01) and 163.6-676.4 (0.12 ± 0.01). The 580 keV peak is created by the following cascades;

559.5-656.1(0.011 ± 0.003), 652.6-575.3 (0.007 ± 0.002) amd 591.3-656.1 (0.010 ± 0.003). The 263, 393 and 470 keV peaks appear to arise from a gamma ray in the 650 keV region feeding the 786 keV level. Further evidence for this gamma ray is shown in Figures 14b, e and f. The Ge(Li)-NaI(Tl) experiment gated on the 656 ± 8 keV region of the germanium side reveals the same 263 keV peak in the coincidence spectrum. Thus the energy of this radiation must be 656 ± 8 keV and defines a level at 1442 ± 8 keV. These peaks in Fig. 15c are thus due to the 656-316.5-469.4 (0.13 ± 0.05) and the 656-393.4-262.9 (0.05 ± 0.02) cascades. The 316 and 393 coincidence peaks are obscured by other peaks in the spectrum.

The 725 keV peak in Figure 15b is due to chance while other peaks in the spectrum indicate the presence of the following cascades; 575.3-149.2 (1.1 ± 0.1), 559.5-316.5 (0.06 ± 0.02), 591.3-316.5 (0.05 ± 0.02), 539.2-350.2 (0.010 ± 0.004), 559.5-393.4 (0.02 ± 0.01), 591.3-393.4 (0.02 ± 0.01), 559.5-316.5-469.5 (0.06 ± 0.02) and 591.3-316.5-469.4 (0.05 ± 0.02). The origin of the peaks at 655 and 676 keV has already been discussed in connection with Fig. 15c. The 263 keV peak appears to be due to a 575-262.9 (0.13 ± 0.03) cascade beginning from the 969.5 keV level. Evidence for this cascade also appears in the Ge(Li)-NaI(Tl) experiments where a narrow gate set on the 575.3 keV peak allows one to place a limit of 575 ± 5 keV on the energy of the transition responsible for the 263 keV coincidence peak. These coincidences cannot be due to the 575.3 keV transition since it is strongly in coincidence with the 149.2 keV transition and is known

to depopulate the 724.5 keV level from β-γ coincidence measurements. One must thus introduce a gamma ray of energy 575 ± 5 keV and intensity 0.10% into Table II. Part of 0.2% coincidence probability associated with the 263 keV coincidence peak is presumably accounted for by the 559.3-393.4-262.9 (0.02 ± 0.01) and the 591-393.4-262.9 (0.02 ± 0.01) cascades. The residue of approximately 0.16 is in good agreement with the value of 0.10 obtained "cleanly" in the Ge-NaI experiment.

Figure 15a presents evidence for the following cascades which have not already been mentioned; 489.6-149.2 (0.59 ± 0.03), 225.0-499.2 (0.13 ± 0.02), 330.9-489.4 (0.52 ± 0.05), 513.7-326.7 (0.36 ± 0.04), 407.5-499.2 plus 500.4(0.06 ± 0.02), 407.5-330.9-489.6 (0.03 ± 0.01) and 470-499.2 plus 500.4-469.4 (1.6 ± 0.3). The peaks at 739 keV and 846 keV arise from the cascades discussed in connection with the 725 keV gate and the 850 keV gate (Figure 15d).

The coincidences displayed in Figure 14f that have not as yet been mentioned are the 183.6-316.5-469.4 (0.07 ± 0.01), the 255.1-469.4 (0.06 ± 0.01), the 316.5-469.4 (11.7 ± 0.4) and the 407.5-470 plus 469.4 (0.06 ± 0.02). The origin of the peaks at 500, 590, 650, 876 and 1018 keV have already been discussed in connection with Figures 15 a,b,c,e and f respectively. The peak at 908 keV is due to the 908-470 keV coincidences mentioned earlier when discussing the 910 keV "gate"

Evidence for the 393.4 plus 413.5-262.5 (6.7 ± 0.3), the 407.5-330.9 (0.03 ± 0.01) and the 407.5-513.7-326.1 (0.012 ± 0.002) cascades is presented in Figure 14e. The other peaks at 470, 580, 650 and 970 have already been discussed in connection with Figures 14f and 15 b,c,

and f respectively. The 725 keV peak is due to chance. The 846 keV peak is due to the 846-350 keV cascade which has been introduced into this spectrum through cumulative errors in the analysis.

Figure 14d presents evidence for the 330.9-489.6-149.2 (0.52 ± 0.05), 350-149.2 (0.3 ± 0.1) and the 350.2-326.1 (1.1 ± 0.1) cascades. The 730 keV peak is due to chance and the origin of the peaks at 490, 638 and 846 keV has already been discussed in connection with Figures 15 a, c and d. Because of the coarse grid used in these experiments, part of the intensity of both the 150, 350 and 638 keV peaks has been diverted to the spectrum shown in Figure 14c. Corrections for this effect have been taken account of in obtaining the coincidence probabilities of Table IV.

The spectrum in Figure 14c adds no new information but serves to confirm evidence already discussed in connection with other "gates". The peak at 265 keV is believed to be spurious; it is created in the i-axis stripping as a residue after the subtraction of a strong 393 plus 413 keV contribution and a 2% adjustment in the intensity or a 2% adjustment in the line shape for these lines would be sufficient to eliminate this peak. The 730 keV peak is again due to chance. Since the 469.4 keV and the 499.2 keV transitions both have Compton edges rising close to the 316.5 keV peak, a slight error in their line shapes would create the combined 846 and 876 keV peak which appears at 860 keV in this spectrum.

The spectrum of Figure 14b also yields no new information. The 725 keV peak is again due to chance, the 319 keV peak can be explained on the basis of a 2% error in the 469 keV line shape and the remaining

peaks have been discussed in connection with Figure 14e, f and Figure 15 b, c, e and f. All the peaks of Figure 14a have been discussed in connection with other gates except the 725 keV peak which is due to chance and the three weak peaks at 225, 408 and 652 which are believed to be associated with the 225.0-350-149.2 (0.020 ± 0.005), the 407.5-330.9-489.6-149.2 (0.03 ± 0.01) and the 652.6-575.3-149.2 (0.010 ± 0.005) cascades.

Coincidence spectra for "gates" covering the 160-180 and the 225-255 keV regions were also examined but are not presented here. In addition to supporting the data already presented, these give evidence for the following cascades; 245.6-969.4 (0.013 ± 0.005), the 183.6-393.4-262.9 (0.023 ± 0.005) and the 183.6-316.5-469.4 (0.07 ± 0.02).

The coincidence probabilities from all the data are shown in Table IV. The experimental coincidence coefficients agree quite well with the values calculated on the assumption that the decay scheme shown in Figure 18 is correct. The decay of each matrix position in the gamma-gamma coincidence array was followed for about 20 hours to make sure that all the cascades observed belonged to the 4.44 hour ^{105}Ru activity.

A γ-γ coincidence experiment was also carried out using a Ge(Li) detector to feed the i axis and a NaI(Tl) detector to feed the j axis. Because of the poor efficiency of the germanium detector, the statistical accuracy of this data was much poorer than that obtained in the NaI(Tl)-NaI(Tl) experiments. However, the excellent resolution of the germanium detector made it possible to derive useful information from peaks fifty counts high. In order to improve the statistical situation, the coincidences associated with several channels on each peak in the germanium spectrum were summed, and then reduced by the

contributions from an equal number of channels associated with an adjacent portion of the Compton continuum. Whenever the term "gate" is used in connection with the NaI-Ge spectra, it implies that the process described above was carried out; the gate being labelled by the energy of the most prominent gamma ray in it. The data obtained in this experiment were analyzed by the method discussed in Chapter III except for the spectra in coincidence with the 326, 330 and 490 keV peaks. The first two peaks were on the edge of the strong 317 keV peak while the third was very near the strong 676 keV Compton edge. For these three spectra it was necessary to estimate the Compton distribution under the peak and subtract this contribution. The coincidence probabilities derived from this analysis and presented in Table V have uncertainties of at least 20%. The data in Table V also solved a number of ambiguities in the NaI-NaI coincidence results not understood at first. A few typical "gated" coincidence spectra are shown in Figure 16. Results from these and spectra in coincidence with other "gates" will be discussed below.

Figure 16a shows the NaI spectrum in coincidence with a 12 keV "gate" set on the 350 keV gamma ray. This gate contains a triplet of gamma rays of energies 350, 350.2 and 351 keV. The centre member of the triplet is the strongest and hence the only one detected in the Ge(Li) singles spectrum. The 350 keV member is in coincidence with the peaks at 150, 470 and 846 keV, the 350.2 keV member is in coincidence with the 326 keV peak and the 351 keV member is in coincidence with the 970 keV peak. The 263 keV peak is due to the 369.2-262.9 cascade because a few 369 keV pulses are included in the gate.

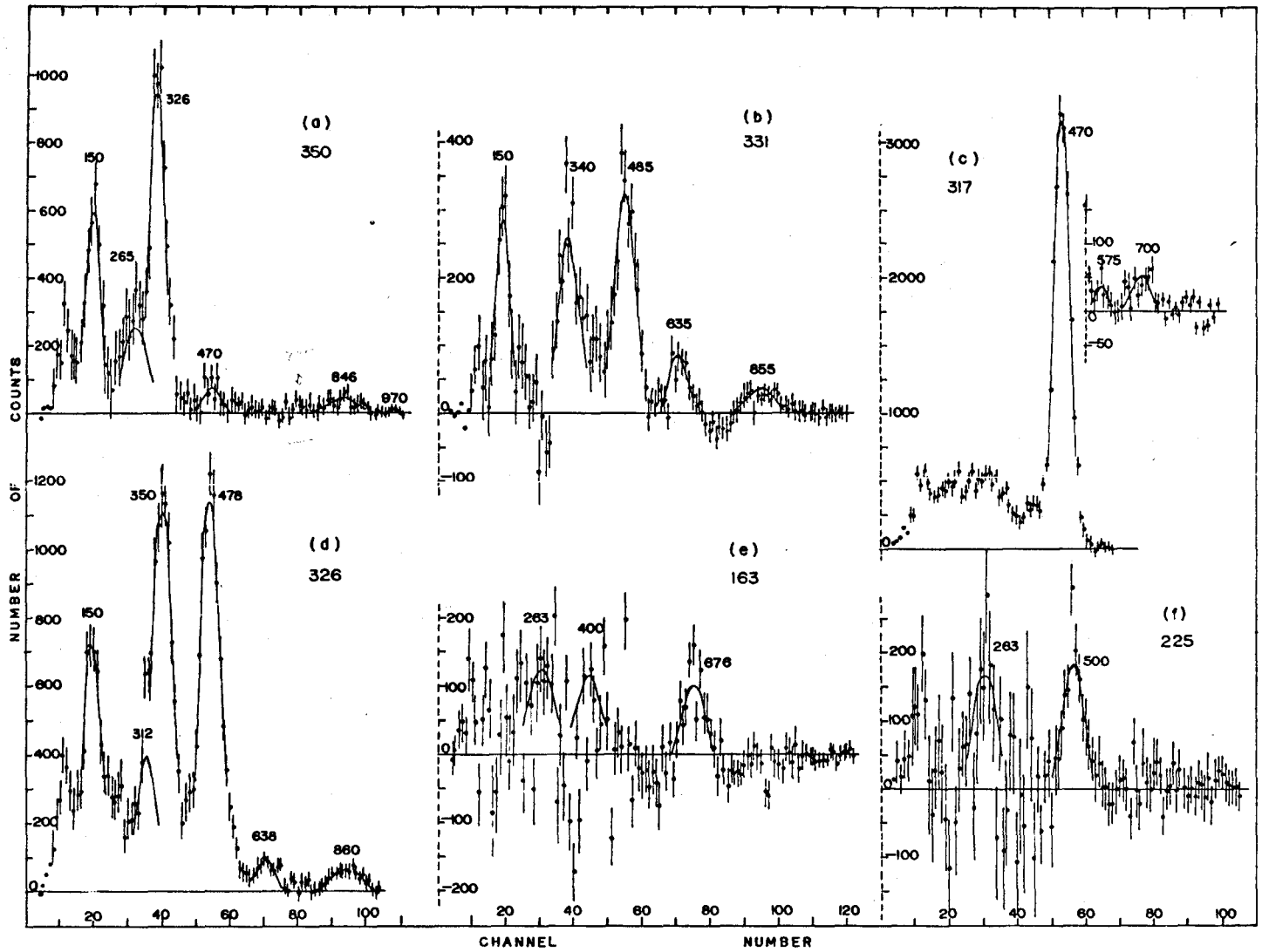

FIGURE 16

GAMMA COINCIDENCE SPECTRA FROM
NaI(Tl)-Ge(Li) SYSTEM

The spectrum in coincidence with a 6 keV gate centered at an energy of 335 keV is shown in Figure 16b. In this spectrum the 150, 485 and 635 keV peaks arise from coincidences with the 330.9 keV photon. The 340 keV peak is due to the combined effect of the 350.2-326.1 and 513.6 Compton edge - 326.1 keV cascades. Finally the weak 855 keV peak arises from the 499.2 Compton edge-845.8 keV cascade.

Figure 16c is the spectrum in coincidence with a 6 keV gate centered on the 317 keV peak. Present is the expected strong 470 keV peak arising from the 316.5-469.5 keV cascade and a weak 575 keV peak due to 316.5 keV photon coincidences with gamma rays of energies 559.5 and 591.3 keV. The 700 keV peak is due to chance.

The spectrum in coincidence with a 6 keV gate centered at 328 keV is presented in Figure 16d. This gate contains appreciable parts of the 330.9 keV and the 326.1 keV gamma rays and a small fraction of the intense 316.5 keV radiation. The 150, 638 and one third of the 478 keV peaks are due to coincidences with the 330.9 keV radiation. The two values listed for the 330.9-489.6-149.2 and the 330.9-638.6 cascades are the values obtained from Figure 16a as well as Figure 16c. The 350 keV peak arises from the 350.2-326.1 keV cascade while the 860 keV peak is due to coincidences between the 875.8 and 845.8 keV radiations and the 469.4 and 499.2 keV Compton edges. The remaining two-thirds of of the 478 keV peak is due to the 316.5-469.4 keV cascades.

Figure 16e shows three peaks which are all in coincidence with the 163.6 keV gamma ray in the gate. Of these, the 414 and 676 keV peaks showed up in the NaI-NaI experiments but the 262.9 peak which arises

from the 163.6-413.5-262.9 cascade was missed.

In Figure 16f only two peaks are observed which are a result of 393.4 Compton edge-262.9 and the 225.0-499.2 coincident events.

The Ge-NaI data produced clear evidence for a number of cascades in spectra which have not been presented in this thesis. A gate set on the 149 keV peak revealed the existence of the 738.3-489.6-149.2 (0.04) cascade in addition to a number of the cascades revealed by the data of Figure 16. The 414 gate showed evidence for the 539.2-413.5 (0.02) coincidences and the 591 keV gate revealed the existence of the 591.3-316.5-469.4 (0.06) keV triple cascade. Gates at 1221 and 1251 keV showed up the 1221.2-499.2 (0.02) and the 1250.9-469.4 (0.02) coincident pairs.

The measurement in the probability matrix at the 653 (Ge)-164(NaI) position is due to a 183.6-656.1 cascade which showed up only in the spectrum in coincidence with a germanium gate at 653 $\pm$ 12 keV. The symbol TR for "trace" indicates that rather insecure evidence was found for a 1059 keV peak in the 639 keV germanium "gate". No coincidences were observed with the 1321.3 and 632.3 keV germanium "gates" thus suggesting that these gamma rays feed either the ground state or the 129.7 keV metastable state.

With the germanium "gate" set on the 822.1 keV gamma ray, peaks appear at 499, 350 and 150 keV indicating that the 822.1 keV radiation feeds the 499.2 keV level. However, the 150 keV peak appeared to be too strong and as the "gate" was widened from 12 keV to 18 keV its intensity increased relative to the other two peaks.These effects can be explained by postulating a second 822 keV radiation of intensity 0.012 % which feeds

the 149.2 keV level. It presumably is the transition from the 969.5 keV state.

The Ge-NaI coincidence experiment clarified the portion of the decay scheme involving the two 470 and two 499 keV radiations. A sketch of this portion of the scheme is given below. The 845 keV germanium

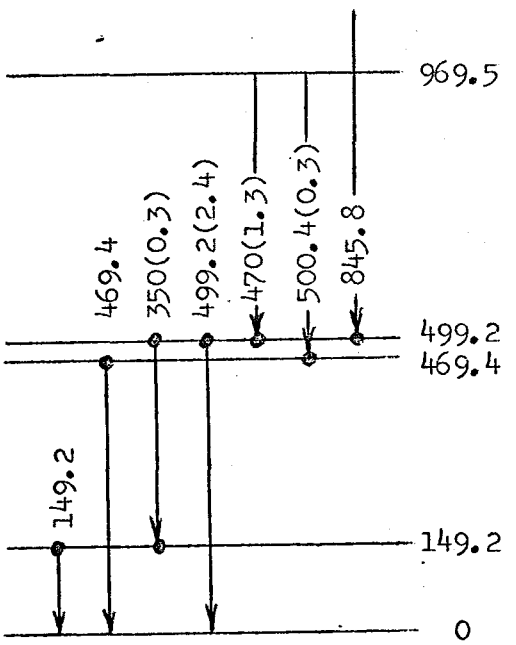

"gated" spectrum yields a value of $(\delta_{845.8\text{-}499.2})/(\delta_{845.8\text{-}350\text{-}149.2})$. Other values for this ratio can be found from the reversed experiments. The mean value of all these experiments is 8 ± 2. From the 350 keV germanium "gate" one obtains a value for $\delta_{470\text{-}350}$ of $0.12 \pm 0.02\%$ while a mean obtained from the 470 and 499 germanium "gates" yields

$$\delta_{470\text{-}499.2} + \delta_{500.4\text{-}469.4} = 1.6\%$$

Combining these measurements, one finds that

$$\delta_{470\text{-}499.2} = 1.0 \pm 0.2\%$$

and $$\delta_{500.4\text{-}469.4} = 0.6 \pm 0.2\%$$

The intensity of the 500.4 keV radiation derived in this fashion is thus $0.6 \pm 0.2\%$, in agreement with the value of $0.30 \pm 0.05\%$ found by analysing the 500.4 + 499.2 keV doublet in the germanium singles spectrum.

The spectra obtained in these experiments would have been improved in quality had it been possible to preserve an adequate counting rate and still avoid a set up with 180^{o} close geometry. In this geometry, Compton edges were accentuated and often created peaks which complicated the interpretation.

5.3.2 Beta Gamma Coincidence Studies

The results of the beta-gamma coincidence experiments described in Chapter III are presented in Table VI. The spectra from which these data were derived are shown as Fermi plots in Figure 17. The energies in the first column of Table VI are those of the coincident gamma ray while those in the second column are beta end-points. The third column presents the NaI(Tl) detector efficiencies upon which the analysis depends, the fourth gives the absolute intensity of each beta group and the final column denotes the level fed by each group. The end-points and intensities of the three highest energy beta groups as measured from the beta singles spectra are also presented.

A large number of gamma rays listed in column one are ground state transitions, as evidenced by the fact that the sum of the beta end-point energy and the gamma ray energy is equal to approximately 1920 keV. The position of most of the gamma rays in the decay scheme was established by γ-γ coincidence measurements; the exceptions are the gamma rays of energies 806.2, 1215.2, 1321.3, 1697.4 and 1720.2 keV whose position in the decay scheme has been established by the β-γ experiments alone. The decay energy can in principle be established from every beta end-point in Table VI. However, the errors on some of these

TABLE VI

Results of β-γ Coincidence Experiments and β Singles Experiments

(keV) Component	(keV) End Point	NaI(Tl)$\varepsilon\omega$	β-Group intensity(%)	(keV) Level Fed
Singles Spectrum	1450 ± 10 1780 ± 20 Ground State		1.9 ± 0.3 0.28 ± 0.07 < 0.02	469.4 129.7 0
149.2	1179 ± 45	0.0140	0.5 ± 0.3	724.5
262.9	1553 ± 17 1121 ± 5	0.0195	0.10 ± 0.03 5.9 ± 0.2	392.6 785.9 and 806.1
316.5	1134 ± 4*	0.0211	10.7 ± 0.4	785.9
350.2	1121 ± 35	0.0222	2.2 ± 0.4	806.1
393.4	1141 ± 7*	0.0230	2.7 ± 0.6	785.9
413.5	1119 ± 9*	0.0235	3.3 ± 0.6	806.1
469.4	1457 ± 5* 1151 ± 7 895 ± 45 529 ± 17	0.0246	1.4 ± 0.1 9.9 ± 0.5 3.9 ± 0.2 6.3 ± 0.3	469.4 785.9 1345.2 1486.6
499.2	975 ± 43 492 ± 24	0.0247	1.7 ± 0.4 2.1 ± 0.5	969.5 1345.2
575.3	1182 ± 10*	0.025	1.0 ± 0.4	724.5
652.6	573 ± 34	0.0254	0.9 ± 0.4	1377.1
676.4	1109 ± 5*	0.0255	16.5 ± 0.8	806.1
724.5	1187 ± 2*	0.0256	48.2 ± 2.5	724.5
806.2+822.1	1142 ± 7 612 ± 39	0.0259	0.4 ± 0.2 0.7 ± 0.4	806.1 1321.3
875.8	567 ± 8*	0.026	4.0 ± 0.2	1345.2
907.7	563 ± 26	0.0261	1.0 ± 0.3	1377.1
969.4	952 ± 5* 527 ± 21	0.0261	2.1 ± 0.2 0.7 ± 0.3	969.5 1377.1
1017.2	428 ± 16*	0.0262	0.39 ± 0.04	1486.6
1215.2	683 ± 36	0.0263	0.096 ± 0.010	1215.2
1321.3	552 ± 15	0.0262	0.31 ± 0.03	1321.3
1697.4 and 1720.2	199 ± 2	0.025	0.15 ± 0.02	1697.5 and 1720.2

*Values used to obtain the total decay energy of 1916 ± 4 keV

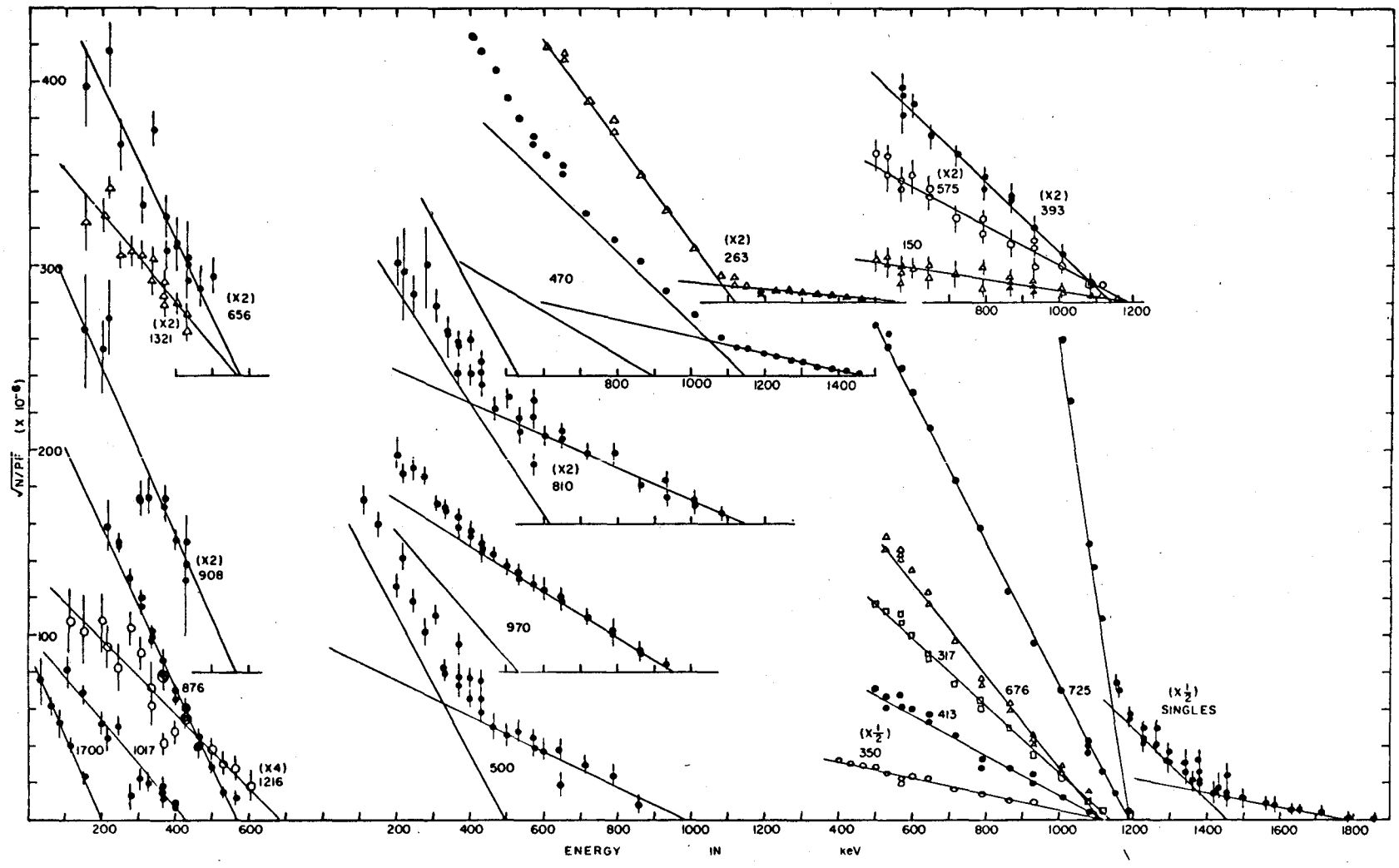

FIGURE 17

SINGLES AND BETA—GAMMA FERMI PLOTS

are rather large or the end points are distorted because more than one gamma ray contributed to the coincidence spectrum. The entries marked with an asterisk represent the best data; the weighted mean of the end point values derived from these is 1916 ± 2 keV. When uncertainties in the calibration are included, the limits of error on the decay energy are increased to 4 keV.

The end points and intensities of the low energy inner beta groups of the β-γ coincidence spectra are unreliable, both because of cumulative errors in analysis and because there is a certain amount of electron scattering from the walls of the spectrometer which tends to increase the number of low energy electrons. This effect was minimized by using a "window" on the beta pulse distribution but the effect could not be entirely removed. This distortion could have been partially due to source thickness, but this did not seem to be an important contributor to the effect since even at the 129-K conversion peak, only approximately 10% of the counts showed up in the "tail". Because of this effect the intensities and energies of the inner beta groups have not been given much weight.

It should be noted that there was no measurable beta intensity feeding the ground state, in marked disagreement with some of the earlier work.

5.4 The Decay Scheme

The results of the measurements discussed above are incorporated in the decay scheme shown in Figure 18. In this figure observed gamma-gamma coincidences are indicated by full circles at the level between the

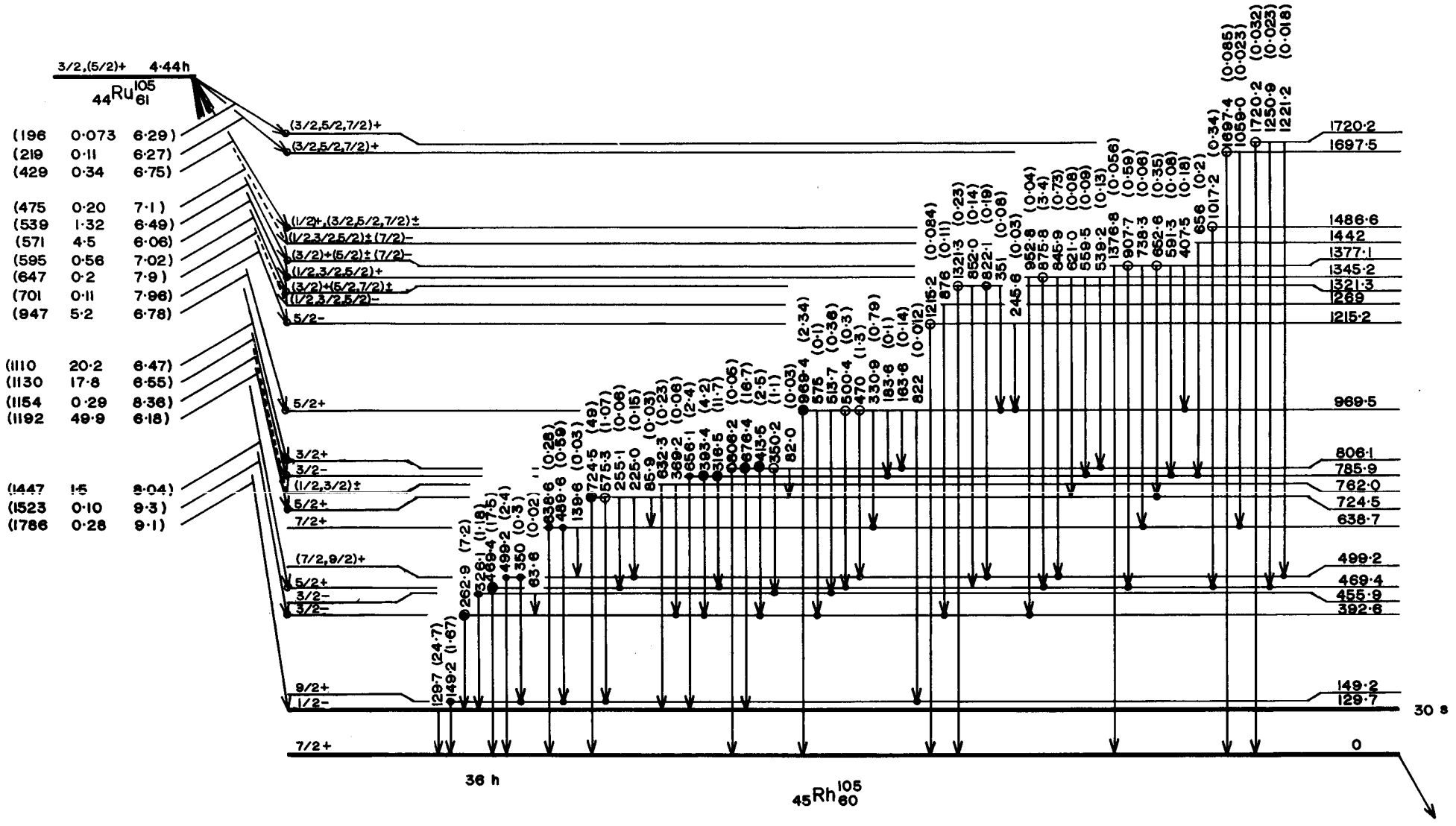

FIGURE 18 DECAY SCHEME OF $^{105}Ru \longrightarrow ^{105}Rh$

two members of the cascade. An observed coincidence between a beta ray and a gamma ray is shown on the gamma transition involved by an open circle. The energies of the transitions are given in keV and the intensities in %.

The transitions of energy 63.6, 82.0, 85.9, 129.7, 139.6, 621.0, 632.3, 806.2 and 852.0 keV have been placed in the decay scheme by energy fit alone. Some of these were intense enough to have been seen in coincidence experiments but were masked by stronger gamma rays of nearly the same energy. The weak radiations of energy 350, 351, 470, 575, 656, 822 and 876 keV have been positioned in the decay scheme to satisfy the coincidence data, but were not observed in the germanium detector measurements. All the rest of the gamma rays shown in the decay scheme were observed both in the singles and coincidence measurements and have been located to satisfy both the energy fit and the coincidence information.

Another test of the decay scheme is revealed by the intensity balance of Table VII. This table compares the net flow of transition intensity out of each level with the observed flow of beta intensity into the level. The radiation flow is simply the difference between the transition intensity de-exciting the level and that feeding it. This will be in error if weak gamma transitions in the decay scheme are missed. The beta intensity feeding each level was deduced from the absolute β-γ coincidence probabilities or, in a few cases, from the Fermi analysis of the singles spectrum.

Since the entry in column three is formed by summing all the β-γ coincidence probabilities for gamma rays de-exciting the level and since the β-γ

TABLE VII

Intensity Balance for the Levels in ^{105}Rh

Level	Gamma Intensity Out - Gamma Intensity In	β Feed Intensity with Appropriate Gamma Ray	$Log_{10}f_0t$
1720.2	0.073 ± 0.005	} 0.15±0.02 (1720.2 and 1697.4)	6.29 ± 0.07
1697.5	0.108 ± 0.009		6.27 ± 0.08
1486.6	0.340 ± 0.017	0.39 ± 0.04 (1017.2)	6.75 ± 0.08
1442 ± 8	0.20 ± 0.05		7.1 ± 0.1
1377.1	1.32 ± 0.04	1.0±0.3(907.7)+0.9±0.4(652.6) = 1.9± 0.5	6.49 ± 0.05
1345.2	4.47 ± 0.15	4.0 ± 0.2(875.8)	6.06 ± 0.05
1321.3	0.560 ± 0.016	0.31±0.03(1321.3)+0.7±0.4(822.1) = 1.0 ± 0.4	7.02 ± 0.06
1269±10	0.20 ± 0.05		7.9 ± 0.3
1215.2	0.113 ± 0.011	0.096 ± 0.010 (1215.2)	7.96 ± 0.08
969.5	5.22 ± 0.16	2.1±0.2(969.4)+1.7±0.4 (499.2 and 500.4)=3.8±0.5	6.78 ± 0.05
806.1	20.2 ± 0.7	16.5±0.8(676.4)+3.3±0.6 (413.5) +2.2±0.4 (350.2)=22.0±1.1	6.47 ± 0.04
785.9	17.8 ± 0.5	2.7±0.6 (393.4)+10.7±0.4(316.5) =13.4±0.7	6.55 ± 0.04
762.0	0.29 ± 0.05		8.36 ± 0.08
724.5	49.9 ± 2.0	48.2±2.5(724.5)+1.0±0.4(575.3) =49.2±2.5	6.18 ± 0.04
638.7	-0.01 ± 0.05		> 9.3
499.2	0.37 ± 0.23		> 8.6
469.4	1.1 ± 1.1	1.4±0.1(469.4)or 1.9±0.3 (Singles)	8.04 ± 0.08
455.9	-0.34 ± 0.12		> 9.2
392.6	0.29 ± 0.35	0.10 ± 0.03 (262.9)	9.27 ± 0.12
149.2	-0.29 ± 0.09		> 9.5
129.7	-3.0 ± 2.5	0.28 ± 0.07 (Singles)	9.08 ± 0.20
Ground State		< 0.02	> 10.4
Total	98.9 ± 3.5%		

measurements were unable to pick up weak transitions, these entries are likely to be on the low side.

In general, the agreement between columns 2 and 3 is excellent; in the few cases where there are discrepancies they can be readily accounted for by missed transitions in column 3.

The total gamma intensity of 98.9 $\pm$ 3.5% is consistent with the quoted error in the absolute intensity for the 725 keV transition.

Column 4 presents the log $f_o t$ values calculated for the partial beta transitions to each of the ^{105}Rh levels. These were deduced from the gamma intensities except for the 469.4, 392.6 and 129.7 and ground states. In these cases the measured beta intensities of column 3 were used.

5.4.1 The Decay of $^{105}Rh \longrightarrow {}^{105}Pd$

The ground state of ^{105}Pd has been determined to be 5/2+ from the hyperfine structure of the atomic states of palladium (Blaise and Cantrel (1953)). The decay of $^{105}Rh \longrightarrow {}^{105}Pd$ has been investigated by many workers whose results are summarized in the Nuclear Data Sheets (1966). More recently Karlsson et al (1964) and Pierson (1965) have examined this decay. The latter author carried out a very complete study and presented the decay scheme shown below. The present measurements confirm the results they obtained for the gamma ray energies and intensities of the four most energetic lines.

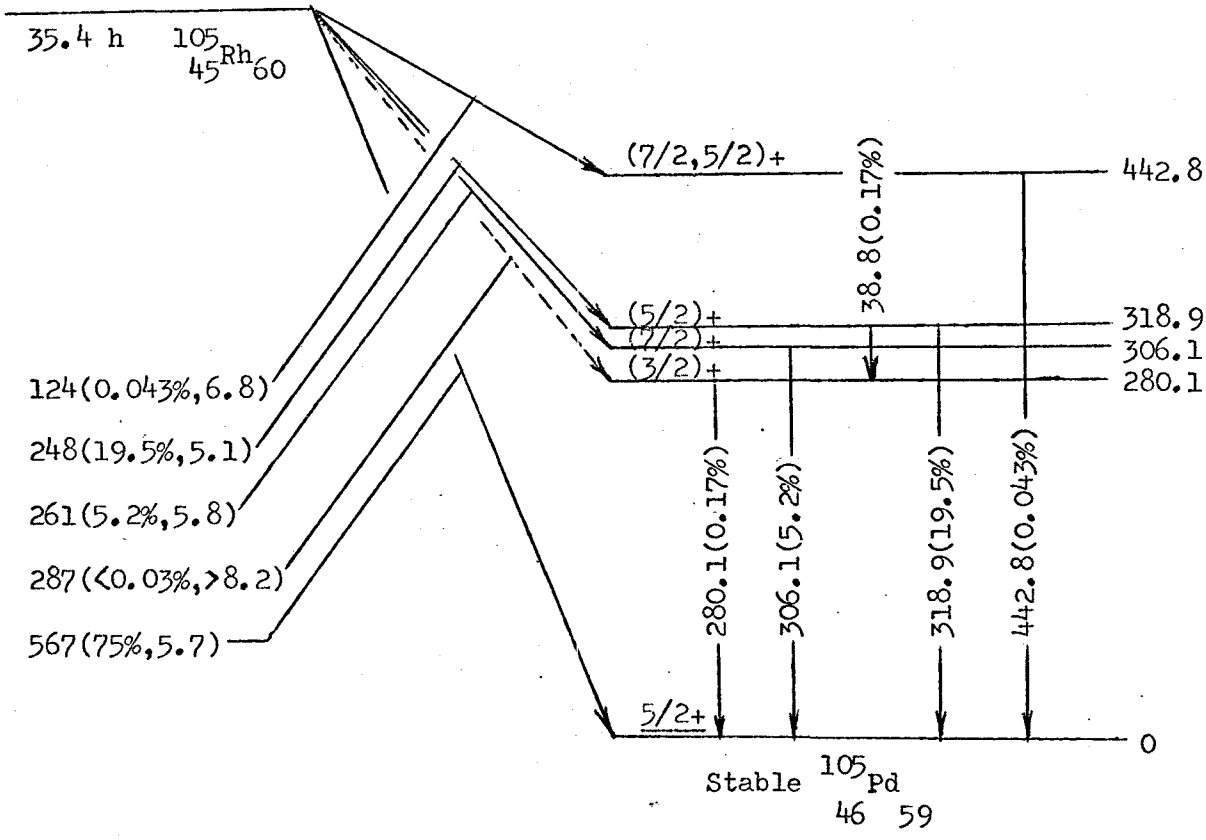

Fig. 19 Decay Scheme of $^{105}Rh \longrightarrow {}^{105}Pd$

Pierson discussed in detail the possible spin assignments for the excited states of ^{105}Pd and the ground state of ^{105}Rh. He concluded that the ground state spin of ^{105}Rh must be 7/2+, basing this conclusion on Coulomb excitation data, the decay of ^{105}Ag to levels in ^{105}Pd, $\log_{10} f_o t$ values and the absence of a beta feed to the 280.1 keV level. It seems to the present author that Pierson has not totally excluded the possibility of a 5/2+ assignment for the ground state of ^{105}Rh. His argument that a $\log_{10} f_o t$ value of > 8.2 for the beta feed to the 280.1 keV level of spin 3/2+ means that the spin of ^{105}Rh cannot be 5/2+ is reasonable but not conclusive, since nuclear structure effects can be enough to increase the $\log_{10} f_o t$ value from a value near 6 to the observed

lower limit of 8.2. Thus one must open the discussion of spins in the ^{105}Ru to ^{105}Rh decay with one piece of secure information: that the ground state spin of ^{105}Rh is either 5/2+ or 7/2+ with the 7/2+ value favored.

5.4.2 The Spins and Parities of Levels in ^{105}Rh

The 129.7 keV transition is known to be E3 in character. Hence, the ground state and the 129.7 keV level must differ in spin by three units and also differ in parity. The 5/2+ choice for the ground state leads to a 11/2- assignment for the upper level while the 7/2+ choice permits either a 1/2- or 13/2- assignment for the isomeric level. The ground state spin of ^{103}Rh has been measured to be 1/2 and the magnetic moment suggests that it has negative parity. ^{103}Rh has a 57 minute isomer 40 keV above the ground state which is de-excited by an E3 transition. Thus one expects to find low lying levels of spins 7/2+ and 1/2- in both ^{103}Rh and ^{105}Rh, and one is led to the 1/2- assignment for the 129.7 keV state in ^{105}Rh. This choice is supported by the shell model since there are no low-lying 11/2- or 13/2- states expected for Z = 45. One concludes that the 1/2-, 7/2+ pair in ^{103}Rh is also found in ^{105}Rh but that the order of the two states has been reversed by the addition of two neutrons in going from ^{103}Rh to ^{105}Rh.

The 149.2 keV ground state transition was measured to be M1 + E2 thus indicating that the 149.2keV state has possible Jπ values of (5/2, 7/2 or 9/2)+. The 9/2+ choice seems logical by comparison

with ^{103}Rh which has a low lying 9/2+ state. This choice is also supported by internal evidence which will be presented later.

The E1 nature of the 676.4 keV transition feeding the 1/2-, 129.7 keV level limits the Jπ choice for the 806.1 keV level to either (1/2 or 3/2)+. On the assumption that the 806.2 keV transition to the 7/2+ ground state has $L \leq 2$, the choice can be limited to the 3/2+ value. It is interesting to note that the E1 transitions, 676.4, 413.5 and 350.2 keV from this level to the 1/2-, 129.7 keV level , the (1/2 or 3/2)- 392.6 keV level and the (1/2 or 3/2)-, 455.9 keV levels respectively have intensity ratios 1:0.15:0.072 similar to those obtained using Weisskopf single particle estimates; namely 1:0.22:0.11 if all the negative parity states have spin 1/2 and 1:0.05:0.02 if the 392.6 and 455.9 keV levels have spin 3/2. At the same time, if one assumes that the 806.2 keV transition is E2, its transition rate is greater than the single particle estimate by a factor of 50. While these arguments do not help to limit the spin choices for the 392.6 and 455.9 keV levels, they do suggest that the 806.2 keV transition may be somewhat collective in nature or the E1 transitions are hindered to this degree.

The 656.1 keV transition feeding the 1/2-, 129.7 keV level is M1 and/or E2 in character. If one assumes the extreme situation in which it is pure E2, then the possible Jπ values for the 785.9 keV level are restricted to the values $\leq 5/2-$. These values are consistent with the M1 and/or E2 character of the 393.4 keV transition from the 785.9 keV to the (1/2 or 3/2)-, 392.6 keV level. The

absence of the ground state transition from the 785.9 keV level makes the 5/2- choice for this level unlikely since a 5/2- assignment would permit an E1 transition to the 7/2+ ground state. From the data this transition has an upper limit in intensity of 0.02%, a factor of at least 10^5 smaller than one would have expected using single particle estimates with the $5/2 \longrightarrow 5/2+$ (E1) 316.5 keV transition as a guide or 10^7 with the (E2) 656.1 keV transition as a guide .

The M1 and/or E2 character of the 469.4, 499.2, 724.5 and 969.4 keV ground state transitions limit the $J\pi$ values for the levels defined by these transitions to the choices $3/2+ \leq J\pi \leq 11/2+$ for the extreme case in which all the transitions are assumed to be E2. The absence of observable transitions from these levels to the 1/2-, 129.7 keV state leads one in each case to reject the 3/2+ choice. Upper limits for the intensities of these four transitions are 0.06%, 0.06%, 0.04% and 0.01% respectively as set by the present experiments. These intensities are at least 10^6, 10^6, 10^7 and 10^6 times weaker respectively than what one would have expected on single particle estimates if the spins of these states had been 3/2+ using the E2 transition to the ground state as the reference value in each case. The 7/2+, 9/2+ and 11/2+ choices for the 969.5 keV level are eliminated by the M1 + E2 character of the 163.6 keV transition which feeds the 3/2+, 806.1 keV state. These arguments thus favour the 5/2+ assignment to the 969.5 keV level.

The E1 nature of the 316.5 keV photon, makes it possible to further restrict the spin choices for the 785.9 keV and 469.4 keV levels. The spin of the former of these states has already been re-

stricted to (1/2 or 3/2)- while the spin of the latter is limited by the expression $5/2+ \leq J\pi \leq 11/2+$. The nature of the 316.5 keV transition immediately defines the spins of these states to be 3/2- and 5/2+ respectively.

If one makes the reasonable assumption that both the 470 and the 255.1 keV transitions have a multipolarity of two or less, the 11/2 spin choice for both the 499.2 and the 724.5 keV levels are rejected leaving available the choices (5/2, 7/2 or 9/2)+ for each of these states. For the 725 keV level, the 5/2+ choice seems to be preferable using the arguments of the next paragraph. For the 499.2 keV level, the 5/2+ choice can be rejected both because there is no observed E1 transition from the 3/2-, 786 keV level and because the 350 keV transition is $\sim 10^3$ times stronger than one would expect if it were E2.

One can argue that the 149.2 keV level must be 9/2+ in character on the basis of the relative intensities of the transitions feeding this level and the ground state from the 5/2+, 969.5 keV level. The fact that the former is 200 times as strong as the latter suggests that the former is mainly M1 and the latter E2. This being so, the 149.2 keV level must be a 9/2+ state. The intensity difference between the 724.5 keV (49%) and the 575.3 keV(1.1%) transitions from the 724.5 keV level to the 7/2+ ground state and the 9/2+, 149.2 keV level can be explained by the former being mainly M1 in character with the latter being pure E2 in character. This enables one to choose 5/2+ for the 724.5 keV level.

From the M1 nature of the 330.9 keV transition and the 5/2+ favored value for the 969.5 keV level,

the Jπ choice for the 638.7 keV level is limited to 5/2+ or 7/2+. The 3/2+ value has been rejected by the argument that no transition to the 1/2-, 129.7 keV level was observed (an upper limit for the intensity of this transition is 0.05% which corresponds to a reduction in intensity for this radiation of more than 10^5 over that expected for an E1). The spin of the 638.7 keV level is further restricted to 7/2+ by assuming that the 489.6 keV (0.59%) and the 638.6 keV (0.28%) transitions to the 9/2+, 149.2 keV level and the 7/2+ ground state are a mixture of M1 and E2.

The 262.9 keV and the 326.1 keV transitions to the 1/2-, 129.7 keV level are both M1; this information restricts the Jπ choice for the 392.6 keV and the 455.9 keV states to (1/2 or 3/2)-. The fact that there are reasonably strong transitions to these states from the 5/2+, 969.5 keV state argues strongly against the 1/2- assignment, since such a spin assignment would require these transitions to be M2 in character. Their observed intensity pattern is reasonable if they are E1.

Assuming that the transitions from the 762 keV level have $L \leq 2$ permits the values of $1/2^{\pm}$, $3/2^{\pm}$ or 5/2- to be postulated for it since this state de-excites only to the 3/2-, 392.6 keV and the 1/2-, 129.7 keV levels. The 5/2- value is not favored due to the absence of an E1 transition to the 7/2+ ground state (an upper limit of 0.03% can be set for this transition which corresponds to a reduction in intensity for this radiation by at least a factor of 10^6).

The parity of the 1345.2 keV level is determined to be positive from the nature of the 875.8 transition de-exciting this level to the 469.4 keV level.

By making use of the Jπ assignments deduced above, one can roughly determine the transition intensities between all these states using single particle estimates. These intensity estimates are in reasonably good agreement with the observed photon intensities measured in this work. These estimates were made on the assumption that transitions accompanied by a change in parity have been hindered by a factor of approximately one hundred compared to those involving no parity change. This factor was established by comparing the E1 and M1 or E2 transitions from the 806.1 keV and the 785.9 keV levels.

Because there are a number of low lying levels with different spin values and also since all the levels fed have to satisfy the beta decay selection rules and therefore cannot differ too widely in Jπ values, the assumption that the transitions from the higher energy levels must have $L \leqslant 2$ is not unreasonable. The possible spin values are given in brackets for the following levels above the 969.5 keV state using the favored spin values of the lower energy states:

1720.2 (3/2+, $5/2^{\pm}$, $7/2^{\pm}$ or 9/2-) by virtue of the transitions to the 7/2+ ground state and the 5/2+, 469.4 keV level.

1697.5 (3/2+, $5/2^{\pm}$, $7/2^{\pm}$, $9/2^{\pm}$ or 11/2+) by virtue of the transition to the 7/2+, ground state.

1486.6 (1/2+, $3/2^{\pm}$, $5/2^{\pm}$, $7/2^{\pm}$, 9/2+) by virtue of the transition to the 5/2+, 469.4 keV level.

1442 ($1/2^{\pm}$, $3/2^{\pm}$, $5/2^{\pm}$, 7/2-) by virtue of the transition to the 3/2-, 785.9 keV level.

1377.1 (3/2+, 5/2±, 7/2-) by virtue of the transitions to the 7/2+, ground state, 5/2+, 469.4 keV state, and the 3/2-, 785.9 keV level.

1345.2 (1/2+,3/2+, 5/2+) by virtue of the transitions to the 5/2+, 469.4 keV level and the 3/2-, 392.6 keV level.

1321.3 (3/2+, 5/2±, 7/2±, 9/2+) by virtue of the transitions to the 7/2+ ground state and the 5/2+, 469.4 keV level.

1269 (1/2±, 3/2±, 5/2±, 7/2-) by virtue of the transition to the 3/2-, 392.6 keV level

1215.2 (3/2+, 5/2±, 7/2±, 9/2+) by virtue of the transitions to the 7/2+ ground state and the 5/2+, 969.5 keV state.

The allowed $\log_{10} f_0 t$ values for the beta transitions to the 3/2+, 806.1 keV level and the 5/2+, 724.5 keV level limit the Jπ value for the ^{105}Ru ground state to be 3/2+ or 5/2+ with the 3/2+ choice favored due to the absence of an appreciable amount of beta decay to the 7/2+ ground state and the 7/2+, 638.7 keV level. The $\log_{10} f_0 t$ values for the beta transitions to levels below 1000 keV agree fairly well with the predicted Jπ values. No arguments about the absence of expected transitions to any state above 1250 keV will be used since most of the transitions from these levels are close to the limits of detection. The allowed $\log_{10} f_0 t$ values for the beta transitions to the 1720.2 keV and the 1697.5 keV levels limit the Jπ values of these levels to (3/2, 5/2 or 7/2)+. The 9/2+ values for the 1486.6 keV, 1321.3 keV and the 1215.2 keV levels are eliminated due to the fact that the beta transitions to these levels are either allowed or first forbidden as determined by their $\log_{10} f_0 t$ values. The $\log_{10} f_0 t$ values for the beta transitions to the 1269 and the 1215.2 keV levels

are rather high to be allowed and these transitions are assumed to be first forbidden. With this assumption the Jπ assignments to these levels can be (1/2, 3/2 or 5/2)- and (5/2 or 7/2)- respectively. The 5/2- choice for the 1215.2 keV level is favored because of the absence of transitions to the 9/2+, 149.2 keV and the 5/2+, 469.4 keV states.

The arguments that have been used above in the determination of the favored Jπ assignments for a state have often been based on single particle estimates, on the absence of a transition or on $\log_{10} f_0 t$ values. These are all admittedly weak arguments since nuclear structure effects can greatly influence the transition probabilities. However, in the absence of any other information, it seems justifiable to carry the argument as far as possible, without denying the possibility that some of the assignments may turn out to be incorrect.

5.4.3 A Comparison with Previous Investigations

The work of Saraf et al (1960), Ricci et al (1960) and Brandhorst (1961) revealed only the more intense transitions in the ^{105}Ru decay and established a few of the more abundantly populated levels found also in the present study. Ricci and Brandhorst report a 210 keV gamma ray based on observed 210-470 keV coincidences. Such coincidence events could be due to Compton back-scattering of the strong 725 keV radiation detected in one detector into the other detector, if the experiment was done in 180° geometry. It is significant that this peak was not found by Saraf who used an anti-Compton

shield between the detectors or in the present work which used a 90^{o} geometry.

Brandhorst and Saraf both observed a 1350 keV radiation which is believed to be entirely due to coincidence summing of the 876 keV and 470 keV photons. Brandhorst also observed a strong 10% beta transition to the ground state which is believed to be due to beta-gamma summing in the plastic detector. Results from a magnetic spectrometer such as the one used in the present work, cannot be distorted by such summing effects.

The gamma-gamma angular correlation results of Arya (1963) cannot be given much weight because the pattern for their "320-475" keV cascade is really created by three cascades, namely, 11.7% (316.5-469.4 keV), 0.52% (330.9-489.6 keV) and 0.36% (513.7-326.1 keV). Similarly their so-called "485-475" keV cascade is due to a mixture of the 1.3% (470-499.2 keV) and 0.3% (500.4-469.4 keV) correlation patterns. The same statements are applicable to the angular correlation studies of Neeson and Arns (1965) involving the same cascades. Inasmuch as the results of Arya and Neeson and Arns for the same cascades are not in agreement and since neither of the authors describe what precautions were taken to analyze the contents of the gates in their spectra, it is difficult to take either set of results seriously. Finally, Neeson and Arns (1965) obtained information on a "317-148 keV" cascade. The present work shows that no such cascade exists; it appears that the coincidences they observed can be attributed to the 0.52% (330.9-489.6-149.2) keV triple cascade.

5.4.4 The Interpretation of the Levels of ^{105}Ru

No firm model dependent predictions of the levels in this decay can be made. However, it is probably worthwhile to outline the arguments and tentative conclusions that can be reached. In principle, one can attempt to describe these levels in terms of the shell model or in terms of the Nilsson model. While both are difficult to apply, the former seems to be more applicable than the latter. In the reasoning that follows, it has been assumed that if there are two states with the same Jπ value resulting from the coupling of particles in one subshell, the one with the lowest seniority will be more stable.

The ground state of ^{105}Ru has been established to be either 3/2+ or 5/2+ with the former choice more likely. The ground state configuration has eleven neutrons distributed between the $d_{5/2}$ and $g_{7/2}$ subshells. Thus in principle, it can be described by any one of the following four configurations (i)$(d_{5/2})^6(g_{7/2})^5$, (ii)$(d_{5/2})^5(g_{7/2})^6$, (iii) $(d_{5/2})^4(g_{7/2})^7$ or (iv) $(d_{5/2})^3(g_{7/2})^8$. In terms of the M-scheme of coupling described by de Shalit and Talmi (1963), these configurations should yield low lying states as follows for the four configurations

(i) v = 1, Jπ = 7/2+ ; v = 3, Jπ = 5/2+; and v = 3, Jπ = 3/2+

(ii) v = 1, Jπ = 5/2+

(iii) v = 1, Jπ = 7/2+ and

(iv) v = 1, Jπ = 5/2+, v = 3, Jπ = 3/2+

Of these four configurations, the most stable one might be expected to be the last since it contains a completed $g_{7/2}$ subshell and there-

fore presumably gains the most stability from pairing energy. Thus if one accepts the Jπ value of the ^{105}Ru ground state as 3/2+, the most likely description for the state is v = 3, $\left[(d_{5/2})^3(g_{7/2})^8\right]_{3/2+}$.

The ground state of ^{105}Rh is 7/2+ and presumably belongs to the $(g_{9/2})^5$ proton configuration. Two 7/2+ states arise from this configuration, with seniorities 3 and 5 respectively. We thus interpret the ground state as v = 3, $(g_{9/2})^5_{7/2+}$ and either the 499.2 keV or the 638.7 keV as the v = 5, $(g_{9/2})^5_{7/2+}$ state. A 7/2+ state is also possible from the v = 1, $\left[(g_{9/2})^4(g_{7/2})^1\right]_{7/2+}$ configuration.

The 129.7 keV level can be interpreted as a hole in the $p_{1/2}$ subshell with six particles in the $g_{9/2}$ subshell. Two $\frac{1}{2}$-states are possible from such a coupling, one with v = 1, and the other with v = 5. Again it is reasonable to interpret the metastable state as the state with the lowest intensity; v = 1, $\left[(p_{1/2})^{-1}\ (g_{9/2})^6\right]_{\frac{1}{2}-}$.

Three 9/2+ states are possible from the coupling of five particles in the $g_{9/2}$ shell, one with v = 1 and two with v = 3. It is attractive to identify the 149.2 keV level with the v = 1, $(g_{9/2})^5_{9/2+}$ state and to associate the 499.2 keV state with one of the v = 3 states of this configuration.

Only one 3/2+ state is possible from the coupling of five $g_{9/2}$ particles. It has seniority three and can be used for a representation of the 806.1 keV level; v = 3, $(g_{9/2})^5_{3/2+}$.

The 5/2+ states at 465.4 keV, 724.5 keV and 969.5 keV can be attributed to the v = 3 or v = 5, $(g_{9/2})^5_{5/2+}$ states or the

$v = 1, \left[(g_{9/2})^4 (d_{5/2})^1\right]_{5/2}$. It is impossible to distinguish between these choices and, in fact, it is quite likely that all three states are mixtures of the three configurations.

The three 3/2- states at 392.6 keV, 455.9 keV and 785.9 keV can be interpreted as belonging to the $v = 3, \left[(p_{1/2})^{-1} (g_{9/2})^6\right]_{3/2^-}$, $v = 5, \left[(p_{1/2})^{-1} (g_{9/2})^6\right]_{3/2-}$ and the $v = 1, \left[(p_{3/2})^{-1} (g_{9/2})^6\right]_{3/2-}$ configurations as well as a vibrational excitation on the $\frac{1}{2}$-, 129.7 keV level. Again it is impossible to make definite assignments.

The 5/2- state at 1215.2 keV can be represented by either the $v = 3, \left[(p_{1/2})^{-1} (g_{9/2})^6\right]_{5/2-}$ state or as the $v = 1, \left[(f_{5/2})^{-1} (g_{9/2})^6\right]_{5/2-}$ state. It appears meaningless to speculate concerning the configurations of the other levels.

Although there is no evidence that this is a deformed nucleus, some of the levels can be described in terms of the Nilsson model on the assumption that one can use this model in the limit of zero deformation.

The ground state of ^{105}Rh can be interpreted as the 7/2+ [413] particle state. The 1/2- isomeric state can be interpreted as the $\frac{1}{2}$ - [301] hole state and the 9/2+, 149.2 keV level can be interpreted as the 9/2+ [404] particle state. The 3/2- states at 392.6 keV, 455.9 keV and 785.9 keV may be associated with the 3/2- [301] or the 3/2- [312] hole states or the 3/2- member of the 1/2- [301] rotational band but it is impossible to distinguish between the various alternatives. The 3/2+, 806.1 keV level can be interpreted as the 3/2+ [431] hole state.

The 5/2+ states at 469.4, 724.5 and 969.5 keV may be associated with the 5/2+ [422] hole state, the 5/2+ [413] and 5/2+ [402] particle states but again there is no way of making a positive correlation. The 638.7 keV level may well be the 7/2+ [404] particle state and the 1215.2 keV level may either be the 5/2- [303] hole state or the 5/2- member of the 1/2- [301] rotational band.

The ground state of ^{105}Ru is probably the 3/2+ [411] state. If the spin should turn out to be 5/2+, an assignment to either the 5/2+ [412] or 5/2+ [413] Nilsscn levels would be appropriate. The 5/2+ [413] Nilsson level is not a logical choice since it would lead to an unhindered allowed beta transition to the 7/2+ [413] ground state of ^{105}Rh. Similarly the 3/2+ [422] choice for the ground state of ^{105}Rh is not very plausible since it would give rise to an unhindered allowed beta transition to the 5/2+ excited state of ^{105}Rh associated with the 5/2+ [422] configuration.

It is very difficult to make a proper assignment to the levels in ^{105}Rh and the ^{105}Ru ground state partly because of the insecure Jπ assignments for these levels. The experiments reported in this thesis have been carried out to the limits of the experimental facilities available at this laboratory. A secure knowledge of the ground state spins of ^{105}Ru and ^{105}Rh would make the interpretation very much easier. According to some members of Dr. Summers-Gill's atomic beam group, such measurements should be possible with their equipment, and the author believes that he has generated some interest within that group in making these measurements in the near future. An investigation of the internal conversion spectra with a magnetic spectrometer

of sufficiently high resolution to determine L_1: L_2: L_3 ratios would yield much more precise information concerning multipole mixtures and hence lead to firmer Jπ assignments. The large $\pi\sqrt{2}$ beta ray spectrometer at Chalk River would probably be adequate for such measurements. Finally, the possibility of carrying out gamma-gamma angular correlation studies using two Ge(Li) detectors would seem to be feasible in the near future. Such measurements might lead to unique spin assignments for some of the levels.

SUMMARY

The beta and gamma ray transitions emitted following the decay of ^{105}Ru have been extensively studied by singles and coincidence techniques. The internal conversion coefficients of the eighteen most intense gamma rays were determined using a $\pi\sqrt{2}$ magnetic spectrometer. This spectrometer was also used to determine the energies and intensities of the more intense gamma rays by the external conversion method. Ge(Li) and NaI(Tℓ) detectors have been used to identify seventy gamma ray transitions, of which all but seven have been classified in the proposed decay scheme. The decay scheme has been thoroughly tested by means of gamma-gamma and beta-gamma coincidence measurements. Twenty-two levels have been established for ^{105}Rh, of which nine had been postulated by earlier workers.

The total decay energy was found to be 1916 ± 4 keV. The intensity balance within the decay scheme as determined by the beta ray and gamma ray measurements, were found to be consistent.

An attempt at an interpretation of some of the levels in both the shell model and the Nilsson model was carried out but it was not possible to arrive at unique assignments for many of the levels.

REFERENCES

Alaga, G., Alder, K., Bohr, A., and Mottelson, B.R. (1955). K. Danske Vidensk. Selsk. Mat.-Fys. Medd. 29, No. 9.

Alaga, G. (1955) Phys. Rev. 100, 432.

Alaga, G. (1957) Nucl. Phys. 4, 625.

Allen, J. S. (1948) Amer. J. Phys. 16, 451.

Artna, A. (1961). Ph.D. Thesis, McMaster University, Hamilton, Ontario.

Arya, A. P. (1963). Nucl. Phys. 40, 387.

Bernstein, A.M. and Brennan, M. H. (1960), Phys. Rev. 120, 927.

Blaise, J., and Cantrel, H. (1953). J. Phys. Radium 14, 135.

Bohr, A. and Mottelson, B. (1953). K. Danske Videnskab. Selskab, Mat.-Fys. Medd., 27, No. 16.

Brandhorst, H. W. (1962) Phys. Rev. 125, 1323.

Brueckner, K. A. and Gammel, J. L. (1958). Phys. Rev. 109, 1023.

Burke, D. G. (1963). Ph.D. Thesis, McMaster University, Hamilton, Ontario.

Chadwick, J. and Ellis, C.D. (1922). Proc. Camb. Phil. Soc. 21, 274.

Chase, R. L. (1960). Rev. Sci. Instr. 31, 945.

Coryell, C. D. and Irvine, J. W. (1955) M.I.T. LNS Annual Progress Report.

Davis, R. (1955). Phys. Rev. 97, 766.

De Shalit, A. and Talmi, I. (1963). "Nuclear Shell Theory". Academic Press, New York, New York.

Duffield, R. B. and Langer, L. M. (1951) Phys. Rev. 81, 203.

Ewan, G. T. and Tavendale, A. J. (1964) Can. J. Phys. 42, 2286.

Fano, U. (1947). Phys. Rev. 72, 26.

Fermi, E. (1934) Zeits. f. Phys. 88, 161.

Fermi functions (1952) "Tables for the Analysis of Beta Spectra", National Bureau of Standards AMS 13.

Frauenfelder, H., Bobone, R., von Goeler, E., Levine, N., Lewis, H. R., Peacock, R.N., Rossi, A., De Pasquali, G. (1957). Phys. Rev. 106, 386.

Freck, D. V. and Wakefield, J. (1962) Nature 193, 669.

Gerholm, T. R. (1956). Ark. Fys. 11, 55.

Goldhaber, M., Grodzins, L., and Sunyar, A.W. (1958) Phys. Rev. 109, 1015.

Gurney, R. W. (1925) Proc. Roy. Soc. A 109, 540.

Habib, E. (1959) Ph.D. Thesis, McMaster University, Hamilton, Ontario.

Haxel, O., Jensen, J.H.D. and Suess, H.E. (1949) Phys. Rev. 75, 1766.

Haxel, O., Jensen, J.H.D. and Suess, H.E. (1950) Z. f. Phys. 128, 295.

Heath, R.L. (1957) "Scintillation Spectrometry Gamma-Ray Spectrum Catalogue" A.E.C. Report IDO-16408.

Heath, R. L. (1962) A.E.C. Report IDO-16784.

Ingraham, M.G. and Reynolds, J.H. (1950) Phys. Rev. 78, 822.

Johns, M. W., Waterman, H., MacAskill, D. and Cox, C.D. (1953). Can. J. Phys. 31, 225.

Karlsson, S. E., Bergman, O. and Scheuer, W. (1964). Arkiv. Fysik 27, 61.

Kennett, T. J., Prestwich, W.V. and Keech, G. L. (1964). Nucl. Instr. 29, 325.

Kitching, J. E. (1966). Ph.D. Thesis, McMaster University, Hamilton, Ontario.

Klein, O., Nishina, Y. (1929). Z. Physik 52, 853.

Konopinski, E. J. and Uhlenback, G. E. (1941) Phys. Rev. 60, 308.

Lee, T.D. and Yang, C.N. (1956). Phys. Rev. 104, 254.

Marion, J. B. (1960) Nucleonics Nov.

Mayer, M. G. (1949) Phys. Rev. 75, 1956.

Mayer, M.G. (1950) Phys. Rev. 78 16.

Mitchell, R. F. and Martin, D.S. (1956). J. Inorg. Nucl. Chem. 2, 286.

Moszkowski, S.A. (1953) Phys. Rev. 89, 474.

Murray, G., Graham, R. L. and Geiger, J. S. (1965) Nucl. Phys. 63, 353.

Neeson, J. F. and Arns, R. G. (1965) Nucl. Phys. 68, 401.

Nilsson, S. G. (1955) K. Danske Videnskab. Selskab, Mat-Fys. Medd. 29, No.16.

Nilsson, S. G. and Mottelson, B. R. (1959) K. Danske Videnskab. Selskab. Mat.-Fys. Skr 1, No. 8.

Nordheim, L. (1950) Phys. Rev. 78, 294.

Nuclear Data Sheets (1966) Nuclear Data Group, Oak Ridge National Laboratory, U. S. A.

Page, L. A. and Heinberg, M. (1957) Phys. Rev. 106, 1220.

Pauli, W. (1933) Rapports du Septième Conseil de Physique Solvay, Brussels, 1933, Paris: Gauthier-Villars et Cie, (1934).

Pierson, W. R. (1965) Phys. Rev. 140, 1516.

Preston, M. A. (1962) "Physics of the Nucleus", Addison-Wesley Publishing Co. Inc., Reading, Mass., U.S.A.

Primakoff, H. (1952) Phys. Rev. 85, 888.

Rainwater, J. (1950), Phys. Rev. 79, 432.

Rayleigh, Third Baron, "The Theory of Sound", Vol. II, 364, London: MacMillan.

Reines, F., and Cowan, C. L. (1953) Phys. Rev. 92, 830.

Reines, F., and Cowan, C. L. (1959), Phys. Rev. 113, 273 .

Ricci, R. A., Monaro, S., and Van Lieshout, R. (1960) Nucl. Phys. 16, 339.

Robinson, R. L., Stelson, P.H., McGowan, F. K., Ford, J.L.C. and Milner, W. T. (1964) Nucl. Phys. 74, 281.

Rose, M. E., Goertzel, G. H., Spinrad, B. I., Harr, J. and Strong, P. (1951). Phys. Rev. 83, 79.

Rose, M. E. (1958) "Internal Conversion Coefficients" Amsterdam: North Holland Publishing Co.

Rossi, A. and De Pasquali, G. (1957) Phys. Rev. 106, 386.

Saraf, B., Harihar, P. and Jambunatha, R. (1960) Phys. Rev. 118, 1289.

Sherwin, C.W. (1948), Nucleonics 2, May 16.

Siegbahn, K. and Svartholm, N. (1946) Nature 157, 872.

Siegbahn, K. (1965) "Alpha-, Beta- and Gamma-Ray Spectroscopy", North Holland Publishing Co., Amsterdam, Netherlands.

Sliv, L. A. and Band, I. M. (1956,1958) "Coefficients of Internal Conversion of Gamma Radiation" Moscow-Leningrad: USSR Academy of Sciences. Reprinted as University of Illinois Reports 57 ICCK 1 and 58 ICCL 1.

Staveley, A. V. (1961) M. Sc. Thesis, McMaster University, Hamilton, Ontario.

Steudel, A. (1952) Z. Physik 132, 429.

Storm, E. L., Gilbert, E. and Israel, H. (1958) Los Alamos Rept. LA-2237.

Tavendale, A. J. and Ewan, G.T. (1963). Nucl. Instr. and Meth. 25, 185.

Weisskopf, V. F. (1951) Phys. Rev. 83, 1073.

Weisskopf, V. F., Gomes, L. C. and Walecka, J.D. (1958) Ann. Phys. (New York) 3, 241.

Wu, C. S., Ambler, E., Hayward, R.W., Hopper, D. D. and Hudson, R. P. (1957) Phys. Rev. 105, 1413.